

Utah State University

DigitalCommons@USU

All Graduate Theses and Dissertations

Graduate Studies

8-2013

Two Scenes from Utah's Stratigraphic Record: Neoproterozoic Snowball Earth, Before and After

Dawn Schmidli Hayes
Utah State University

Follow this and additional works at: <https://digitalcommons.usu.edu/etd>



Part of the [Geology Commons](#)

Recommended Citation

Hayes, Dawn Schmidli, "Two Scenes from Utah's Stratigraphic Record: Neoproterozoic Snowball Earth, Before and After" (2013). *All Graduate Theses and Dissertations*. 1705.
<https://digitalcommons.usu.edu/etd/1705>

This Dissertation is brought to you for free and open access by the Graduate Studies at DigitalCommons@USU. It has been accepted for inclusion in All Graduate Theses and Dissertations by an authorized administrator of DigitalCommons@USU. For more information, please contact digitalcommons@usu.edu.



TWO SCENES FROM UTAH'S STRATIGRAPHIC RECORD:
NEOPROTEROZOIC SNOWBALL EARTH, BEFORE AND AFTER

by

Dawn Schmidli Hayes

A dissertation submitted in partial fulfillment
of the requirements for the degree

of

DOCTOR OF PHILOSOPHY

in

Geology

Approved:

Dr. Carol Dehler
Major Professor

Dr. Dave Liddell
Committee Member

Dr. John Shervais
Committee Member

Dr. Paul Link
Committee Member

Dr. Adolph Yonkee
Committee Member

Dr. Mark McLellan
Dean of the School of
Graduate Studies

UTAH STATE UNIVERSITY
Logan, Utah

2013

Copyright © Dawn Hayes 2013

All Rights Reserved

ABSTRACT

Two Scenes from Utah's Stratigraphic Record:
Neoproterozoic Snowball Earth, Before and After

by

Dawn Schmidli Hayes, Doctor of Philosophy

Utah State University, 2013

Major Professor: Dr. Carol M. Dehler
Department: Geology

This research is focused on strata deposited in northern Utah during the Cryogenian Period (850 – 635 Ma) of the Neoproterozoic Era, a period that derives its name from the widespread evidence for multiple, likely global, glacial events during this time, commonly referred to as “Snowball Earth” glaciations. This dissertation includes detailed studies of two Cryogenian successions in northern Utah that bracket potential “Snowball Earth” events: the upper part of the Uinta Mountain Group (deposited prior to the glaciations) and the dolomite member of the Kelly Canyon formation (hypothesized to have formed in the aftermath of a global glaciation that terminated at either 665 or 635 Ma). Both successions contain a lithostratigraphic, geochemical, and biotic record of the Earth's oceans before and after the largest-magnitude glaciations in the history of our planet.

The pre-glacial upper part of the Uinta Mountain Group in the area mapped for this study contains evidence of several (at least three) relatively short periods of ocean anoxia in which ferruginous conditions dominated and euxinia did not occur. There is no evidence that biota (organic-walled microfossil assemblages) were influenced by these brief anoxic events, but evidence from the composite Uinta Mountain Group stratigraphic record does suggest a gradual change in biota similar to that in the Chuar group. It is likely this biotic transition is related to nearshore eutrophication in the oceans, but additional redox geochemical information is needed to fully support this conclusion.

The dolomite member of the Kelley Canyon Formation on Antelope Island (post-glacial component of this study) contains idiosyncratic lithologic features thought to be characteristic of 635 Ma deglacial strata, yet its C-isotope values do not lend unequivocal support to this global correlation, and regional correlations and U-Pb zircon ages suggest it is ~30 million years older. These results challenge the popular notion that Neoproterozoic post-glacial cap carbonates can be correlated based upon their lithologic “style,” and they also lend additional support to the possibility of a “Snowball Earth” event at ~665 Ma.

(138 pages)

PUBLIC ABSTRACT

Two Scenes from Utah's Stratigraphic Record: Neoproterozoic Snowball Earth, Before and After

This research is focused on rock units deposited in northern Utah before and after global glacial events of unprecedented magnitude, commonly referred to as “Snowball Earth” glaciations. The rock units deposited prior to the beginning of these glaciations (~770 to 740 million years ago) include the Uinta Mountain Group in Utah's Uinta Mountains. Rock units deposited after the glaciations (either ~665 or ~635 million years ago) include parts of the Kelley Canyon Formation on Antelope Island in the Great Salt Lake. These rocks, deposited in shallow ocean environments, record the history of life and ocean chemistry just before and after the largest-magnitude glaciations in the history of our planet.

The results of this research indicate that shallow ocean conditions before the Snowball Earth glaciations fluctuated between oxic and anoxic, with smaller-scale fluctuations (millions of years) not seeming to affect shallow marine life but larger-scale changes (occurring over several tens of millions of years) corresponding with changes in the types of organisms present. After the glaciations, major & geologically “instant” ocean chemical changes are documented in Utah's rocks; the results of this research challenge some existing ideas about the popular yet hotly contested Snowball Earth hypothesis and have the potential to change the Precambrian part of the geologic timescale.

Dawn Schmidli Hayes

ACKNOWLEDGMENTS

I would like to thank my advisor, Dr. Carol Dehler, for all of her support in completing this research - and for making sure that my adventures in geology were always as interesting and fun as possible! I would also like to thank my committee members, Drs. Paul Link, Adolph Yonkee, Dave Liddell, Susanne Janecke, and John Shervais, for their support and assistance throughout the completion of my dissertation research. I also have several colleagues to thank for their extreme generosity, both with their time and the use of their laboratory facilities. This research would not have been possible without Dr. Viorel Atudorei at the University of New Mexico, Drs. Dave Johnston and Erin Beirne at Harvard University, Dr. Mark Schmitz and Debbie Pierce at Boise State University, the University of Arizona Laserchron center, and microfossil identification assistance from both Robin Nagy (USU) and Dr. Susanna Porter (UC Santa Barbara). I also thank all of my field companions: Ashley and Muffet Hayes, Pearl Dehlerson, Hannah McDonough, Christian Bjerrum, Lily Horne, Dallas Nutt, JR Hoggan, Michael Strange, Robin Butz, Francis MacDonald, Emmy Smith, and Paul and Guy Hoffman.

Funding for this research was provided by the National Science Foundation (NSF EAR-0819759), the Geological Society of America (2011 Student Grant), EDMap (2011-2012 project), Sigma Xi Scientific Society, the Society for Organic Petrology, and the Utah State University J. Stewart Williams Graduate Fellowship.

Dawn Schmidli Hayes

CONTENTS

	Page
ABSTRACT.....	iii
PUBLIC ABSTRACT.....	v
ACKNOWLEDGMENTS.....	vi
LIST OF TABLES	ix
LIST OF FIGURES	x
 CHAPTER	
1. GENERAL INTRODUCTION.....	1
1.1- Introduction	1
1.2- References	7
2. LINKING THE EASTERN AND WESTERN UMG: GEOLOGIC MAP AND STRATIGRAPHY OF THE NEOPROTEROZOIC UINTA MOUNTAIN GROUP, DAGGET AND UINTAH COUNTIES, UT	
2.1- Abstract	11
2.2- Introduction	12
2.3- Geologic setting.....	15
2.4- Methods	20
2.5- Results and discussion	27
2.6- Conclusions	30
2.7- References	38
3. EVIDENCE FOR FERRUGINOUS NEOPROTEROZOIC OCEANS AND A POTENTIALLY GLOBAL BIOTIC TURNOVER: INSIGHTS FROM A NEW GEOCHEMICAL AND MICROFOSSIL RECORD, UINTA MOUNTAIN GROUP, UT	
3.1- Abstract	43
3.2- Introduction	44
3.3- Background	46
3.4- Methods	52
3.5- Results and discussion	56
3.6- Conclusions	63

3.7- References.....	70
4. A NEWLY DESCRIBED NEOPROTEROZOIC POST-GLACIAL CAP CARBONATE SEQUENCE, ANTELOPE ISLAND, GREAT SALT LAKE: DISCOVERY OF THE CRYOGENIAN-EDIACARAN BOUNDARY IN NORTHERN UTAH?	
4.1- Abstract	74
4.2- Introduction	75
4.3- Stratigraphy and sedimentology	77
4.4- Chemostratigraphy	81
4.5- Detrital zircon geochronology	82
4.6- Regional correlations and age constraints.....	82
4.7- Discussion and conclusions.....	83
4.8- References.....	85
5. GENERAL SUMMARY AND CONCLUSIONS	89
5.1- Summary and conclusions	89
5.2- References.....	91
APPENDICES	92
APPENDIX A: <i>Geology</i> submission data repository	93
APPENDIX B: <i>Precambrian Research</i> submission data repository	101
APPENDIX C: Geologic map.....	122
VITA.....	125

LIST OF TABLES

Table		Page
1	Comparison of western, central, and eastern UMG	35
2	Summary of fossil occurrences from previous studies	53
3	Total organic carbon (TOC) averages and ranges	60
4	$\delta^{13}\text{C}$ averages and ranges by section	61

LIST OF FIGURES

Figure	Page
1	Location of Neoproterozoic glacial deposits worldwide.....2
2	Extent and generalized stratigraphy of Neoproterozoic strata in UT.....3
3	Eutrophication evidence from previous work.....13
4	Stratigraphic columns of eastern & western UMG14
5	Simplified geologic map of the Neoproterozoic Uinta Mountain Group.....16
6	Stratigraphy, age data, C-isotope curves, and microfossils.....17
7	Facies photographs, descriptions, and interpretations.....31
8	Thin section photographs.....33
9	Detrital zircon relative probability plots and paleocurrent data.....34
10	Generalized geologic map of the Uinta Mountain Group.....48
11	Stratigraphic columns of Eastern & Western UMG49
12	Correlation of the UMG and Chuar Group.....51
13	Flowchart illustrating the interpretation of iron speciation values.....57
14	Redox and C-isotope data from the Leidy/Marsh Peak area.....59
15	Microfossils in the Leidy/Marsh Peak strata.....66
16	Comparison of C-isotope, TOC, microfossil, and redox data67
17	Illustration of chemocline changes in a shallow-shelf eutrophication70
18	Antelope Island location map.....78
19	Composite measured section of Neoproterozoic units on Antelope Island...79
20	Facies photographs from Antelope Island.....80

CHAPTER 1

GENERAL INTRODUCTION

The Neoproterozoic Cryogenian Period (850 – 635 Ma) derives its name from the widespread evidence for multiple, likely global, glacial events referred to as “Snowball Earth” during this time (Hoffman et al., 1998). Formerly referred to collectively as the “Varanger glaciation,” it has become common to refer to the older of these Cryogenian glacial episodes (~716 – 665 Ma) as “Sturtian” and the younger (~635 Ma) as “Marinoan” (Halverson et al., 2004). General geographic locations, a timeline and a composite C-isotope record for strata deposited during the Cryogenian Period are shown in Figure 1, with the two stratigraphic intervals of interest in this study highlighted on the timeline. Strata of Cryogenian age are abundant in Utah (Figure 2). The Cryogenian strata of Utah that are included in this dissertation research are 1) the pre-glacial Uinta Mountain Group that outcrops throughout the Uinta Mountain Range in northern Utah, southern Wyoming, and western Colorado and 2) the post glacial (either Sturtian or Marinoan) cap carbonate sequence that outcrops on Antelope Island in the Great Salt Lake. There are several other localities in northern Utah, central Utah, and southern Idaho where post-glacial Cryogenian rocks are exposed (Figure 2) in addition to Antelope Island; these additional post-glacial Cryogenian strata are not the focus of this dissertation, but their relationships with the Antelope Island strata are considered.

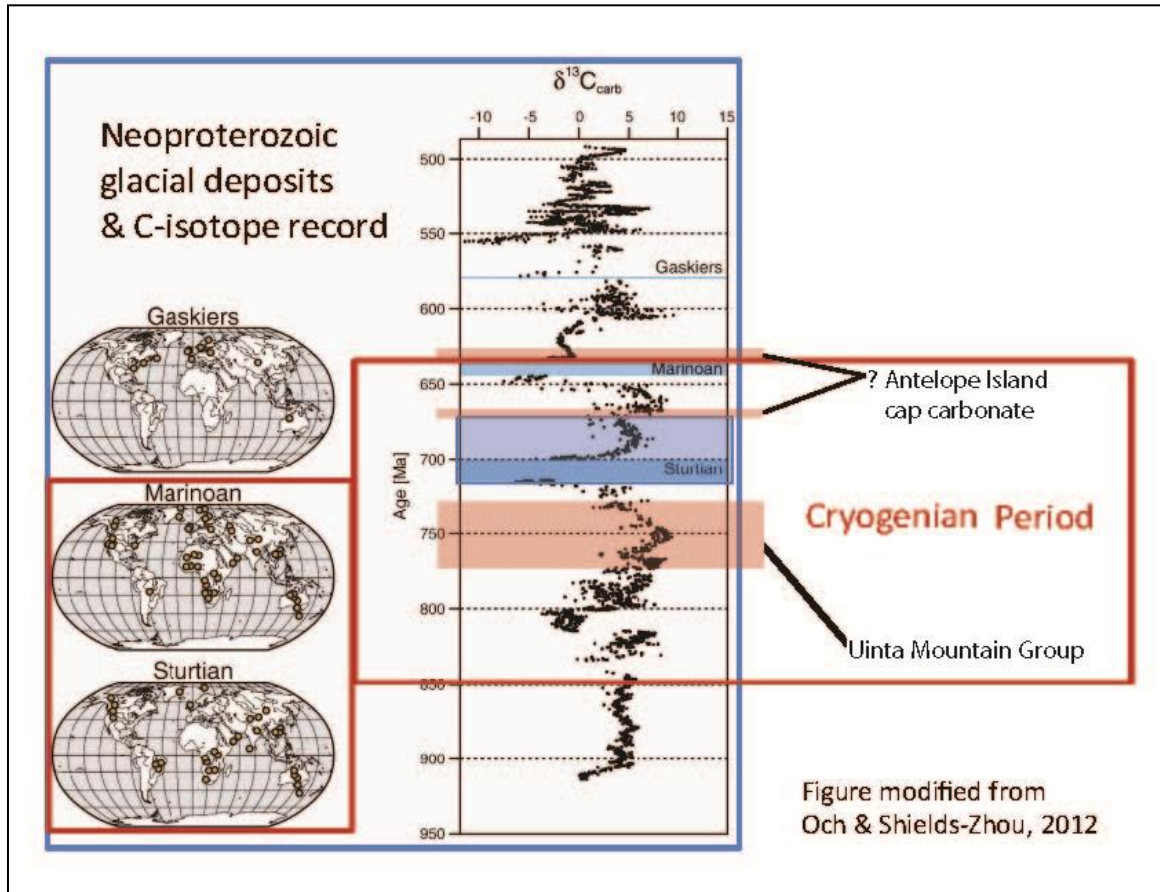


Figure 1. Locations of Neoproterozoic glacial deposits worldwide are shown with yellow dots on the maps. Transparent red boxes on the age/C-isotope graph denote ages of UT strata included in this study (pre-glacial Uinta Mountain Group and post-glacial (Marinoan or Sturtian?) cap carbonate on Antelope Island); blue boxes show timing of glacial episodes (modified from Och and Shields-Zhou, 2012).

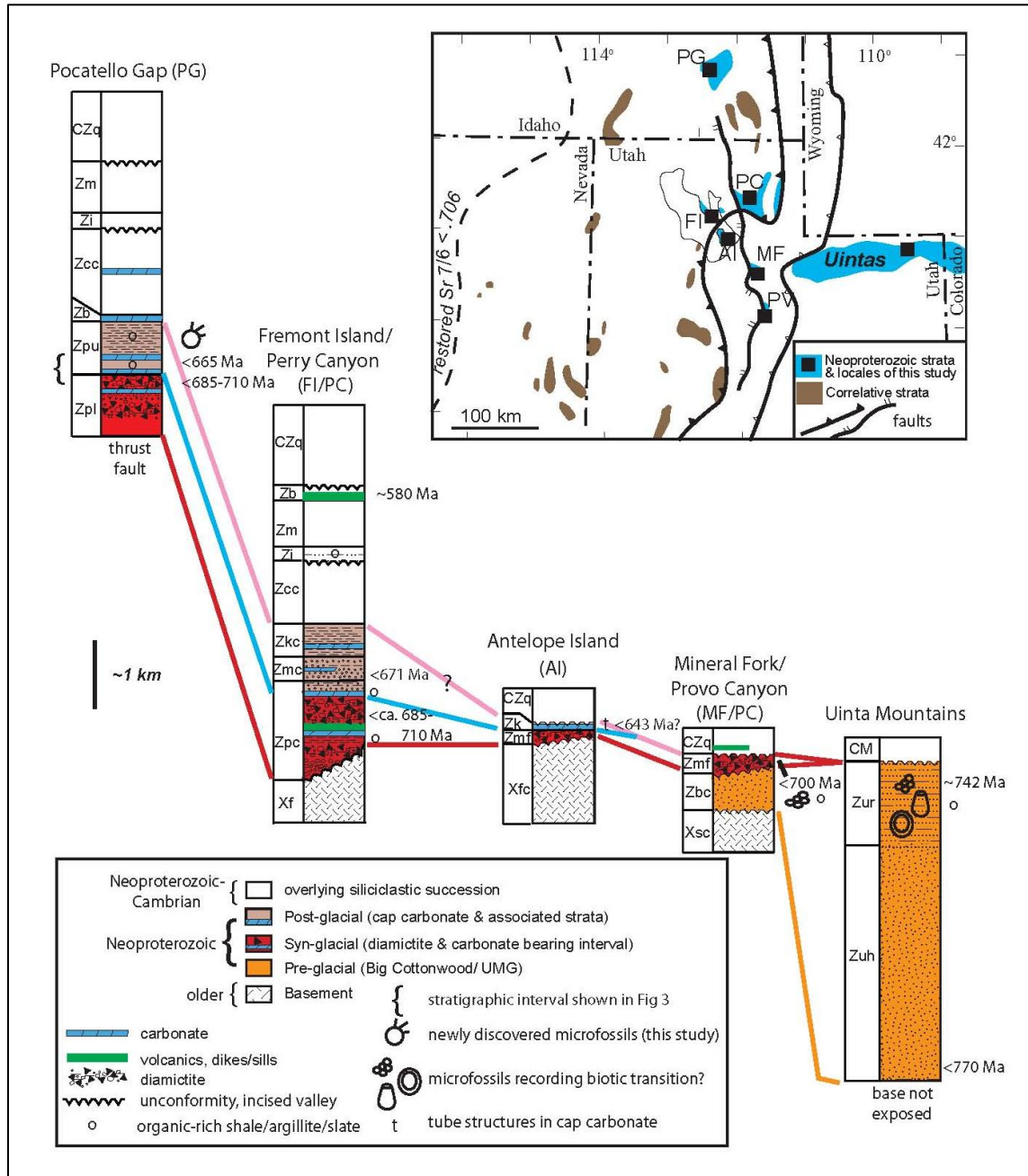


Figure 2. Extent and generalized stratigraphy of Neoproterozoic strata in Utah, including the pre-glacial Uinta Mountain Group and the syn- and post-glacial strata on Antelope Island which are the focus of this dissertation. Figure modified from Dehler, unpublished work.

Several previous Neoproterozoic microfossil diversity studies yield evidence for a relatively sudden biotic change prior to the first well-constrained Sturtian glacial episode at 716.5 Ma (Knoll et al., 1981; Knoll, 1994; Macdonald et al., 2010; Vidal and Knoll, 1982; Vidal and Moczydlowska, 1992). In an event interpreted by Nagy et al. (2009) as a mass extinction of eukaryotic phytoplankton followed by bacterial dominance in the Neoproterozoic Chuar Group, diverse assemblages of complex acritarchs are replaced by more uniform assemblages consisting of simple leiosphaerid acritarchs, bacteria, and vase-shaped microfossils. Nagy et al. (2009) propose that a eutrophication event – a biotic bloom caused by increased nutrient availability, often leading to water column anoxia – is the most plausible explanation for this change in microfossil assemblage. One objective of my dissertation is a study of pre-Sturtian strata in Utah to determine if the Neoproterozoic (Cryogenian) 770-742 Ma Uinta Mountain Group (UMG) contains biotic and geochemical evidence of a eutrophication event similar to the one recorded in coeval strata of the Grand Canyon's Chuar Group.

This study is novel because the results of iron speciation tests have not yet been published for siliciclastic-dominated pre-Sturtian Cryogenian strata in this region; thus, data generated from this research will fill an existing knowledge gap in the Proterozoic record of ocean geochemistry (Canfield et al., 2008). The research is also very exciting in that it allows for a comparison of ocean biogeochemical records from two coeval but very physically different marine depositional systems that likely shared the same ocean – a relatively shallow mixed-siliciclastic carbonate shelf

(Chuar Group) and a more proximal siliciclastic-dominated delta (UMG) – which could potentially “pave the way” for correlating these two Western U.S. successions with other same-aged strata worldwide. A broader significance is that microfossil and ocean geochemical data from this particular time will contribute to our current understanding of eukaryotic biodiversity and environmental conditions just prior to the most extreme glaciations in Earth’s history. Information from this study is especially important for bolstering the amount of data available for generating a much-needed Cryogenian biostratigraphic framework.

Although Cryogenian strata recording glacial episodes are found globally, it is not completely clear where to “draw the line” between the Sturtian and Marinoan glaciations, and this is especially problematic when the Cryogenian stratigraphic record does not contain evidence of two distinct glaciations, as is often the case. While some radiometric ages confirm two distinct ~10-million-year-scale glacial events that appear to be globally synchronous (Halverson, 2006), others challenge the notion that Cryogenian glacial events can be easily binned into only two discrete intervals (Calver et al., 2004; Fanning and Link, 2004; Kendall et al., 2006; Lund et al., 2003; Schaefer and Burgess, 2003).

Glacial deposits from the Cryogenian Period are often capped by lithologically unusual carbonates (“cap carbonates” that record negative $\delta^{13}\text{C}$ values) (Corsetti and Kaufman, 2003; Corsetti and Lorentz, 2006; Halverson, 2006; Halverson et al., 2004; Hoffman et al., 1998; Hoffman and Schrag, 2002; James et al., 2001; Kaufman et al., 1997; Kennedy, 1996; Lorentz et al., 2004; Macdonald et al.,

2009; Macdonald et al., 2010; Nogueira et al., 2003; Porter et al., 2004; Prave, 1999; Pruss et al., 2010; Xiao et al., 2004). Based on their stratigraphic relationships and their lithologic and carbon isotopic characteristics, many of these cap carbonates have been unofficially classified as Sturtian or Marinoan without geochronologic constraints that would assign them clearly to one of these intervals rather than the other. This informal classification is based partly on an analysis of 12 cap carbonates by Kennedy et al. (1998) that describes the “Sturtian-style” cap carbonates as darker-colored, organic-rich, and finely-laminated with negative basal $\delta^{13}\text{C}$ values that increase over a few to a few tens of meters to mildly positive values and the “Marinoan-style” cap carbonates as lighter-colored, with unusual features (such as seafloor fans, tubestones, sheetcrack cements, and tepee-like structures), and negative $\delta^{13}\text{C}$ values. Although this unofficial cap carbonate classification scheme can be easily applied to the 12 examples included in that particular study, it is unclear whether it “works” for the >15 Neoproterozoic cap carbonates discovered since 1998 (Arnaud et al., 2011).

Recent evidence suggests this classification scheme may be oversimplified and may not apply to all Neoproterozoic cap carbonates (Corsetti and Lorentz, 2006). My research tests this hypothesis through a detailed study of the newly discovered “Marinoan-style” cap carbonate unit on Antelope Island in northern Utah. By generating detailed facies descriptions, a C-isotope record, U-Pb detrital zircon maximum ages, it is possible to test both regional and global correlations with other Cryogenian strata. This work will yield information about the number

and timing of Cryogenian glacial events in this region and globally. This information has very important implications for testing current Snowball Earth models.

The products of the research in the Uinta Mountain Group include 1) a 1:24,000 scale geologic map of portions of the Leidy Peak and Marsh Peak USGS 7.5' quadrangles (with an accompanying report), part of an EDMAP project submitted in October, 2012, and 2) a manuscript that will be submitted to the peer-reviewed publication *Precambrian Research* in May, 2013. The final product of the research on Antelope Island is a manuscript that was submitted to the peer-reviewed publication *Geology* in March, 2013.

REFERENCES

- Arnaud, E., Halverson, G.P., and Shields-Zhou, G., 2011, Chapter 1 The geological record of Neoproterozoic ice ages: Geological Society, London, Memoirs, v. 36, p. 1-16.
- Calver, C.R., Black, L.P., Everard, J.L., and Seymour, D.B., 2004, U-Pb zircon age constraints on late Neoproterozoic glaciation in Tasmania: *Geology*, v. 32, p. 893-896.
- Canfield, D.E., Poulton, S.W., Knoll, A.H., Narbonne, G.M., Ross, G., Goldberg, T., and Strauss, H., 2008, Ferruginous conditions dominated later neoproterozoic deep-water chemistry: *Science*, v. 321, p. 949-952.
- Corsetti, F.A., and Kaufman, A.J., 2003, Stratigraphic investigations of carbon isotope anomalies and Neoproterozoic ice ages in Death Valley, California: *Geological Society of America Bulletin*, v. 115, p. 916-932.
- Corsetti, F.A., and Lorentz, N.J., 2006, On Neoproterozoic Cap Carbonates as Chronostratigraphic Markers, *Neoproterozoic Geobiology and Paleobiology*, in Xiao, S., and Kaufman, A.J., eds., Volume 27: Topics in Geobiology, Springer, Dordrecht, Netherlands, p. 273-294.

- Fanning, C.M., and Link, P.K., 2004, U-Pb SHRIMP ages of Neoproterozoic (Sturtian) glaciogenic Pocatello Formation, southeastern Idaho: *Geology*, v. 32, p. 881-884.
- Halverson, G.P., 2006, A Neoproterozoic Chronology, *in* Xiao, S.H., and Kaufman, A.J., eds., *Neoproterozoic Geobiology and Paleobiology: Topics in geobiology*: Dordrecht, Netherlands, Springer, p. 300.
- Hoffman, P.F., Kaufman, A.J., Halverson, G.P., and Schrag, D.P., 1998, A Neoproterozoic snowball earth: *Science*, v. 281, p. 1342-1346.
- Hoffman, P.F., and Schrag, D.P., 2002, The snowball Earth hypothesis: Testing the limits of global change: *Terra Nova*, v. 14, p. 129-155.
- James, N.P., Narbonne, G.M., and Kyser, T.K., 2001, Late Neoproterozoic cap carbonates: Mackenzie Mountains, northwestern Canada: Precipitation and global glacial meltdown: *Canadian Journal of Earth Sciences*, v. 38, p. 1229-1262.
- Kaufman, A.J., Knoll, A.H., and Narbonne, G.M., 1997, Isotopes, ice ages, and terminal Proterozoic earth history: *Proceedings of the National Academy of Sciences*, v. 94, p. 6600-6605.
- Kendall, B., Creaser, R.A., and Selby, D., 2006, Re-Os geochronology of postglacial black shales in Australia: Constraints on the timing of "Sturtian" glaciation: *Geology*, v. 34, p. 729-732.
- Kennedy, M.J., 1996, Stratigraphy, sedimentology, and isotopic geochemistry of Australian Neoproterozoic postglacial cap dolostones: Deglaciation, delta C-13 excursions, and carbonate precipitation: *Journal of Sedimentary Research*, v. 66, p. 1050-1064.
- Kennedy, M.J., Runnegar, B., Prave, A.R., Hoffmann, K.-H., and Arthur, M.A., 1998, Two or four Neoproterozoic glaciations?: *Geology*, v. 26, p. 1059-1063.
- Knoll, A.H., Blick, N., and Awramik, A.M., 1981, Stratigraphic and ecologic implications of late Precambrian microfossils from Utah: *American Journal of Science*, v. 281, p. 247-263.
- Knoll, A.H., 1994, Proterozoic and early Cambrian protists: evidence for accelerating evolutionary tempo: *Proceedings of the National Academy of Sciences of the United States of America*, v. 106, p. 1281-1292.

- Lorentz, N.J., Corsetti, F.A., and Link, P.K., 2004, Seafloor precipitates and C-isotope stratigraphy from the Neoproterozoic Scout Mountain Member of the Pocatello Formation, southeast Idaho: Implications for Neoproterozoic earth system behavior: *Precambrian Research*, v. 130, p. 57-70.
- Lund, K., Aleinikoff, J.N., Evans, K.V., and Fanning, C.M., 2003, SHRIMP U-Pb geochronology of Neoproterozoic Windermere Supergroup, central Idaho: Implications for rifting of western Laurentia and synchronicity of Sturtian glacial deposits: *Geological Society of America Bulletin*, v. 115, p. 349-372
- Macdonald, F.A., McClelland, W.C., Schrag, D.P., and Macdonald, W.P., 2009, Neoproterozoic glaciation on a carbonate platform margin in Arctic Alaska and the origin of the North Slope subterranean: *Geological Society of America Bulletin*, v. 121, p. 448-473.
- Macdonald, F.A., Schmitz, M.D., Crowley, J.L., Roots, C.F., Jones, D.S., Maloof, A.C., Strauss, J.V., Cohen, P.A., Johnston, D.T., and Schrag, D.P., 2010, Calibrating the Cryogenian: *Science*, v. 327, p. 1241-1243.
- Nagy, R.M., Porter, S.M., Dehler, C.M., and Shen, Y., 2009, Biotic turnover driven by eutrophication before the Sturtian low-latitude glaciation: *Nature Geoscience*, v. 2, p. 414-417.
- Nogueira, A.C.R., Riccomini, C., Sial, A.N., Moura, C.A.V., and Fairchild, T.R., 2003, Soft-sediment deformation at the base of the Neoproterozoic Puga cap carbonate (southwestern Amazon craton, Brazil): Confirmation of rapid icehouse to greenhouse transition in snowball Earth: *Geology*, v. 31, p. 613-616.
- Och, L.M. and Shields-Zhou, G.A., 2012, The Neoproterozoic oxygenation event: Environmental perturbations and biogeochemical cycling: *Earth-Science Reviews*, v. 110, p. 26-57.
- Porter, S.M., Knoll, A.H., and Affaton, P., 2004, Chemostratigraphy of Neoproterozoic cap carbonates from the Volta Basin, West Africa: *Precambrian Research*, v. 130, p. 99-112.
- Prave, A.R., 1999, Two diamictites, two cap carbonates, two delta C-13 excursions, two rifts: The Neoproterozoic Kingston Peak Formation, Death Valley, California: *Geology*, v. 27, p. 339-342.
- Pruss, S.B., Bosak, T., Macdonald, F.A., McLane, M., and Hoffman, P.F., 2010, Microbial facies in a Sturtian cap carbonate, the Rasthof Formation, Otavi Group, northern Namibia: *Precambrian Research*, v. 181, p. 187-198.

- Schaefer, B.F., and Burgess, J.M., 2003, Re-Os isotopic age constraints on deposition in the Neoproterozoic Amadeus Basin: Implications for the 'Snowball Earth': *Journal of the Geological Society*, v. 160, p. 825-828.
- Vidal, G., and Knoll, A.H., 1982, Radiations and extinctions of plankton in the late Proterozoic and early Cambrian: *Nature*, v. 287, p. 57-60.
- Vidal, G., and Moczydlowska, M., 1992, Patterns of phytoplankton radiation across the Precambrian-Cambrian boundary: *Journal of the Geological Society*, v. 149, p. 654-647
- Xiao, S., Bao, H., Wang, H., Kaufman, A.J., Zhou, C., Li, G., Yuan, X., and Ling, H., 2004, The Neoproterozoic Quruqtagh Group in eastern Chinese Tianshan: evidence for a post-Marinoan glaciation: *Precambrian Research*, v. 130, p. 1-26.

CHAPTER 2

LINKING THE EASTERN AND WESTERN UMG: GEOLOGIC MAP, STRATIGRAPHY, AND DEPOSITIONAL ENVIRONMENT OF THE NEOPROTEROZOIC UINTA MOUNTAIN GROUP, DAGGET AND UINTAH COUNTIES, UTAH¹

2.1 - Abstract

Strata of the upper Neoproterozoic Uinta Mountain Group (UMG) were mapped in parts of the Leidy Peak and Marsh Peak 7.5' quadrangles in Dagget and Uintah counties, Utah. A 1:24,000 scale digital map (an ArcGIS project) of the area that includes detailed unit descriptions, stratigraphic columns with correlations, and two geologic cross sections was the final product. In this area, 5 stratigraphic units (Zhp, Zrp1, Zrp2, Zrp3, Zrp4) of the UMG were designated, described, and mapped. Facies associations, paleocurrent measurements, and detrital zircon provenance data suggest that units Zrp1-4 were deposited in a tidally-influenced marginal marine environment in which relative sea level fluctuated fairly regularly (at least four s transgressive-regressive cycles are recorded) and sediment sources from both the east and north were important. When these results are considered with available geochemical and microfossil data for these units and others in the UMG, the correlation of Zrp1-4 with the lower Red Pine Shale in the western Uinta Mountains is favored over the correlation of these newly described units with the Box Canyon shale intervals of the formation of Hades Pass.

¹ Coauthored by Hayes, D.S., and Dehler, C.M.

2.2- Introduction

There are three main outcomes of this mapping project: 1) it generates a detailed map (1:24,000 scale) where previous mapping was done only very generally at the 1:100,000 scale (Sprinkel, 2006), 2) it provides detailed descriptions of the UMG in an area where none existed previously and helps “fill in the blanks” in the existing geochemical and microfossil record for the Uinta Mountain Group as a whole (Figure 3), and 3) it allows an understanding of key units in the upper UMG in the central part of the Uinta Mountains (Figures 4 and 5).

This mapping area was chosen because it contains some of the best known exposures of the upper UMG shale units hypothesized to capture the geochemical and biotic transition previously discussed in the introductory chapter of this dissertation. This rationale is discussed in more detail in Chapter 3 of this dissertation. The mapping project discussed here in Chapter 2 provides a detailed stratigraphic framework for the geochemical and microfossil records presented in Chapter 3. This necessary context allows for 1) an integration of stratigraphy with geochemistry and micropaleontology in the Leidy/Marsh mapping area and 2) correlation of all data from this new mapping area with the existing data set for the Uinta Mountain Group as a whole, which is shown in Figure 3. This also allows for a comparison of geochemical and microfossil trends at two very different scales (millions of years versus several tens of millions of years).

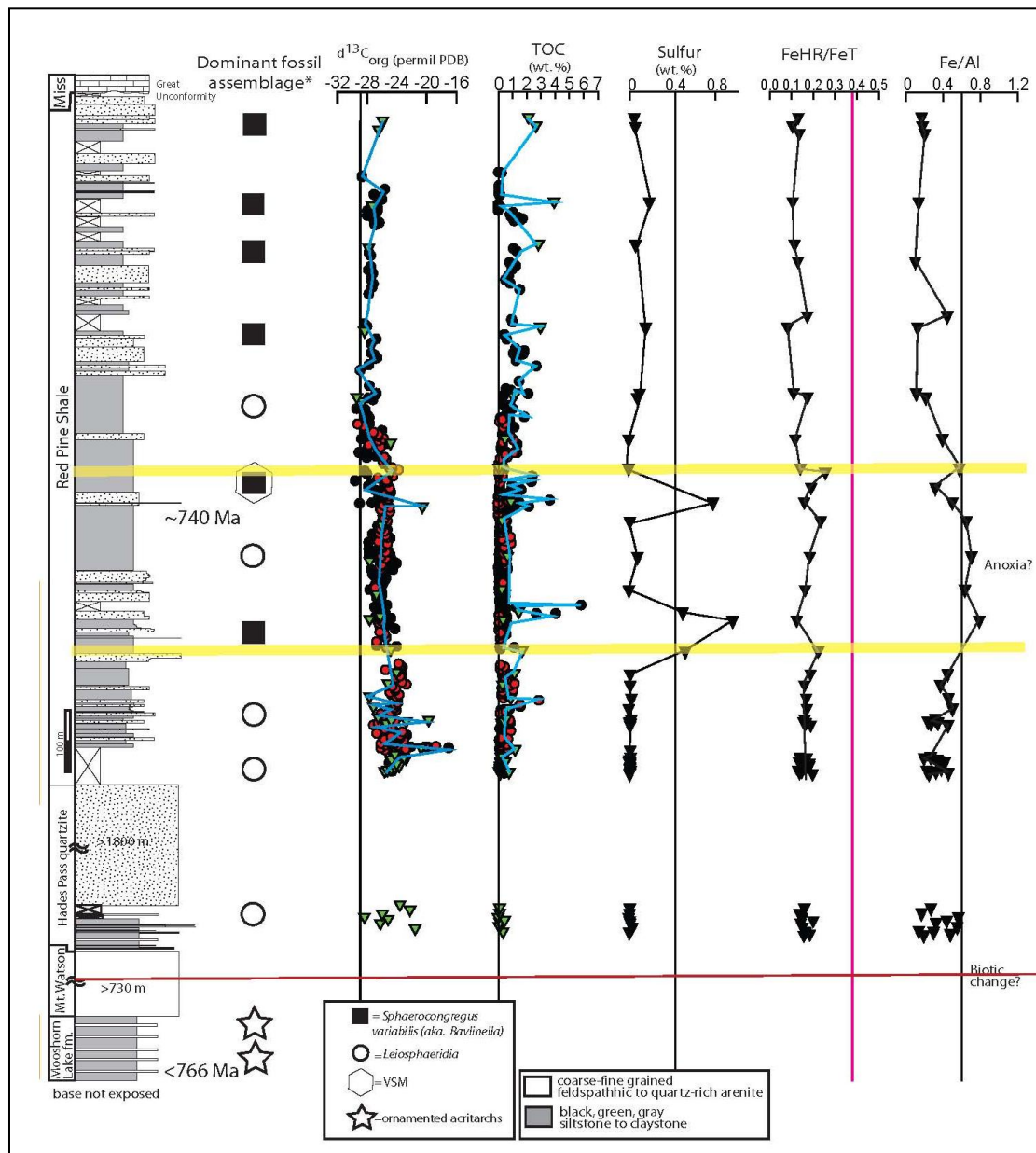


Figure 3. Eutrophication evidence from previous work. Data modified from Hayes (2010) combined with a similar data set from a measured section near Leidy Peak into a composite section. Note the scale change between the lower strata (formations of Moosehorn Lake, Mt. Watson, and Hades Pass) and the upper strata (Red Pine Shale). Fe/Al values above 0.60 suggest deposition under anoxic conditions. Note facies-independent co-occurrence of elevated sulfide, possible anoxic conditions (bracketed by yellow lines), and transition in microfossil assemblage and diversity (marked with red line).

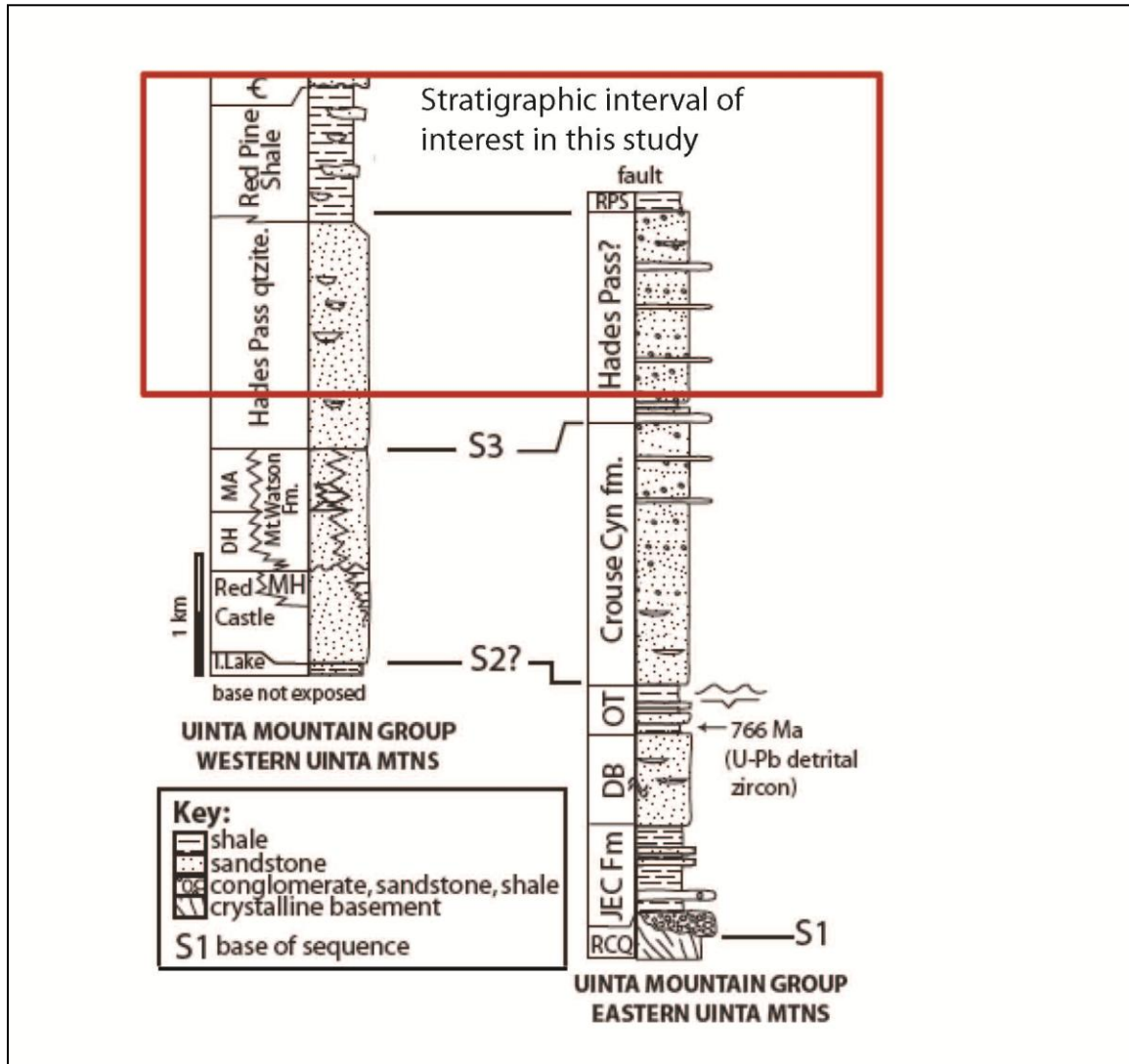


Figure 4. Stratigraphic columns of Eastern & Western UMG showing hypothesized correlation. S1, S2, and S3 indicate lower-order fining upward sequences, which show fluvial or more proximal marine units at the base, becoming proximal to distal marine at the top. C = Cambrian; DH = formation of Deadhorse Pass; MA = formation of Mount Agassiz; MH = formation of Moosehorn Lake; RCQ = Paleoproterozoic (?) Red Creek Quartzite; JEC = Jesse Ewing Canyon Formation; DB = formation of Diamond Breaks; OT= formation of Outlaw Trail; RPS = Red Pine Shale. 742 Ma upper age constraint is based on correlation with the Chuar Group of the Grand Canyon using paleontologic, C-isotope, and paleoenvironmental data. Figure modified from Dehler et al., 2010.

2.3 - Geologic setting

Stratigraphy, age, and correlation

The Uinta Mountain Group, located in northeastern Utah near the Utah-Wyoming border (Figure 5), is one of the only mid-Neoproterozoic successions in the United States that remains well-preserved. It is a thick, siliciclastic succession of relatively unmetamorphosed shale and sandstone (Wallace and Crittenden, 1969). High (0.68) H/C ratios from organic-rich shale in the Neoproterozoic Uinta Mountain Group suggest that little thermal alteration of these rocks has taken place (Strauss and Moore, 1992). The UMG is dominated by quartz arenite to arkosic arenite, yet has significant shale intervals, some as thick as 1800 m (Red Pine Shale) (Bryant, 1992; Dehler et al., 2007; Myer, 2008). The stratigraphy in the western Uinta range is markedly different than that in the east. The western units appear to be more easily divisible, as Wallace (Wallace, 1972) demonstrated by informally naming and subdividing the 4 km thick succession into 7 units, and was followed by Sanderson (Sanderson, 1984) who formally named one unit (Mount Watson Formation). Although it is not completely clear how the eastern and western parts of the Uinta Mountain Group correlate, Figure 4 provides a working model, and it has been determined that strata in the northern part of the Uinta Mountain Group are dominated by sediments derived from the Wyoming craton, and strata from the southern part are dominated by sediments from Paleoproterozoic and Mesoproterozoic sources to the east (Ball and Farmer, 1998; Condie et al., 2001; Dehler et al., 2010; Mueller et al., 2007; Sanderson, 1984).

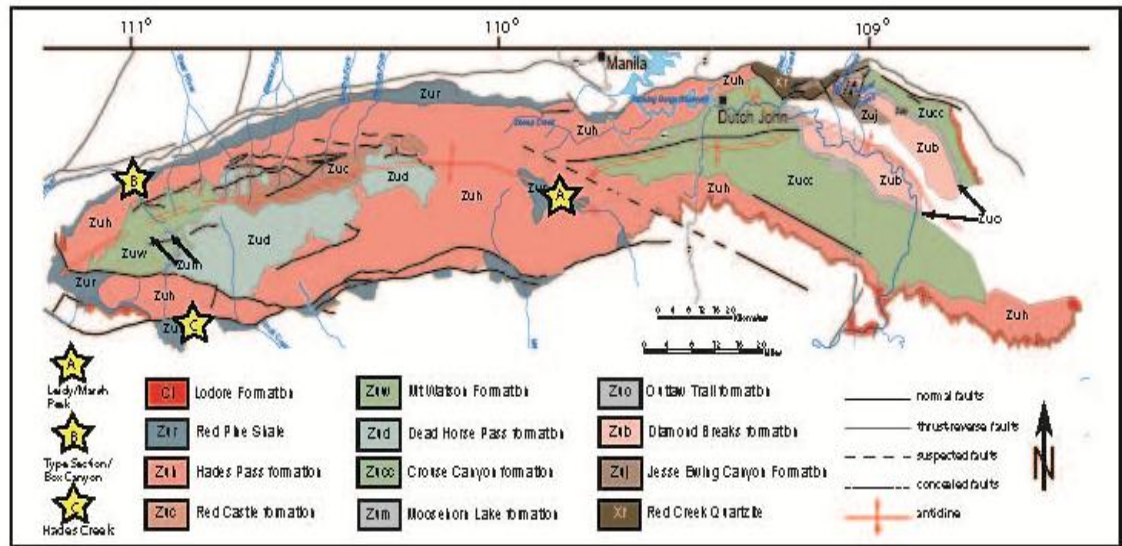


Figure 5. Simplified geologic map of the Neoproterozoic Uinta Mountain Group in northern Utah, southwestern Wyoming, and northwestern Colorado. Note that likely correlative units in the western and eastern Uinta Mountains are denoted with similar map colors but different names/map unit symbols. Samples discussed in this study were collected from the upper Uinta Mountain Group (formation of Hades Pass & Red Pine Shale formation) at the two locations shown on the map (Leidy/Marsh Peak to the east, and Box Canyon and the Red Pine Shale Type Section to the west).

The UMG likely correlates with the Chuar Group of Arizona based on microfossil assemblages, carbon isotope data, and U-Pb zircon geochronology (Dehler et al., 2002; Dehler et al., 2007); this is illustrated in Figure 6. Since the Chuar Group is ~770 to 742 Ma (Karlstrom et al., 2000) and the formation of Outlaw Trail in the UMG has a maximum depositional age of 766+/- 4 Ma, the UMG's best age constraint is ~770-742 Ma (Dehler et al., 2010).

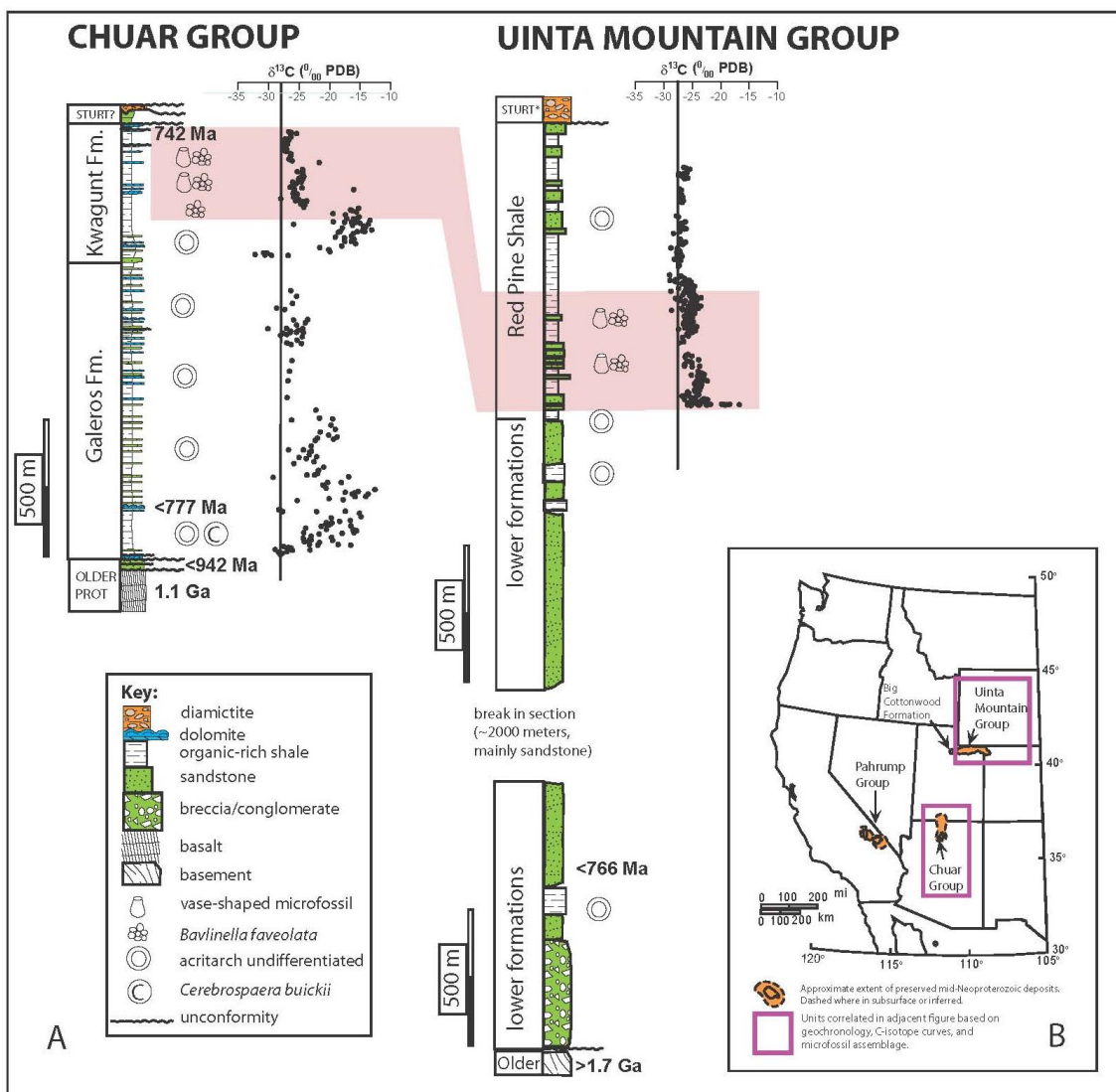


Figure 6. Stratigraphy, age data, C-isotope curves, and microfossil assemblage data from the Chuar and Uinta Mountain Groups is shown above, with the proposed correlation shown shaded in pink (part A). Current outcrop extent of these strata and others hypothesized to be correlative are shown above shaded in orange, and the Chuar and Uinta Mountain Group locations are highlighted with purple boxes (part B). Figure modified from both Dehler et al. (2010) and Dehler (unpublished work).

Depositional environment

Wallace (1972) interpreted the western UMG to represent fluvio-marine deposition defining a marine shoreline that roughly coincides with the modern Uinta divide. Sanderson (1984) interpreted the Mt. Watson Formation, and the entire western UMG, to represent braided fluvial deposition in an aulocogen. Dehler et al. (2002) interpret the uppermost unit of the western UMG, the Red Pine Shale, to indicate marine deltaic deposition. Recent research in the western UMG provides evidence for several transitions back and forth between fluvial and marginal marine environments throughout deposition of the entire group (Kingsbury, 2008; Kingsbury-Stewart et al., in press; Osterhout, 2011).

The informally divided UMG in the easternmost Uinta Mountains is dominated by trough-crossbedded sandstone with lesser shale and conglomerate, and is interpreted to represent dominantly braided fluvial and deltaic deposition (Brehm, 2007; De Grey and Dehler, 2005; Dehler et al., 2007; Rybczynski, 2009). Paleocurrent data from De Grey and Dehler (2005) show a southwesterly flowing river system. Paleocurrent data from both Brehm and Rybczynski (Brehm, 2007; Rybczynski, 2009) show significant westerly and northwesterly flow. These data, in combination with facies analyses, indicate a complicated basin and suite of depositional systems (Condie et al., 2001). De Grey and Dehler (2005) suggests that the green fine-grained facies in the eastern UMG south of Browns Park (formation of Outlaw Trail) represents a delta plain and indicates a marine transgression.

Tectonic setting

The Uinta Mountain Group was deposited in an intracratonic extensional basin with a roughly east-west-trending northern basin edge (Dehler et al., 2010). This deposition took place on autochthonous Laurentian continental crust (Karlstrom and Houston, 1984). The term “intracratonic extensional basin” is preferred over the previously used term “rift basin” since there are neither volcanic nor significant rift-associated facies in the Uinta Mountain Group (Prave, 1999). More coarse-grained deposits and a greater percentage of immature sandstones are found upsection throughout the Uinta Mountain Group strata on the northern side of the range, suggesting a basement-bounding fault trending roughly east-west during UMG deposition (Brehm, 2007; Dehler, 2010; Hansen, 1964; Rybczynski, 2009; Wallace, 1972).

The Uinta Mountains – the core of which expose the UMG - are an east-west-trending range in northeastern Utah and northwestern Colorado that are structurally defined by the boundary between Archean crust to the north and Paleoproterozoic crust to the south (Stone and Stevens, 1993), and more recently by the Laramide-age Uinta Arch, an east-west-trending anticline that spans the length of the range (Figure 5). The timing of Laramide uplift in this area is constrained between 70-40 Ma, during the latest Cretaceous to Middle Eocene. The Uinta Mountains of northeastern Utah and southwestern Wyoming are the westernmost Laramide orogenic structure, and they have received much attention due to their east-west trend; this trend is perpendicular to that of most other Laramide uplifts

and basins. The unusual trend of the Uinta Mountains is thought to be controlled by uplift of Precambrian strata along pre-existing Precambrian basin-bounding faults – especially the North Flank Fault - reactivated by Laramide stresses (Marshak et al., 2000; Paulsen and Marshak, 1999).

Associated with the Uinta arch are east-west-trending reverse faults on the north and south flanks of the range. These structures expose Proterozoic rocks in the middle of the arch, and Paleozoic and younger rocks along the flanks of the range. Extension is recorded in both the eastern and western parts of the Uinta range by a series of east-west to west-northwest trending normal faults and northeast-trending normal faults, with the greatest area of extension expressed in the Browns Park half-graben in the far eastern part of the Uinta Mountains. The area north of Browns Park records the structurally deepest part of the range and it is here that the oldest rocks are exposed. The eastern Uinta range, including Browns Park, has been incised by the Green River since Pliocene(?) time (Hansen, 1964).

2.4 - Methods

Geologic mapping

The mapping area for this project is located where Duchesne, Daggett, and Uintah counties converge in northeastern Utah (Appendix C). This includes the Neoproterozoic strata located just east of the 110° longitude line (the line along which the UMG is informally divided into eastern and western groups) in portions of the Leidy Peak, Marsh Peak, White Rocks Lake, and Paradise Park 7.5-minute

quadrangles. This rectangular area is bounded by the 109° 54' to 109° 47' W longitude and 40° 49' to 40° 41' N latitude lines, and it is approximately equivalent to two thirds of a typical 7.5-minute quadrangle in its areal extent.

Mapping was conducted at a 1:12,000 scale, with a 1:24,000 scale map as the ultimate product (Appendix C). Field mapping, 1:12,000 scale aerial photography mapping, and GoogleEarth imagery were used to make the final product. Contacts, faults, strike and dip, and paleocurrent measurements were mapped in the field (using the iPad application GISRoam) and digitized into ArcMap 10.0 onto a 1:24,000-scale topographic base. Measuring of several stratigraphic sections (six total; Appendix C) through areas containing strata of interest was the first task. The strata were thoroughly described and facies characteristics were analyzed. Paleocurrent analysis was as extensive as sedimentary structure availability allowed in the map area. Samples were acquired within each of the measured sections for compositional, textural, and geochemical characterization, as well as for geochronology and micropaleontology. Mapping emphasized the UMG only and was not focused on the overlying Phanerozoic units, as other workers have been attentive to these younger units (Sprinkel, 2002).

Measured sections

Six new sections containing significant amounts of shale in what was hypothesized to be either the formation of Hades Pass or the Red Pine Shale of the Uinta Mountain Group were measured and described in detail. This mapping locality was selected because it was likely to contain evidence of the hypothesized

microfossil transition due to eutrophication. Previous but very limited sampling of the shale in the Leidy Peak area yielded evidence of a change in microfossil assemblage upsection, from ornamented acritarchs to leiosphaerids (Nagy and Porter, 2005). Data from Hayes (2010) indicated a similar shift in microfossil diversity upsection, but no ornamented acritarchs species were recovered from the single measured section at the Leidy Peak locality included in this 2010 study.

Rock samples were collected from these new measured sections in the Leidy/Marsh Peak map area using both a uniform and stratified sampling method. Samples were collected at ~1.5 meter vertical spacing to generate a geochemical and micropaleontological record comparable with those available from previous studies in the Red Pine shale and Chuar Group (Dehler et al., 2005; Dehler et al., 2007; Hayes, 2010; Nagy and Porter, 2005; Nagy et al., 2009). The six measured section locations selected for sampling are shown in Appendix C.

Correlation of measured sections

In order to accurately subdivide and map the strata in the proposed mapping area – and to possibly integrate data from this mapping area with existing UMG data sets- the six measured sections from the map area were correlated with one another (Appendix C). In most cases, correlating sections within the map area was accomplished by walking out contacts in the field and analyzing aerial photography. In other cases, correlating sections within the map area required both careful lithologic analysis of distinct sandstone marker beds along with identification of minor faults. Whenever possible, suites of distinctive beds (“packages” or facies

associations) were used for correlation rather than single marker beds.

Paleocurrent data and detrital zircon provenance data also aided in correlation of these sandstone units.

Sequence stratigraphic correlation was applied in this field area; there are at least three relatively thick (30-60m) shale units that may record smaller-scale marine transgressions prior to the likely 3rd order transgression recorded by the 1100+m thick Red Pine Shale. Thickness measurements of the shale units across the field area may provide additional information about the geometry of the UMG paleo-basin, allowing the following hypotheses to be tested: 1) the contact between the formation of Hades Pass and the Red Pine Shale is gradational, and 2) the Red Pine Shale continues eastward across the 110° line, and thus should be mapped farther east than it currently is mapped.

Chemostratigraphic (C-isotope ratios and redox geochemistry) and biostratigraphic (microfossil assemblage) data were used to test the mapping-based correlations in the field area. These methods were used in conjunction with litho- and sequence stratigraphic methods to correlate shale units in the field area with other UMG shale units; specifically, the two shale units mapped in the formation of Hades Pass by Wallace (1972) and previously sampled (Box Canyon location) for microfossil assemblage and C-isotope and redox geochemistry (Hayes, 2010) were compared with those in this mapping area, as was the Red Pine Shale Formation in the western Uinta Mountains.

Facies and paleocurrent analyses

Detailed descriptions of all outcrops encountered during field work in the mapping area were used to group the strata into facies associations based on grain size, sedimentary structures, and unit architecture. Measured stratigraphic sections, facies descriptions, and field photographs were used to document facies associations, interpret the depositional environment, and present stratigraphic subdivisions shown on the map (Appendix C).

Brunton compass measurements of the orientation of cross-strata foresets in the field were used to constrain paleoflow. All paleoflow data points were corrected for bed orientation using Stereoplot and then analyzed and displayed using Oriana by Kovach Computing. To better constrain paleoenvironmental interpretations, these data are presented as Rose diagrams (showing dip directions) corresponding with facies descriptions.

Sedimentary petrography

To document variations in provenance and enhance paleoenvironmental interpretations, a suite of thin sections from the different facies associations identified were analyzed using petrographic descriptions and the Gazzi-Dickinson (Ingersoll et al., 1984) point-count method with at least 300 randomly selected points per count. All thin sections were stained for plagioclase and potassium feldspar. All detrital zircon samples were point-counted.

Detrital zircon analysis

To better constrain the maximum depositional age and provenance of units in the mapping area, detrital zircon extraction and U/Pb dating of zircons was conducted. Since funding for these analyses was limited, the transition from the formation of Hades Pass to the Red Pine Shale Formation was a focus and fine-grained greenish-yellow quartz to subfeldspathic arenite facies were targeted based on previous results in the UMG (Dehler et al., 2010). Zircon crystals were extracted from samples at Utah State University and Boise State University by traditional methods of crushing and grinding, followed by separation with a Rogers water table, heavy liquids (methylene iodide), and a Frantz magnetic separator. Generally, 500-1000 zircon grains (or as many as could be obtained, if less) were incorporated into a 1-inch-radius epoxy mount together with fragments of the Sri Lankan zircon standard. Prior to isotopic analysis, the mounts were sanded to ~20 micron depth, polished, imaged, and then cleaned.

U-Pb analyses were conducted by laser ablation- multicollector- inductively coupled plasma mass spectrometry (LA-MC-ICPMS) at the Arizona LaserChron Center (Gehrels et al., 2008). Laser ablation of zircon grains was accomplished with a New Wave UP193HE Excimer laser (operating at a wavelength of 193 nm) using a spot diameter of 30 microns. Ablated material was carried (in He gas) into the plasma source of a Nu HR ICPMS, where U, Th, and Pb isotopes were measured simultaneously. Measurements were made in static mode, using Faraday detectors with 3×10^{11} ohm resistors for ^{238}U , ^{232}Th , ^{208}Pb - ^{206}Pb , and discrete dynode ion

counters for ^{204}Pb and ^{202}Hg . Each analysis consisted of one 15-second integration on peak with the laser off (for determination of background levels), 15 one-second integrations with the laser firing, and a 30 second delay to purge the previous sample and prepare for the next analysis. ^{204}Hg interference with ^{204}Pb was accounted for by measurement of ^{202}Hg during laser ablation and subtraction of ^{204}Hg according to the natural $^{202}\text{Hg}/^{204}\text{Hg}$ of 4.35, and a Hg correction was applied if needed.

Common Pb correction was accomplished using the Hg-corrected ^{204}Pb and assuming initial Pb compositions from Stacey and Kramers (1975). Uncertainties of ± 1.5 for initial $^{206}\text{Pb}/^{204}\text{Pb}$ and ± 0.3 for $^{207}\text{Pb}/^{204}\text{Pb}$ were applied to assumed compositions based on variation in Pb isotopic compositions in modern crustal rocks. Analysis of fragments of a Sri Lanka zircon standard with a known age of 563.5 ± 3.2 Ma (2-sigma error) occurred every fifth measurement and were used to correct for Pb/U and Pb isotope fractionation. Analyses >20% discordant (by comparison of $^{206}\text{Pb}/^{238}\text{U}$ and $^{206}\text{Pb}/^{207}\text{Pb}$ ages) or >5% reverse discordant were not included in the results. Data are shown on concordia diagrams and age-probability diagrams using Isoplot (Ludwig, 2008). Age-probability diagrams combine age and uncertainty as a normal distribution for each grain, and then sum distributions from all grains into a single sample distribution. Composite age probability plots were made using an Excel program (available from www.geo.arizona.edu/alc).

2.5 - Results and discussion

In the area mapped (Appendix C), the Uinta Mountain Group was divided into 5 map units. These include, in stratigraphic order, 1) the formation of Hades Pass (Zhp), 2) the Leidy Peak shale unit (Zrp1), 3) the Lower Marsh Ridge shale unit (Zrp2), 4) the cyclic unit (Zrp3), and 5) the Upper Marsh Ridge shale unit (Zrp4). Detailed descriptions for each of these map units are included in Appendix C.

The formation of Hades Pass, interpreted as representing fluvial-deltaic deposits (Figure 7A) with a thin (<5 m) uppermost layer of supratidal deposits in the Leidy/Marsh Peak area, is dominated by NW-directed paleocurrents (Figure 9). This paleoflow direction contrasts with those previously reported from this unit in other parts of the Uinta Mountains, which are dominantly S and SE-directed (Dehler et al., 2010). Detrital zircon data (Figure 9) for this unit show a variety of sources, including Archean (2.5 – 2.8 Ga) grains from the southern Wyoming Province, Paleoproterozoic (1.65 – 1.85 Ga) grains from the Mojave, Yavapai, and Mazatzal provinces, Early Mesoproterozoic (1.5 – 1.6 Ga) grains likely from reworked lower Belt Supergroup equivalents, Early-Middle Mesoproterozoic (1.4 – 1.45 Ga) grains with an A-type igneous Laurentian and/or Belt Supergroup source, and Middle-Late Mesoproterozoic (9.3 – 1.2 Ga) grains likely sourced from the Grenville orogen and foreland (Dehler et al., 2010). The detrital zircon signature changes significantly in the Leidy/Marsh Peak area across the transition from the “classic Hades” (fluvial-deltaic) facies to its overlying supratidal facies (Figure 7A); it becomes less mixed,

with increasing Grenville orogen contribution and some younger (Neoproterozoic) grains (Figure 9).

The Leidy Peak shale unit (Zrp1) overlying the formation of Hades Pass, consists of clayshale that coarsens upward to silty shale and siltstone; these finer-grained intervals are overlain by a distinct medium-to-coarse-grained arkosic to quartz arenite layer less than 1 m thick (Figure 8), a red flaggy-weathering fine-to-medium-grained quartz arenite, and a purple-red fine-grained quartz arenite (Figure 7B; Figure 8). Paleocurrent measurements in the upper sandstones of Zrp1 show two distinct patterns: the lower sandstone with apparent herringbone cross-bedding has both SE and NW-directed values, likely reflecting tidal influence, and the upper sandstone shows SE-directed currents (Figure 9). The depositional environment of the Leidy Peak shale unit is thus interpreted as transitioning from distal prodelta to delta plain/channel; this shallowing-upward unit may record a small-scale transgressive-regressive cycle or the progradation of a delta.

The Lower Marsh Ridge shale unit (Zrp2) that overlies Zrp1 also consists of an overall coarsening-upward package of sediments including clayshale, silty shale, siltstone, both arkosic and quartz arenite channels, and an upper fine-to-medium-grained quartz to feldspathic arenite (Figures 7, 8). The depositional environment of the Lower Marsh Ridge shale unit is interpreted as varying from distal prodelta to tidal flat with several delta channel deposits; like unit Zrp1, Zrp2 may record a small-scale transgressive-regressive cycle and/or delta progradation.

The cyclic unit (Zrp3) that overlies the Lower Marsh Ridge shale unit is quite distinct in the map area. It consists mainly of meter-scale cycles of alternating coarse arkosic arenite and siltstone (Figures 7, 8), with a capping layer of fine-grained quartz arenite. Paleocurrent measurements for the upper part of this unit are bimodal, trending generally WNW and SE and reflecting tidal influence (Figure 9). The depositional environment of the cyclic unit is mainly tidal flat, with a transition to supratidal at the top. Detrital zircon signatures from the uppermost part of the unit match those from the same facies below, indicating that the source areas may have remained the same since the deposition of Zrp1 (Figure 9).

The Upper Marsh Ridge shale unit (Zrp4), overlying the cyclic unit, consists of silty shale and siltstone (Figure 7); these finer-grained intervals are overlain by a yellow-green fine-grained subarkosic to quartz arenite, and a purple-red fine-grained quartz arenite. Paleocurrent measurements in the upper sandstone of Zrp4 show two distinct patterns: both SE and N-directed values are present, with the SE-directed current dominating (Figure 9). The depositional environment of the Upper Marsh Ridge shale unit is interpreted as transitioning from prodelta gradually to supratidal (shallowing-upward) and then to nearshore with a tidal influence. Like unit Zrp1, this likely represents a small-scale transgressive-regressive cycle or the progradation of a delta. Even though the facies are similar, the detrital zircon signature from the supratidal facies of unit Zrp4 is distinctly different from those below; it appears to record a major shift in provenance to Archean-dominated sources that is likely related to increased input from the Wyoming Province to the

north (Figure 9). The increased feldspar content of this sample relative to those from similar facies below (Figure 8; Appendix B) lends support to the idea that uplift of the Wyoming Province to the north (a consequence of Rodinian rifting) during the time of deposition may have caused this provenance shift.

2.6 - Conclusions

Facies variations through time in the map units in this area suggest a transition from a fluvial-deltaic environment (Zhp) to a tidally-influenced deltaic one containing a few potentially subtidal shale units (Zrp1-4). Each of the map units Zrp1-4 records an overall shallowing-upward sequence, with Zrp1, 2, and 4 containing significantly thicker intervals of shale (~30-50 m) and Zrp3 lacking >dm-scale shale intervals. Overall, Zrp1 through most of Zrp4 appear to record an interval of relatively deeper-water deposition between two fairly thick, likely fluvial to fluvial-deltaic, sandstone intervals (Zhp and upper part of Zrp4). Zrp1, 2, and 4 may represent either small-scale fluctuations in relative sea level (each would record a flooding and subsequent regression) or cycles of delta progradation. The strata unfortunately do not allow these two possibilities to be easily distinguished, but the scale of the shale intervals in these units – and their lateral continuity throughout the field area – seems to favor the contribution of relative sea level fluctuations over delta lobe progradation. This is supported by both the available detrital zircon data for this specific and other areas of the UMG (Dehler et al., 2010), sequence stratigraphic interpretation of other UMG units (Kingsbury, 2008;

	<p>Depositional environment:</p> <p>fluvial to fluvial-deltaic</p>
	<p>Depositional environment:</p> <p>upper tidal to supratidal</p>
	<p>Depositional environment:</p> <p>prodelta to distal prodelta</p> <p>Description:</p> <p>mostly grey to greenish-grey clayshale and silty shale (occasionally brown to reddish-brown in color); fine light/dark laminations in some areas; contains dm-thick fine sandstone interbeds occasionally</p>

Figure 7A. Facies photographs, descriptions, and interpretations.


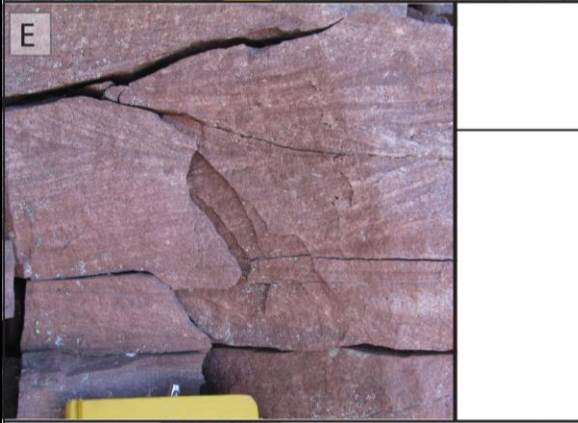

	<p>Depositional environment: subtidal, delta front</p>
	<p>Depositional environment: lower to middle tidal</p>
	<p>Depositional environment: tidal flat (middle-upper tidal)</p> <p>Description: meter-scale cycles of alternating reddish coarse arkosic arenite and greenish-grey siltstone to silty shale</p>

Figure 7B. Facies photographs, descriptions, and interpretations.

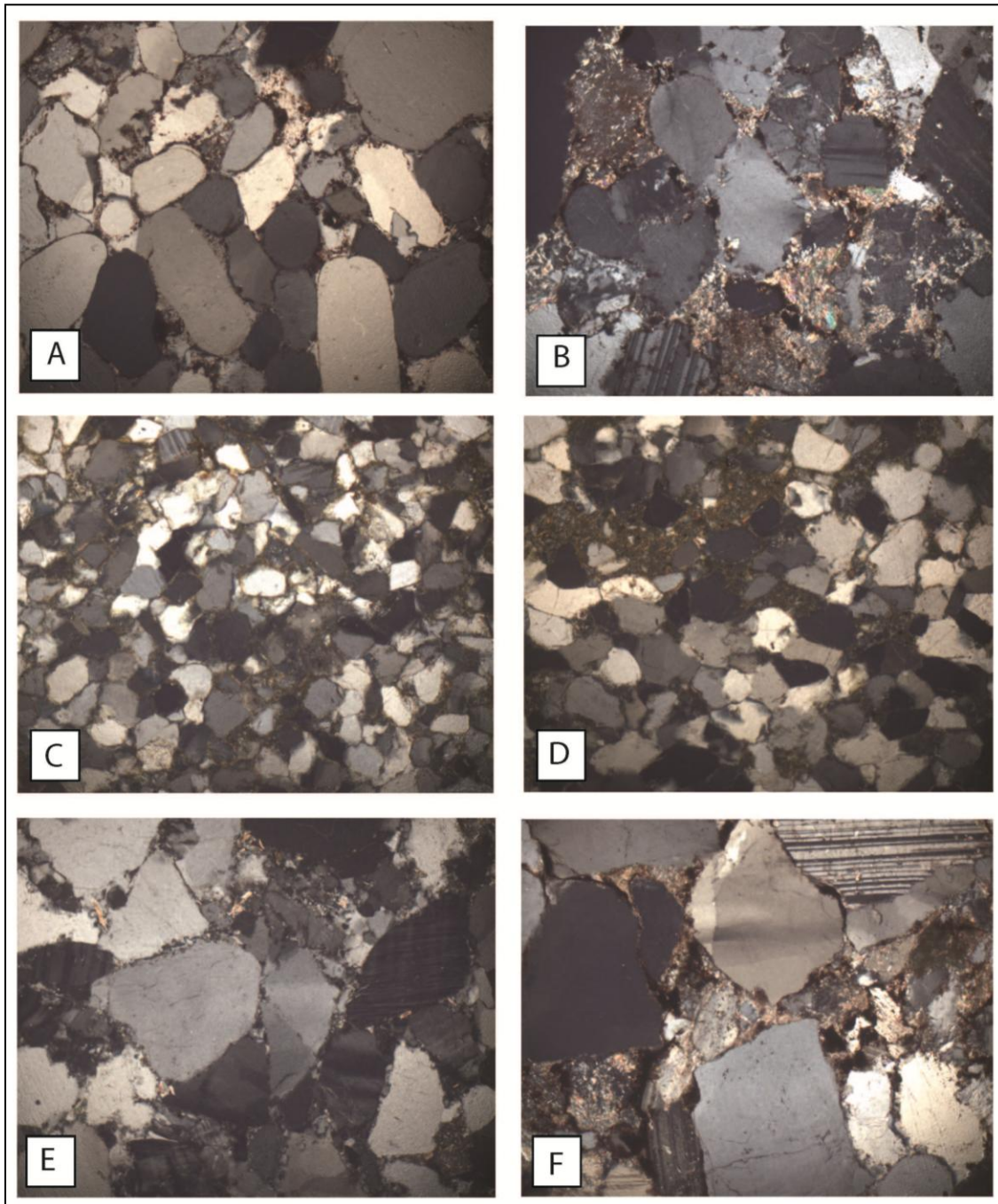


Figure 8. Thin section photographs. Magnification = 100x, xpl. A. 27DH11. Quartz arenite with Fe cement. B. 29DH11. Feldspathic arenite. C. 111DH12. Quartz arenite, supratidal facies, detrital zircon sample. D. 112DH12. Quartz arenite, supratidal facies, detrital zircon sample. E. Subfeldspathic arenite (facies unique to Leidy Peak shale unit). F. 40DH11. Coarse feldspathic arenite (facies unique to map unit Zrp3).

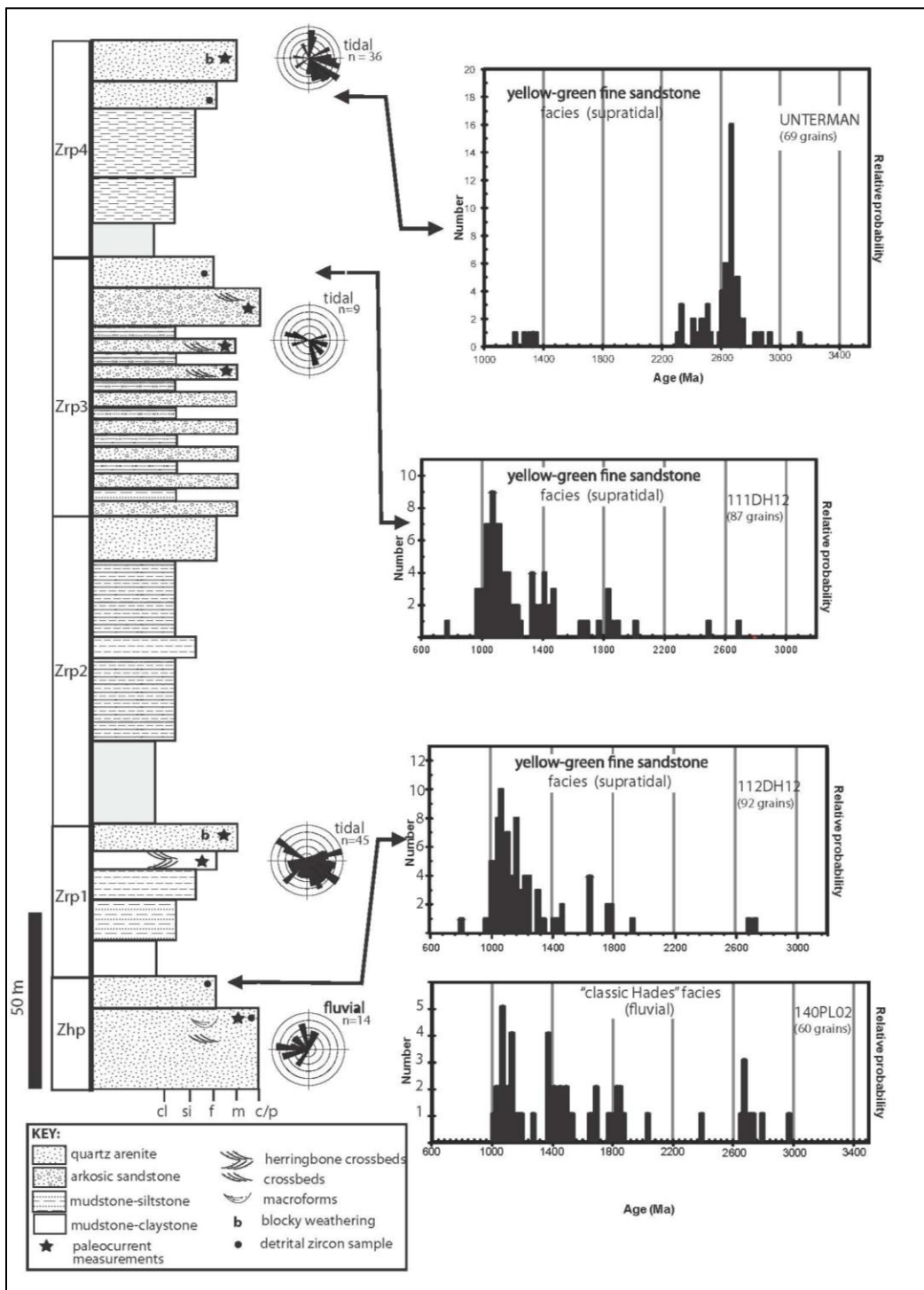


Figure 9. Detrital zircon relative probability plots and paleocurrent data. Zhp = formation of Hades Pass, Zrp1 = Leidy shale unit, Red Pine Shale Formation, Zrp2 = Lower Marsh Ridge shale unit, Red Pine Shale Formation, Zrp3 = cyclic unit, Red Pine Shale Formation, Zrp4 = Upper Marsh Ridge shale unit.

Kingsbury-Stewart et al., in press), and the cyclicity of low-amplitude sea-level changes recorded in other coeval units (Dehler et al., 2005).

Paleocurrent measurements from the facies in the Leidy/Marsh Peak area suggest a transition from fluvial input from the east (Zhp) to a mainly tidal signature (Zrp 1 – 4), a change that is also supported by facies changes in this stratigraphic interval. Interestingly, the upper formation of Hades Pass (Zhp) paleoflow measurements in this location are not consistent with those from this same unit in the western Uinta Mountains (Table 1).

Table 1. Comparison of western, central and eastern UMG paleoenvironments. Generalized summary of paleocurrent, detrital zircon provenance, and depositional environment interpretation data for the UMG by general region. W and E UMG data summarized from Dehler et al., 2010.

	Western UMG	Central UMG (this study, Leidy & Marsh Peak, upper UMG)	Eastern UMG
Paleocurrents	W-flowing longshore, W/SW prograding deltaic, N tidal	WNW fluvial, NW/N and SE tidal	NW and SSE tidal, W/SW fluvial
Depositional environments	Fluctuating fluvial, deltaic, nearshore marine	Fluvial to deltaic, some nearshore marine	Mainly fluvial, some deltaic & marine in lower units
Detrital zircon provenance	Generally more mixed during transgression, less mixed during regression	Very mixed in fluvial, less mixed in supratidal middle, Archean-dominated supratidal	Mixed & Neoproterozoic (in lower marine facies; no data for upper fluvial facies)

This may be due to the fact that the Leidy/Marsh Peak location is much farther east and may have thus been influenced more by fluvial input from the east. It could also suggest a “kink” in the UMG paleo-shoreline, which would imply that the UMG depositional basin may not have been as completely open to the south as proposed in previous paleogeographic models (Dehler et al., 2010). The main current directions in the tidally-influenced upper units (N/NW to SE) suggest the shoreline in the Leidy/Marsh region was oriented roughly S/SW to NE; most of the paleocurrent measurements in the tidally-influenced part of unit Zrp1 support this interpretation as well. This differs from both the inferred E-W orientation of the shoreline in the W UMG and N-S orientation in the upper part of the E UMG and does not provide a convenient “intermediate” angle between them, but instead a jog in the other direction.

The detrital zircon provenance changes through time in the Leidy/Marsh Peak area suggest that the input of Wyoming Province material from the north decreased with the transition from fluvial (Zhp) deposits to tidally-influenced ones (Zrp1-4) – at least for the two older supratidal intervals sampled. The youngest supratidal sample (upper Zrp4) shows a sudden shift back to northern-derived Wyoming Province input that is very comparable to that reported by Dehler et al. (2010) across the transition from the formation of Hades pass into the overlying Red Pine Shale in the western Uinta Mountain Group. When compared to the detrital zircon provenance data from the western Uinta Mountain Group and correlative Big Cottonwood Formation (Dehler et al., 2010), the Leidy/Marsh DZ

data set from the stratigraphically lower supratidal facies most closely matches the sample signatures of the formation of Moosehorn Lake (UMG) and middle Big Cottonwood Formation; these samples show a dominant population of 1.1 Ga grains with much smaller populations of 1.5-1.9 Ga and Archean grains. The Leidy/Marsh DZ data set from the uppermost supratidal facies is markedly different and composed of mostly Archean grains, much like that reported by Dehler et al. (2010) for the Red Pine Shale Formation and formation of Deadhorse Pass in the western Uinta Mountains. The detrital zircon provenance signatures from the supratidal facies in the Leidy/Marsh area do not very closely match the two reported from the lower eastern Uinta Mountain Group's Jesse Ewing Canyon and Outlaw Trail formations, both of which show a more mixed provenance with slightly dominant Archean peaks (Dehler et al., 2010).

Dehler et al. (2010) suggest that the appearance of more mixed DZ signatures (rather than Archean-dominated) in the western UMG units occurs during transgression and represents the "tapping" of a more southerly/southeasterly sediment source; if the same is true for the Leidy/Marsh area, then the DZ data set from the two stratigraphically lower supratidal samples would reflect input from this source and a potentially elevated sea level. Since the units in the Leidy/Marsh area are likely correlative with those in the upper UMG, a match in DZ provenance with the upper UMG (Red Pine Shale Formation) is expected, and the data from the uppermost DZ sample in the Leidy/Marsh area support this hypothesis and the correlation of these units. The hypothesis regarding corresponding DZ provenance

and relative sea level changes in the UMG (Dehler et al., 2010) is further supported by the stratigraphy in the Leidy/Marsh area suggesting that the deeper-water part (Zrp1 – lower part of Zrp4) of the overall shallowing-upward succession is associated with the more mixed DZ signature versus the Archean-dominated DZ signature (top of Zrp4).

Both the paleocurrent and detrital zircon data, when combined with existing organic C-isotope and microfossil data (Hayes, 2010; Hayes and Dehler, in prep – see Ch. 3 of this dissertation; Myer, 2008), suggest that the units mapped in the Leidy/Marsh Peak area (Zrp1 – 4) are probably lateral equivalents of the lower Red Pine Shale rather than the Box Canyon shale intervals in the lower formation of Hades Pass. This would imply that the lower Red Pine Shale in the western Uinta Mountains was deposited in a slightly deeper-water part of the paleo-UMG basin than the Red Pine Shale units mapped in the Leidy/Marsh area, which is consistent with paleogeographic models previously proposed by Dehler et al. (2010).

2.7 – References

- Ball, T.T., and Farmer, G.L., 1998, Infilling history of a Neoproterozoic intracratonic basin: Nd isotope provenance studies of the Uinta Mountain Group, western United States: *Precambrian Research*, v. 87, p. 1-18.
- Brehm, A., 2007, Re-evaluation of the Jesse Ewing Canyon Formation: implications for neoproterozoic paleogeography and tectonic setting of northeastern Utah: Logan, Utah State University.
- Bryant, B., 1992, Geologic and structure maps of the Salt Lake City 1 x 2 quadrangle, Utah and Wyoming: U.S. Geological Survey Miscellaneous Investigations Series Map I-1997, scale 1:250,000.

- Condie, K.C., Lee, D., and Farmer, G.L., 2001, Tectonic setting and provenance of the Neoproterozoic Uinta Mountain and Big Cottonwood groups, northern Utah: constraints from geochemistry, Nd isotopes, and detrital modes: *Sedimentary Geology*, v. 141, p. 443-464.
- De Grey, L.D., and Dehler, C.M., 2005, Stratigraphy and facies analysis of the eastern Uinta Mountain Group, Utah-Colorado border region., *in* Dehler, C., Pederson, J., Sprinkel, D., Kowallis, B., eds., *Uinta Mountain Geology*, Volume 33, Utah Geological Association, p. 31-47.
- Dehler, C.M., Fanning, C.M., Link, P.K., Kingsbury, E.M., and Rybczynski, D., 2010, Maximum depositional age and provenance of the Uinta Mountain Group and Big Cottonwood Formation, northern Utah: Paleogeography of rifting western Laurentia: *Geological Society of America Bulletin*, v. 122, p. 1686-1699.
- Dehler, C.M., Crossey, L.J., Atudorei, V., Bloch, J.D., Karlstrom, K.E., and Anonymous, 2002, Characterization of the Red Pine Shale, Uinta Mountain Group: Mid-Neoproterozoic paleogeography of NE Utah Abstracts with Programs - Geological Society of America.
- Dehler, C.M., Elrick, M., Bloch, J.D., Crossey, L.J., Karlstrom, K.E., and Des Marais, D.J., 2005, High-resolution delta C-13 stratigraphy of the Chuar Group (ca. 770-742 Ma), Grand Canyon: Implications for mid-Neoproterozoic climate change: *Geological Society of America Bulletin*, v. 117, p. 32-45.
- Dehler, C.M., Porter, S.M., De Grey, L.D., Sprinkel, D.A., and Brehm, A., 2007, The Neoproterozoic Uinta Mountain Group revisited; a synthesis of recent work on the Red Pine Shale and related undivided clastic strata, northeastern Utah, *U. S. A: Proterozoic geology of western North America and Siberia*, v. 86, p. 151-166.
- Gehrels, G.E., Valencia, V., Ruiz, J., 2008, Enhanced precision, accuracy, efficiency and spatial resolution of U-Pb ages by laser ablation-multicollector-inductively coupled plasma-mass spectrometry: *Geochemistry Geophysics Geosystems*, v. 9.
- Hansen, W.R., 1964, *Geology of the Flaming Gorge area, Utah-Colorado-Wyoming*: U.S. Geological Survey Professional Paper 490, p. 196.
- Hayes, D.H., 2010, Stratigraphic, microfossil, and geochemical analysis of the Neoproterozoic Uinta Mountain Group: Evidence for a eutrophication event?: Logan, Utah State University

- Ingersoll, R.V., Fullard, T.F., Ford, R.L., Grimm, J.P., Pickle, J.D., and Sares, S.W., 1984, The effect of grain size on detrital modes; a test of the Gazzi-Dickinson point-counting method: *Journal of Sedimentary Research*, v. 54, p. 103-116.
- Karlstrom, K., and Houston, R., 1984, The Cheyenne belt: Analysis of a Proterozoic suture in southern Wyoming: *Precambrian Research*, v. 25, p. 415-446.
- Karlstrom, K.E., Bowring, S.A., Dehler, C.M., Knoll, A.H., Porter, S.M., Des Marais, D.J., Weil, A.B., Sharp, Z.D., Geissman, J.W., Elrick, M.B., Timmons, J.M., Crossey, L.J., and Davidek, K.L., 2000, Chuar Group of the Grand Canyon: Record of breakup of Rodinia, associated change in the global carbon cycle, and ecosystem expansion by 740 Ma: *Geology*, v. 28, p. 619-622.
- Kingsbury, E.M., 2008, Geologic mapping and sequence stratigraphic analysis of the neoproterozoic Uinta Mountain Group, Kings Peak 7.5' quadrangle, Duchesne and Summit Counties, Utah: Pocatello, Idaho State University.
- Kingsbury-Stewart, E.M., Osterhout, S.L., Link, P.K., and Dehler, C.M., in press, Sequence stratigraphy and formalization of the Middle Uinta Mountain Group (Neoproterozoic), central Uinta Mountains, UT: A closer look at the western Laurentian Seaway at ca. 750 Ma: *Precambrian Research*.
- Ludwig, K.R., 2008, User's manual for Isoplot 3.7. A geochronological toolkit for Microsoft Excel., Berkeley Geochronology Center Special Publication 4: Berkeley, California, University Press, 39 p.
- Marshak, S., Karlstrom, K., and Timmons, J.M., 2000, Inversion of Proterozoic extensional faults: An explanation for the pattern of Laramide and Ancestral Rockies intracratonic deformation, United States: *Geology*, v. 28, p. 735-738.
- Mueller, P.A., Foster, D.A., Mogk, D.W., Wooden, J.L., Kamenov, G.D., and Vogl, J.J., 2007, Detrital mineral chronology of the Uinta Mountain Group: Implications for the Grenville flood in southwestern Laurentia: *Geology*, v. 35, p. 431-434.
- Myer, C.A., 2008, Sedimentology, stratigraphy, and organic geochemistry of the Red Pine Shale, Uinta Mountains, Utah: A prograding deltaic system in a mid-Neoproterozoic interior seaway: Logan, Utah State University.
- Nagy, R.M., and Porter, S.M., 2005, Paleontology of the Neoproterozoic Uinta Mountain Group: *Uinta Mountain Geology: Utah Geological Association Publication*, v. 33, p. 49-62.

- Nagy, R.M., Porter, S.M., Dehler, C.M., and Shen, Y., 2009, Biotic turnover driven by eutrophication before the Sturtian low-latitude glaciation: *Nature Geoscience*, v. 2, p. 414-417.
- Osterhout, S.L., 2011, Geologic mapping, lithostratigraphic and sequence stratigraphic analysis of the Neoproterozoic Uinta Mountain Group, Mount Powell 7.5' Quadrangle, Duchesne and Summit Counties, Utah: Pocatello, Idaho State University.
- Paulsen, T., and Marshak, S., 1999, Origin of the Uinta recess, Sevier fold-thrust belt, Utah: influence of basin architecture on fold-thrust belt geometry: *Tectonophysics*, v. 312, p. 203-216.
- Prave, A.R., 1999, Two diamictites, two cap carbonates, two delta C-13 excursions, two rifts: The Neoproterozoic Kingston Peak Formation, Death Valley, California: *Geology*, v. 27, p. 339-342.
- Rybczynski, D., 2009, Correlation, paleogeography, and provenance of the neoproterozoic eastern Uinta Mountain Group, Goslin Mountain Area, northeastern Utah: Logan, Utah.
- Sanderson, I.D., 1984, The Mount Watson Formation, an interpreted braided-fluvial deposit in the Uinta Mountain Group (Upper Precambrian), Utah: *The Mountain Geologist*, v. 21, p. 157-164.
- Sprinkel, D.A., 2002, Progress report geologic map of the Dutch John 30' x 60' quadrangle, Utah-Colorado-Wyoming (year 3 of 3): Utah Geological Survey Open-File Report 399, scale 1:62,500.
- , 2006, Interim geologic map of the Dutch John 30' x 60' quadrangle, Daggett and Uintah Counties, Utah, Moffat County, Colorado, and Sweetwater County, Wyoming, Utah Geological Survey, p. Open File Report 491 DM.
- Stacey, J.S., and Kramers, J.D., 1975, Approximation of terrestrial lead isotope evolution by a two stage model: *Earth and Planetary Science Letters*, v. 26, p. 207-221.
- Stone, P., and Stevens, C.H., 1993, Large-magnitude Permian shortening and continental-margin tectonics in the southern cordillera – Discussion: *Geological Society of America Bulletin*, v. 105, p. 279-283.

- Strauss, H., and Moore, T., 1992, Abundances and isotopic compositions of carbon and sulfur species in whole rock and kerogen samples., *in* Schopf, J.W., and Klein, C., eds., *Proterozoic Biosphere: a Multidisciplinary Study*: Cambridge, Cambridge University Press, p. 229-242.
- Wallace, C.A., and Crittenden, M.D., 1969, The stratigraphy, depositional environment and correlation of the Precambrian Uinta Mountain Group, western Uinta Mountains, Utah, *in* Lindsey, J.B., ed., *Geologic Guidebook of the Uinta Mountains*, Intermountain Association of Geologists 16th Annual Field Conference, p. 127-142.
- Wallace, C.A., 1972, A basin analysis of the upper Precambrian Uinta Mountain Group, Utah: Ph.D. Dissertation, University of California Santa Barbara.

CHAPTER 3

EVIDENCE FOR FERRUGINOUS NEOPROTEROZOIC OCEANS AND POTENTIALLY GLOBAL BIOTIC TURNOVER: INSIGHTS FROM A NEW GEOCHEMICAL AND MICROFOSSIL RECORD, LOWER RED PINE SHALE FORMATION, UINTA MOUNTAIN GROUP, UTAH²

3.1 - Abstract

Iron speciation and organic carbon geochemistry from a new shale record in a previously unstudied part of the upper Uinta Mountain Group (UMG) reveals three intervals dominated by anoxic and ferruginous (rich in ferrous iron) bottom waters. These intervals occur in shallow nearshore marine (tens of meters) depositional environments, supporting the hypothesis that ferruginous conditions had returned to Neoproterozoic oceans by <800 Ma and suggesting that global atmospheric oxygen levels at that time were much lower than today. These short-lived periods of anoxia in the newly described upper UMG shale units are not accompanied by sulfidic conditions and seem to have no effect on the local biota on a short-term (e.g. formation-level) time scale. This is evidenced by the persistence of a static organic-walled microfossil assemblage dominated heavily by simple leiosphaerid forms throughout all units in this particular stratigraphic interval. However, when this new shale record is put into a broader stratigraphic context, microfossil data from the UMG as a whole strongly suggest that a biotic change (from high-diversity,

² Coauthored by Hayes, D.S., and Dehler, C.M.

ornamented eukaryotic assemblages to monospecific prokaryotic ones) occurs gradually over the deposition of the entire group. Additional iron speciation data corresponding stratigraphically with the existing microfossil data are needed to determine whether or not this biotic transition, like that in the coeval Chuar Group of the Grand Canyon, could be driven by a global shallow-ocean eutrophication event.

3.2 - Introduction

Several previous Neoproterozoic microfossil diversity studies yield evidence for a relatively sudden biotic change prior to the first Neoproterozoic Cryogenian glaciation at 716.5 Ma (Knoll et al., 1981; Knoll, 1994; Macdonald et al., 2010; Vidal, 1982; Vidal and Moczydlowska, 1992). In an event interpreted by Nagy et al. (2009) as a mass extinction of eukaryotic phytoplankton followed by bacterial dominance, diverse assemblages of complex acritarchs are replaced by more uniform assemblages consisting of simple leiosphaerid acritarchs, bacteria, and vase-shaped microfossils.

Data from the Chuar Group of the Grand Canyon (770-742 Ma) suggest this biotic change was caused by eutrophication and may not be directly related to any glaciations. Evidence for this interpretation includes total organic carbon values indicative of increasing primary productivity as well as iron speciation values that suggest sustained anoxia of the water column tens of millions of years prior to “Sturtian” glaciation (Nagy et al., 2009). Data from the Uinta Mountain Group suggests that a similar eutrophication event may be recorded in shale units of the

formation of Hades Pass and the Red Pine Shale of Utah's Neoproterozoic Uinta Mountain Group.

If shale units in the upper UMG contain biotic evidence of eutrophication, the microfossil assemblage in the strata should shift upsection from a higher-diversity assemblage to one with less-diverse, simpler organisms (Nagy et al., 2009).

Increasing total organic carbon content, potentially indicative of increasing primary productivity, would also be an expected upsection trend after a positive $\delta^{13}\text{C}_{\text{org}}$ excursion. Since eutrophication ultimately results in oxygen depletion due to increased organic decay rates, evidence of anoxia should be present in sediments deposited during or just after eutrophication. Where the UMG contains geochemical evidence of eutrophication, iron speciation signatures should indicate sustained sediment pore-water and water column anoxia (Johnston et al., 2010). If eutrophication was regional and possibly even global, the microfossil change(s) should correlate with the chemical change(s) and not be facies-dependent.

Preliminary results from Hayes (2010) suggesting eutrophication may be recorded in the upper UMG shale units of the western UMG include a significant shift in microfossil assemblage from a higher-diversity ($H' = 0.60$) fauna that includes some ornamented acritarchs to a lower-diversity ($H' = 0.11$) fauna dominated by smooth leiosphaerids and microfossils of a prokaryotic origin (*Sphaerocongregus* sp.). This change co-occurs with an increase in total organic carbon values that directly follows a positive carbon-isotopic excursion, suggesting increased primary productivity that may have been the result of elevated sediment influx and nutrient

availability. Both the biotic change and period of increased total organic carbon values correspond stratigraphically with the onset of an interval of anoxia (indicated by total iron to aluminum ratios above 0.50) and spikes in sulfur concentration that could indicate a temporary period of euxinia.

The research discussed in this paper documents and explores further the stratigraphic, microfossil, and geochemical characteristics of the upper UMG shale units, adding additional key sampling and mapping localities to 1) determine whether or not the biotic change is consistently recorded in this unit, 2) determine if biotic changes in the UMG shale record correlate with geochemical indicators of paleoenvironmental eutrophication, and 3) constrain the timing, duration, and severity of the proposed eutrophication event in the UMG. This study's broader significance is that information about UMG microfossils and paleoenvironment may contribute to our understanding of eukaryotic biodiversification and Cryogenian pre-glacial oceanic and atmospheric conditions on Earth.

3.3 - Background

Geologic setting

The Neoproterozoic Uinta Mountain Group (UMG) is exposed only in the east-west-trending Uinta Mountains in north-central Utah, southwest Wyoming, and northeastern Colorado (Figure 10). The UMG is a relatively thick siliciclastic succession of cross-bedded quartzite and sandstone, siltstone, and shale. In most of the Uinta Mountains, its base is not exposed and it is unconformably overlain by Paleozoic strata (Figure 11). The western part of the UMG (up to ~ the 110°

longitude line) is divided into 4 informal formations and two formal ones (Figures 10 and 11). The oldest, the formation of Red Castle, is interpreted as representing both fluvial and nearshore marine deposition; much of the formation of Hades Pass in the upper UMG also records fluvial-deltaic deposition from the north (Sanderson, 1984; Kingsbury-Stewart et al., in press; Wallace, 1972), with some evidence for west-directed paleoflow as well. The rest of the western UMG records mainly shallow marine siliciclastic deposition with west-directed paleocurrents, southern and western-prograding deltas, and a generally north-directed tidal current component (Dehler et al., 2010; Kingsbury-Stewart et al., in press). Farther east, where the UMG is informally divided into six units that differ from those in the western UMG, the section is much thicker (~7 km vs. the ~4km in the west); it also consists of cross-bedded quartzite and sandstone with less siltstone and shale, but contains relatively more conglomerate than in the west (Figure 11). Where the base of the eastern UMG is exposed, it overlies the Paleoproterozoic Red Creek Quartzite (Hansen, 1965). The oldest unit in the eastern UMG, the Jessie Ewing Canyon Formation, represents a suite of southward-prograding alluvial fans and deltas combined with westward and northward-flowing braided fluvial, deltaic, and marginal marine depositional systems (Brehm, 2007; Dehler et al., 2007). The overlying eastern UMG was deposited mainly by a W/SW-flowing braided fluvial system affected by at least two marine transgressions that resulted in the deposition of significantly thick shale units, including parts of the formation of Outlaw Trail and the Red Pine Shale (Figure 11; Dehler et al., 2007; Rybczynski, 2009).

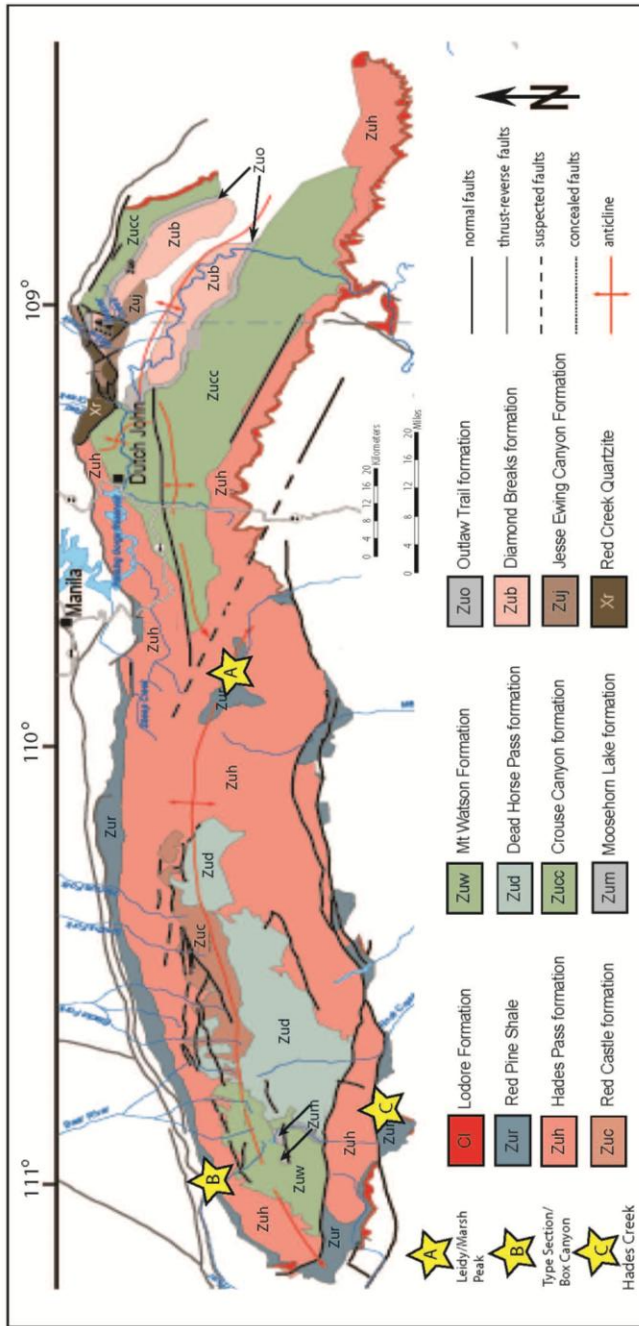


Figure 10. Generalized geologic map of the Uinta Mountain Group, showing exposure of units in the Uinta Mountains. Samples discussed in this paper are from the three localities (A, B, & C) shown with stars. Map modified from Sprinkel, 2006.

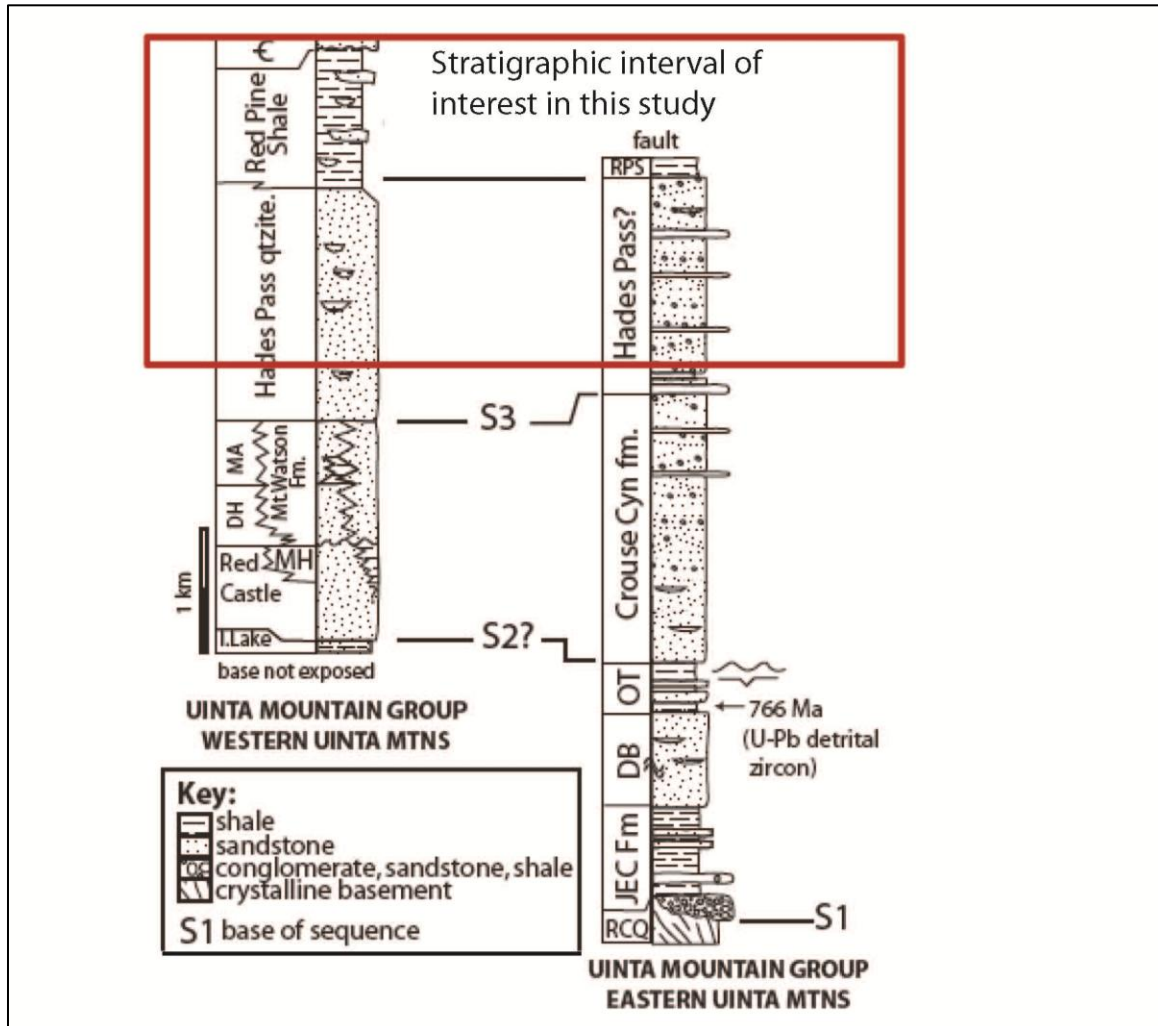


Figure 11. Stratigraphic columns of Eastern & Western UMG showing hypothesized correlation. S1, S2, and S3 indicate lower-order fining upward sequences, which show fluvial or more proximal marine units at the base, becoming proximal to distal marine at the top. C = Cambrian; DH = formation of Deadhorse Pass; MA = formation of Mount Agassiz; MH = formation of Moosehorn Lake; RCQ = Paleoproterozoic (?) Red Creek Quartzite; JEC = Jesse Ewing Canyon Formation; DB = formation of Diamond Breaks; OT = formation of Outlaw Trail; RPS = Red Pine Shale. 742 Ma upper age constraint is based on correlation with the Chuar Group of the Grand Canyon using paleontologic, C-isotope, and paleoenvironmental data. Red box highlights stratigraphic interval sampled for this study. Figure modified from Dehler et al., 2010.

Deposition of these and other shale units in the UMG in a marine setting in contact with global ocean waters is supported by several lines of evidence; these include sedimentary structures and facies, paleocurrent directions, microfossil assemblages, and multiple sets of geochemical data (e.g. Dehler et al., 2010; Hayes, 2010).

Uinta Mountain Group strata record deposition in an intracratonic extensional basin, resting entirely on autochthonous continental crust, formed during early Rodinian rifting (Dehler et al., 2007; Karlstrom and Houston, 1984). Paleomagnetic constraints suggest the UMG was deposited just north of the equator ($<5^{\circ}$ N; Weil et al., 2006). The UMG likely correlates with the Chuar Group of Arizona (Figure 12) based on microfossil assemblages, carbon isotope data, and U-Pb zircon geochronology (Dehler et al., 2002b; Dehler et al., 2007). Since the Chuar Group is ~ 770 to 742 ± 6 Ma (Karlstrom et al., 2000) and the formation of Outlaw Trail in the UMG has a maximum depositional age of 766 ± 4 Ma, the UMG's best age constraint is ~ 766 - 742 Ma (Dehler et al., 2010). This, along with correlation of the UMG with the nearby Big Cottonwood Formation (Dehler et al., 2010), places the UMG stratigraphically below the earliest Cryogenian glacial diamictite deposits in Utah and western North America in general (Fanning and Link, 2004, Fanning and Link, 2008; MacDonald et al., 2010).

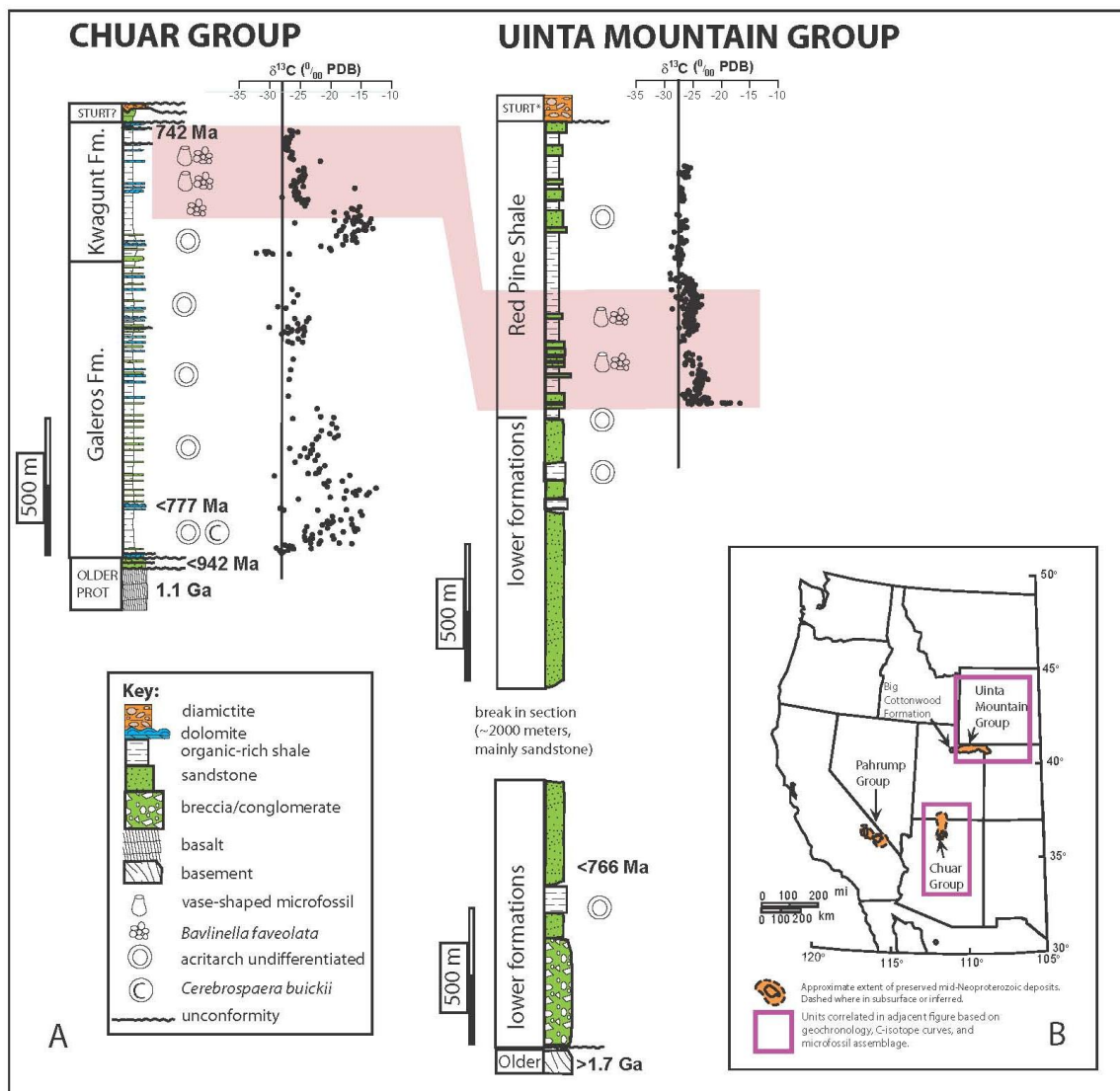


Figure 12. Correlation of the UMG and Chuar Group. A) stratigraphic, microfossil, and C-isotope data for the UMG and Chuar Group with hypothesized correlation shown in shaded pink area. B) map showing outcrop extent of these and correlative strata in the western United States. Figure modified from Dehler et al., 2010.

Micropaleontology

The first microfossil assemblages to be identified in the UMG include mainly *Chuaria circularis*, *Leiosphaeridia* sp., other acritarchs and filaments (Vidal and Ford, 1985). Later analyses identified vase-shaped microfossils, *Leiosphaeridia* sp., *Sphaerocongregus variabilis*, ornamented acritarchs, filaments, and *Chuaria circularis* (Dehler et al., 2007; Nagy and Porter, 2005). Most sections analyzed by Nagy and Porter (2005) were dominated by either *Leiosphaeridia* sp. and filaments or by *Sphaerocongregus variabilis*; these researchers report ornamented acritarchs from a single sample in the Leidy Peak area and vase-shaped microfossils from the upper parts of the upper UMG's Red Pine Shale. This is significant because transitions from more diverse assemblages including ornamented acritarchs to *Leiosphaeridia* sp., *Sphaerocongregus variabilis*, and filament-dominated assemblages may have been caused by regional or global ocean eutrophication (Nagy et al., 2009). Table 2 below contains a list of previously reported taxa from the Uinta Mountain Group.

3.4 - Methods

Geochemical Analyses

Collection and preparation of geochemical samples followed the method of Dehler et al. (2005). Approximately 20 grams of shale chips from each sample were cleaned in 10% HCl, rinsed thoroughly in deionized water, brought to a pH of 5.5, and dried in an oven at 50 °C overnight. Rock samples were then crushed in a zirconium shatter box to ~200 mesh.

Table 2. Summary of fossil occurrences from previous paleontological studies of the upper Uinta Mountain Group. Setting Road data from Vidal and Ford, 1985; “RP” and “LP” samples from Nagy and Porter, 2005; all other data from Hayes, 2010.

Locality	Sample ID #	Fossils
Type Section	RP04-3	<i>Leiosphaeridia</i> sp., filaments
Type Section	RP04-10	<i>Leiosphaeridia</i> sp., filaments
Type Section	RP00B-8	<i>Leiosphaeridia</i> sp., filaments
Type Section	RP00B-32	<i>Leiosphaeridia</i> sp.
Type Section	RP00B-40	Vase-shaped microfossils (VSMs)
Lower Hades	RP01A-50	<i>Leiosphaeridia</i> sp., filaments, <i>Sphaerocongregus variabilis</i>
Lower Hades	RP01A-63	<i>Leiosphaeridia</i> sp., filaments
Lower Hades	RP01A-68	<i>Leiosphaeridia</i> sp., filaments
Lower Hades	RP01A-70	<i>Leiosphaeridia</i> sp., filaments
Lower Hades	RP01A-85	<i>Sphaerocongregus variabilis</i>
Hades	RP03B-1	---barren---
Hades	RP03B-24	<i>Chuarina circularis</i>
Hades	RP03B-25	<i>Leiosphaeridia</i> sp.
Leidy Peak	LP10-03-01-2	Ornamented acritarchs, filaments, ?VSMs
Leidy Peak	LP10-03-01-4	<i>Leiosphaeridia</i> sp., filaments
Leidy Peak	LP10-03-01-6	<i>Leiosphaeridia</i> sp., filaments
Setting Road	---	<i>Taeniatum</i> sp., filaments
Setting Road	---	<i>Leiosphaeridia</i> sp.
Setting Road	---	<i>Valeria lophostriata</i>
Setting Road	---	cf. <i>Stictosphaeridium</i> sp.
Setting Road	---	<i>Trachysphaeridium</i> sp. A
Setting Road	---	<i>Trachysphaeridium laminaritum</i>
Setting Road	---	<i>Trachysphaeridium laufeldi</i>
Setting Road	---	<i>Tasmanites rifeicus</i>
Box Canyon	multiple (13)	<i>Leiosphaeridia</i> sp.
Leidy Peak	multiple (10)	<i>Leiosphaeridia</i> sp.
Type Section	multiple (10)	<i>Leiosphaeridia</i> sp. (lower) and <i>Sphaerocongregus</i> (upper)
Hades (comp)	multiple (13)	<i>Leiosphaeridia</i> sp. (lower) and <i>Sphaerocongregus</i> (upper)
Setting Road	multiple (8)	---barren---

Powders to be used for organic carbon analysis were rinsed with deionized water until their pH reached 5.5, then dried. The portion of each sample to be used for organic carbon analysis was cleaned again in 10% HCl, returned to a pH of 5.5, and dried; however, the powdered sample portion used for Fe speciation and S analysis was not treated with acid. Organic carbon mass spectrometer analysis of these samples (~100 μ g each) was conducted at the University of New Mexico's Department of Earth and Planetary Sciences stable isotope laboratory using a Delta Plus continuous flow mass spectrometer to obtain $\delta^{13}\text{C}_{\text{org}}$ values and total organic carbon weight percent of each sample. These organic carbon values (TOC and $\delta^{13}\text{C}_{\text{org}}$) were used as a correlation tool; they were also compared with microfossil, stratigraphic, and iron geochemistry results to infer paleo-ocean geochemical conditions at the time of deposition.

Chromium reducible sulfur was extracted from 5-8 grams of rock powder for each sample; this sulfur was then converted to silver sulfide, isolated through filtration, massed, combined with 4-5 mg of vanadium pentoxide to aid in combustion, and loaded into tin capsules. Continuous flow sulfur mass spectrometry was conducted on those samples containing sufficient (>0.25 mg) silver sulfide to determine $\delta^{34}\text{S}_{\text{pyrite}}$ values; due to the low amounts of sulfide in most samples, only 8/75 contained enough sulfur for analysis.

Iron speciation analysis, using a modified version of the Poulton and Canfield lab procedure (Poulton and Canfield, 2005), was also conducted on ~100 mg of rock powder per sample to determine the ratio of highly reactive iron (pyrite-derived

and dithionite-soluble) to total iron, with the total iron analysis and total aluminum analysis conducted by SGS geochemical laboratory in Toronto, Canada using a four-acid digestion followed by ICP - AES analysis. Sulfur extractions, sulfur isotope analysis, and iron speciation sequential extractions were performed at Harvard University. Iron speciation values were then calculated and used to assess the paleo-ocean redox state at the time the sediments were deposited.

Micropaleontological Analysis

Microfossil samples were prepared by an independent palynological laboratory using standard hydrofluoric acid maceration techniques. The microfossils (both the total kerogen and > 10 micron fraction) were mounted on glass slides for high-powered light microscopy. Light microscopy (400 – 1000x) was used to qualify morphological characters useful for taxonomic identification. Abundance counts (at 400x) were completed by recording the identity of the first 100 fossils encountered using standard point-counting techniques; this number of individuals is used because no statistically significant difference in population composition occurs with an increased number of counted individuals beyond 100 (Nagy, 2008). Example specimens of taxa encountered were photographed, and England Finder coordinates were recorded to mark the position of unusual fossils on each of slides (always with slide label to bottom left).

Geochemical and paleontological statistics

When applicable, statistical tests were conducted to determine the significance of any trends. Biologic diversity and evenness of each micropaleontological sample were calculated using Multivariate Statistics Package (MVSP version 3.13q) software utilizing the Shannon Method with a natural logarithm base. A special t-test for comparing diversity indices was then used, with the calculation done by hand (Zar, 2010; see supplemental data in Appendix B). Correlations were conducted in Microsoft Excel to examine potential relationships between biotic and geochemical factors; this includes correlations of 1) diversity index vs. FeHR/FeT, 2) diversity index vs. Fe/Al; 3) diversity index vs. TOC, and 4) diversity index vs. $\delta^{13}\text{C}_{\text{org}}$.

3.5 - Results & Discussion

Redox Geochemistry

Total iron (FeT, weight %) in the Leidy/Marsh and Box Canyon samples ranges from 1.25 to 5.77%, with an average value of 3.44%. The majority of this iron is in the operationally defined unreactive portion (FeT - FeHR), with the other 34% in the highly reactive portion (FeHR/FeT). Of this highly reactive iron, the portion locked up in crystalline oxides is relatively high (~25%). Magnetite constitutes ~9% of the highly reactive iron in these samples, and iron carbonates make up a relatively small fraction (~1.4 %) of the FeHR pool. Pyrite concentrations are very low in all of these samples, making up less than 0.05% of the highly reactive

iron, and resulting in very little successful sulfide extraction for sulfur isotope analysis (<10% of samples).

The redox conditions of the depositional environment were mainly inferred using the FeHR/T and Fe/Al values for each sample, with FeHR/T values greater than 0.22 indicating possible anoxia, FeHR/T values greater than 0.38 indicating anoxia, FePyrite/FeHR values greater than 0.80 indicating euxinia, and Fe/Al values greater than 0.50 also suggesting anoxia, especially during relatively rapid sedimentation (Sperling et al., in review; see Appendix B and Figure 13).

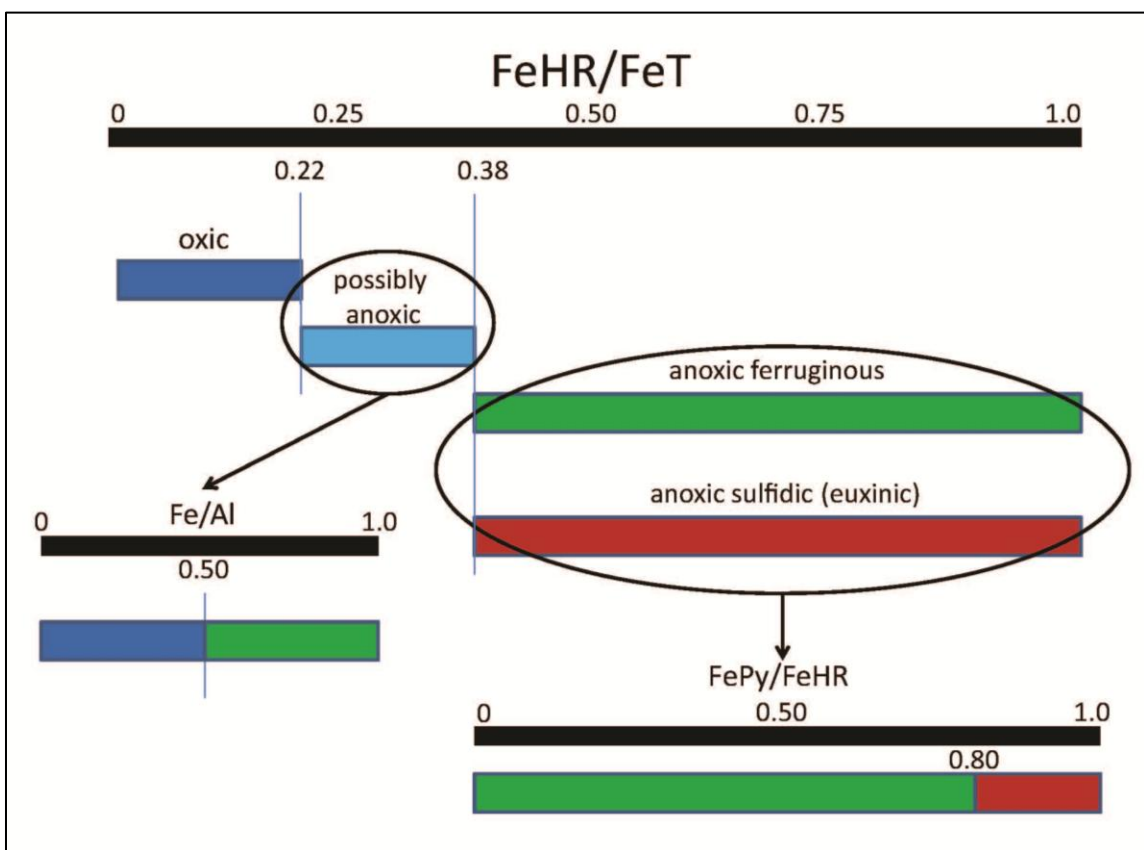


Figure 13. Flowchart illustrating the interpretation of iron speciation values.

Fluctuations in concentrations of vanadium were also considered as an independent redox proxy (supplemental data). Three of the map units in the Leidy/Marsh Peak area (Zrp1, Zrp2, and Zrp4) show brief periods of anoxia where ferruginous (not euxinic/sulfidic) water column conditions existed during deposition (Figure 14; supplemental data). Unsurprisingly, these periods of anoxia are recorded in the shale and siltstone-dominated portions of these three map units where water depth is interpreted to have been relatively greater than in the sandstone-dominated portions. No evidence for anoxia is found in units Zhp and Zrp3, placing them above the oxic-anoxic water interface during deposition and further supporting their depositional environment interpretations as fluvial-deltaic and tidal flat, respectively.

Organic Carbon Data

The ranges and average total organic carbon (TOC) values for each measured section in the Leidy/Marsh Peak map area along with the Box Canyon and Red Pine Shale Type sections in the western UMG are shown in Table 3, and the full data set is displayed in Appendix B. The highest individual TOC value (5.91%) as well as the highest average TOC value (0.77%) come from the Hades Creek and Red Pine Type Sections in the western Uinta Mountains. The rest of the sections (Box Canyon and the five in the Leidy/Marsh area) show relatively low TOC values and limited TOC variability; all of these are very low in TOC compared with those reported

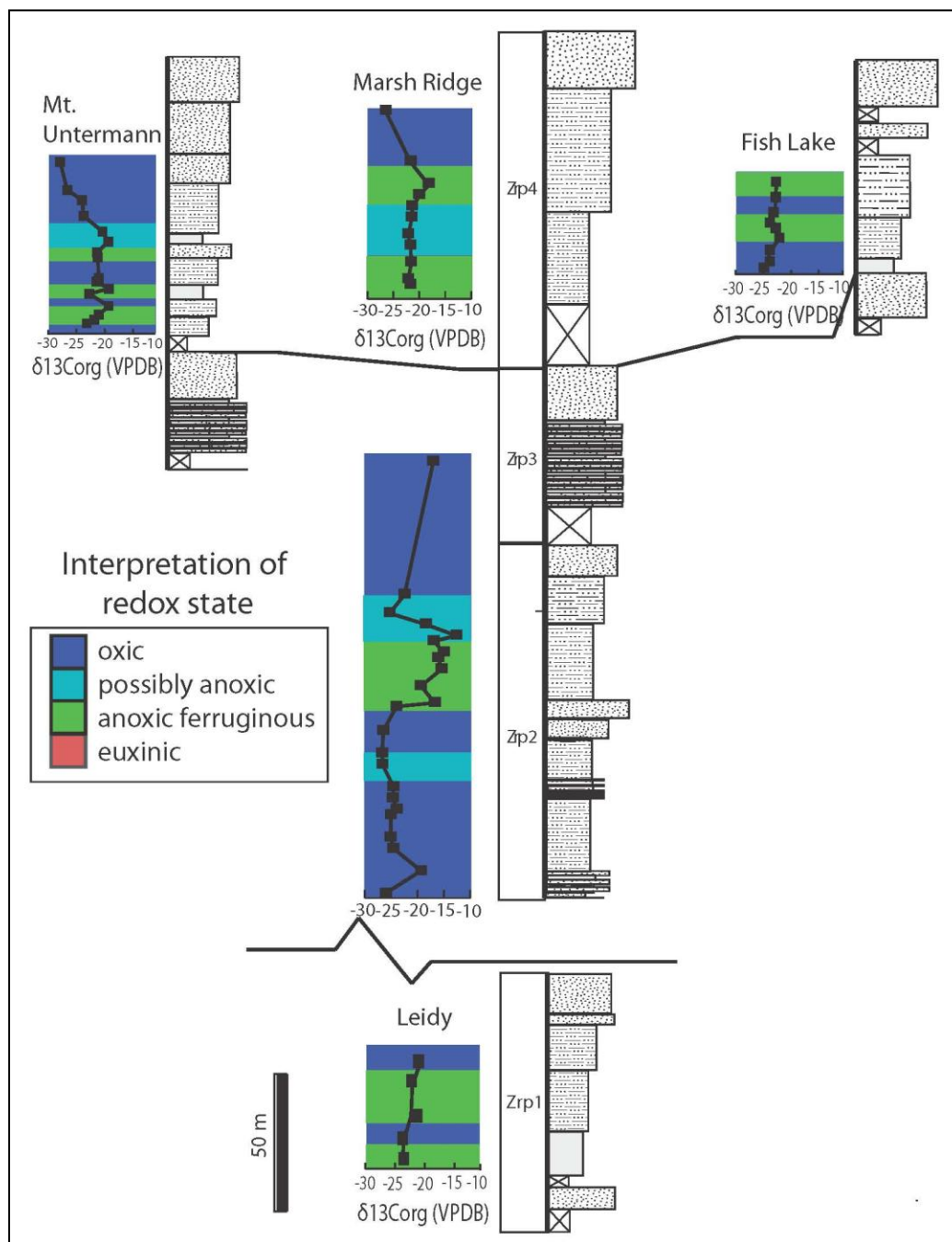


Figure 14. Redox and C-isotope data from the Leidy/Marsh Peak area.

previously from measured sections in the Uinta Mountain Group's Red Pine Shale (Hayes, 2010; Myer, 2008).

Table 3. Total organic carbon (TOC) averages and ranges by section.

Locality/Section	Range of TOC values (weight %)	Average TOC value (weight %)
Box Canyon	0.00 – 0.82 %	0.30 %
Leidy Peak	0.08 – 0.30 %	0.16 %
Marsh Peak Ridge 1	0.05 – 0.76 %	0.14 %
Marsh Peak Ridge 2	0.04 – 0.08 %	0.06 %
Fish Lake	0.04 – 0.17 %	0.08 %
Mt. Untermann	0.03 – 0.17 %	0.08 %
Red Pine Shale Type Section	0.25 – 1.70 %	0.77 %
Hades Creek Section	0.06 – 5.91 %	0.69 %

The range and average $\delta^{13}\text{C}$ organic carbon values for each measured section in the Leidy/Marsh Peak area and the Box Canyon and Red Pine Shale Type sections in the western UMG are shown in Table 4, and curves for the Leidy/Marsh Peak area sections are shown in Figure 14. The Box Canyon and Hades Creek sections show the most negative averages, and the Leidy/Marsh Peak sections seem to show an overall trend of increasing values (more positive upward) from the Leidy Peak shale unit to the first Marsh Ridge shale unit, then decreasing values (more negative upward) from the first Marsh Ridge shale unit to the second. The first Marsh Ridge Shale unit hosts a +10 per mil positive excursion (from ~ -25 to less than -15) that

persists from ~25 to 75 m in the section (Figure 14). In the Red Pine Shale Type Section, values also change dramatically (from ~-24 to -19 per mil) at the base, but this continues over only a few meters. Based on its magnitude, “shape,” and the extreme rarity of such positive values in Uinta Mountain Group samples, it is likely that this positive $\delta^{13}\text{C}_{\text{org}}$ excursion in the lower Marsh Ridge shale unit correlates with the one in the Red Pine Shale in the western UMG; higher sedimentation rates in the nearer-shore facies (Leidy/Marsh Peak area) than in the deeper-water facies (western UMG Red Pine Shale) would explain the longer stratigraphic span of the excursion in the eastern strata.

Table 4. $\delta^{13}\text{C}$ averages and ranges by section.

Locality/Section	Range of $\delta^{13}\text{C}$ (per mil, VPDB)	Average $\delta^{13}\text{C}$ (per mil, VPDB)
Box Canyon	-29.42 to -22.58	-26.17
Leidy Peak	-26.52 to -21.08	-23.82
Marsh Peak Ridge 1	-25.74 to -13.61	-21.26
Marsh Peak Ridge 2	-25.52 to -18.40	-21.41
Fish Lake	-23.68 to -22.03	-22.68
Mt. Untermann	-27.48 to -19.72	-22.30
Red Pine Shale Type Section	-29.34 to -19.70	-25.29
Hades Creek Section	-29.46 to -23.90	-26.24

Micropaleontology

Throughout the Leidy/Marsh Peak map area, the dominant fossil assemblage is *Leiosphaeridia sp.* (supplemental data); both thin-walled and thick-walled forms are found, and they range in size from ~5 to 40 μm in diameter (Figure 15). Other commonly found but non-dominant taxa are filaments (both thick/unsegmented and thin/segmented; Figure 15), *Operculosphaeridia sp.* (Figure 15), and colonial forms (Figure 15), possibly of the genus *Satka*. *Sphaerocongregus variabilis* is very rare, as are ornamented acritarchs (Figure 15). Diversity indices (Shannon-Weiner, log base e method; see supplementary data) indicate a range of values (0.191 – 1.333) with an average diversity index of 0.603; this is relatively high compared with average values from the UMG's Red Pine Shale in the western Uinta Mountains (0.310).

To test the hypothesis of whether or not the Leidy/Marsh Peak shale units correlate with the Box Canyon shale units of the western UMG, microfossil data from the Box Canyon units was re-analyzed and compared with new data. Diversity indices for the Box Canyon units show a higher diversity index average (0.869) than the Leidy/Marsh Peak units (0.603); a special t-test for comparing diversity indices indicates that the Box Canyon diversity is significantly higher than the Leidy/Marsh Peak diversity (see Appendix B). One major difference between the Box Canyon and Leidy/Marsh Peak microfossil assemblages is that Box Canyon contains several filament-rich samples not found in the Leidy/Marsh Peak area. Additionally, a possibly heavily perforated thin-walled *Leiosphaeridia sp.* specimen was found in

the Box Canyon shale units that does not match any known Neoproterozoic acritarch taxonomic affinity (Figure 15 – England Finder Coordinates = R-33).

3.6 - Conclusions

The Uinta Mountain Group basin is typical with respect to what is currently known about Proterozoic ocean basins; anoxia was common in subsurface marine waters, and total iron concentrations are slightly lower than those reported for average shale (Canfield et al., 2008). Highly reactive to total iron (FeHR/FeT) concentrations greater than 0.38 reflect deposition under an anoxic water column, and significantly lower FeHR/FeT values suggest oxic bottom water conditions (Canfield et al., 1992; Poulton and Raiswell, 2002; Raiswell and Canfield, 1998; Raiswell et al., 2001). This enrichment in FeHR is due to enhanced precipitation of highly reactive iron, either pyrite in sulfidic (euxinic) basins or ferric oxides, magnetite, and/or siderite in ferruginous (anoxic but non-sulfidic) basins. In the Leidy/Marsh Peak shale units, FeHR/FeT values fluctuate, generally hovering around the oxic-anoxic threshold (0.38) but not approaching the ferruginous-euxinic FePy/HR threshold (0.80). The iron speciation data set from the Leidy/Marsh sections of the UMG suggests that anoxia, when it occurred, was accompanied by ferruginous conditions (Fe²⁺ in the water column) but not euxinia. This lends further support to the idea that the Neoproterozoic return of ferruginous conditions in subsurface ocean waters occurred after 800 Ma (Canfield et al., 2008; Johnston et al., 2010) and additional strength to correlations between the UMG and Chuar Group. Although the UMG shale units in the Leidy/Marsh Peak area do not

record a transition to euxinic conditions like that observed in the coeval Chuar Group, it is possible that this euxinic episode is recorded in the upper part of the slightly younger upper Red Pine Shale of the western UMG. Total organic carbon, sulfur, microfossil and Fe/Al data suggest that this is likely (Hayes, 2010).

Based on the microfossil and geochemical results of this study, it can be confidently concluded that 1) a biotic change like that observed in the Chuar Group is not recorded in the shale units of the Leidy/Marsh Peak area, 2) biotic variations in this new Leidy/Marsh peak UMG shale record neither correlate with paleoredox fluctuations nor the large positive C-isotope excursion in the Lower Marsh Peak shale unit, and 3) C-isotope and TOC values in this new UMG shale record do not always correlate with geochemical indicators of paleo-anoxia. This, however, does not mean that the Uinta Mountain Group contains no record of the biotic transition and eutrophication event recorded in the coeval Chuar Group; instead, it may allow the location of the hypothesized eutrophication-related biotic transition in the UMG to be more accurately pinpointed.

It seems likely that the biotic transition in the UMG occurs over a relatively long section of strata – perhaps almost the entire group - compared with the transition recorded in the coeval Chuar Group (Figure 16). There is evidence for anoxia, sulfur enrichment, total organic carbon enrichment, and “post-eutrophication” microfossil assemblages (*Sphaerocongregus variabilis*, VSMs, and very low diversity) in the upper Red Pine Shale, the uppermost part of the UMG (Hayes, 2010). Just below that interval, in the lower Red Pine Shale, Leidy/Marsh

Peak and Box Canyon shale units, there is evidence for some anoxic periods without euxinia and possibly “transitional” microfossil assemblages (smooth *Leiosphaeridia*-dominated with intermediate diversity), with the stratigraphically lower Box Canyon units showing slightly higher diversity than the lower Red Pine Shale and Leidy/Marsh Peak units (see supplemental data). Below >700 m of sandstone-dominated strata, in the formation of Moosehorn Lake (Figure 16), microfossil assemblages with taxa similar to “pre-eutrophication” ones in the Chuar Group are reportedly common (Waanders and Sprinkel, unpublished data). Preliminary assessment of a single sample (MH6-23-08-1) from the formation of Moosehoorn Lake reveals the presence of three species that are known from throughout the Galeros Formation, lower Chuar Group: cf. *Trachysphaeridium laminaritum*, cf. *Trachysphaeridium laufeldi*, and a new yet undescribed species characterized by a coating of numerous ~1-3 µm elliptical organic plate scales (S. Porter, pers. comm.; Figure 15).

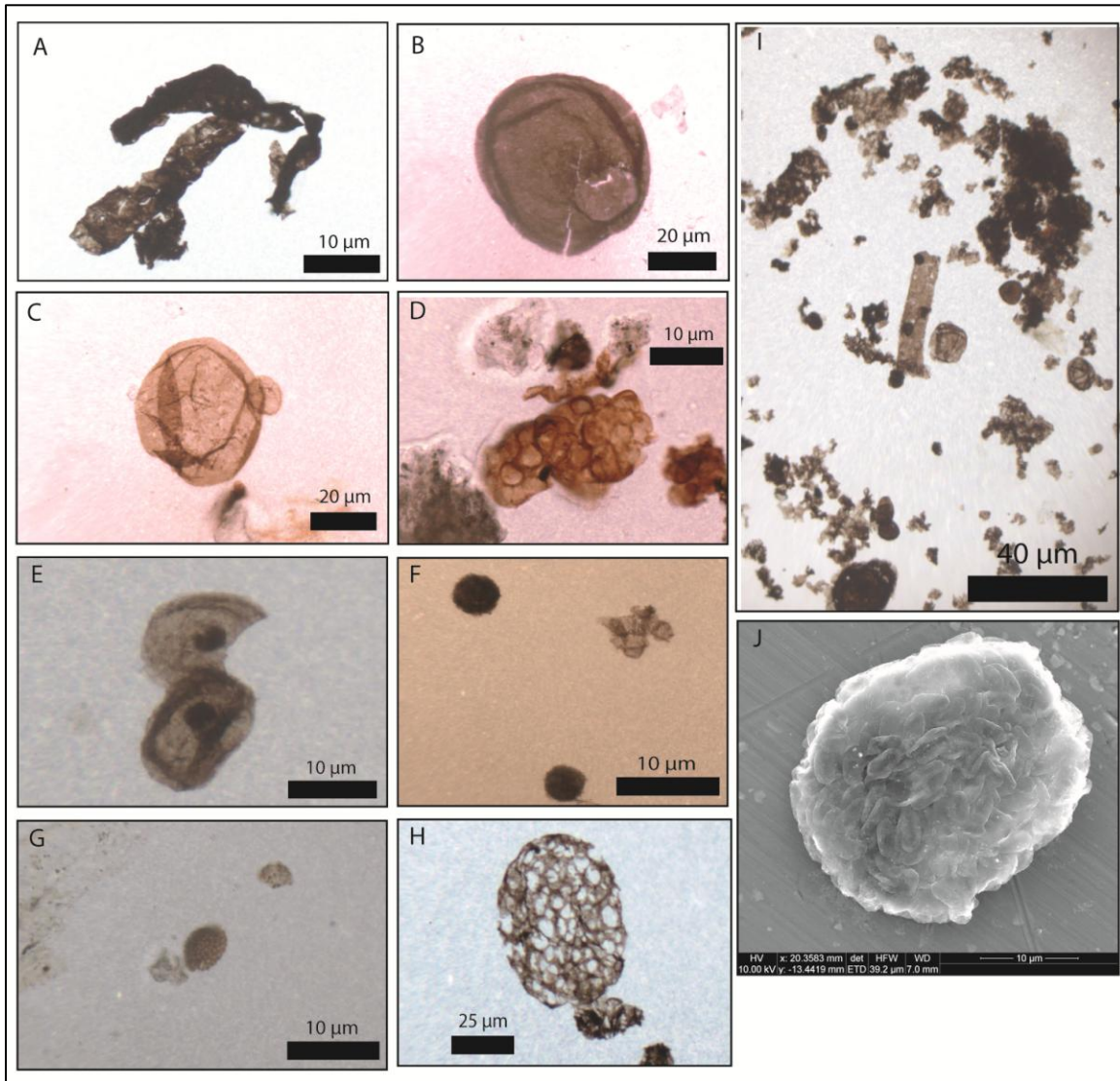


Figure 15. Microfossils from the Leidy/Marsh Peak strata. A) Thick filaments (DHBCC14) B) Thick-walled *Leiosphaeridia* sp. (DHLPA1) C) Thin-walled *Leiosphaeridia* sp. (DHLPA1) D) Colonial form (DHLPA1) E) Two operculosphaerids (52DH11) F) Two possible ornamented acritarchs (58DH11) G) Ornamented acritarch, unidentified species (104DH12) H) Perforated thin-walled leiosphaerid (?) acritarch (DHBCC6) I) Several taxa together (filaments, thick and thin-walled leiosphaerids of varying size, degraded organic material) (58DH11) J) new undescribed species from the fm. of Moosehorn Lake (SEM image, courtesy of S. Porter)

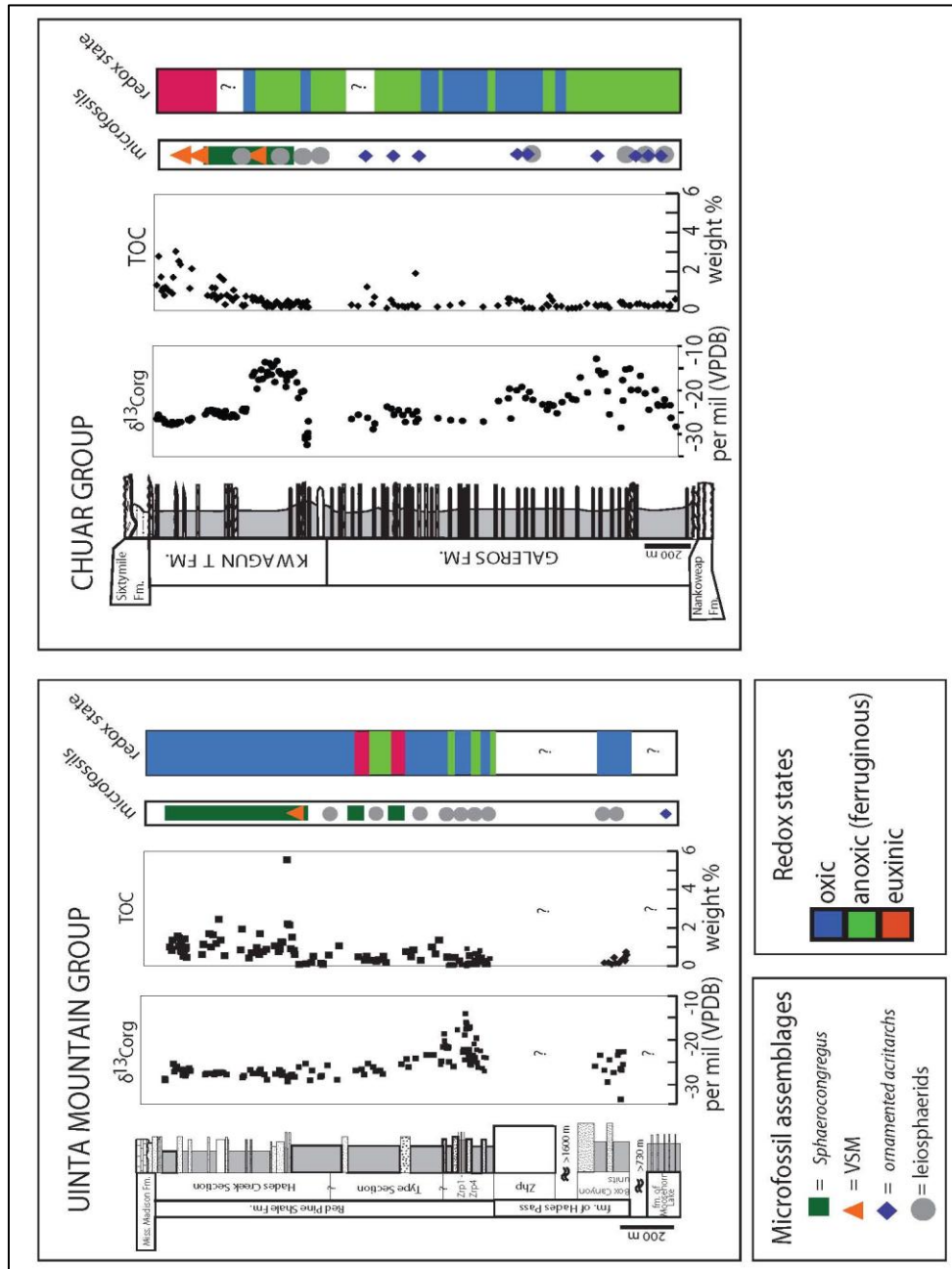


Figure 16. Comparison of C-isotope, TOC, microfossil, and redox data from the Uinta Mountain Group and Chuar Group. Note the large positive C-isotope excursion, upsection increase in TOC, microfossil assemblage changes, and euxinic redox states observed in both groups, strongly suggesting a correlation between these similar-aged units.

In combination, these observations strongly suggest that a biotic transition is present in the Uinta Mountain Group, and that it can be pinpointed somewhere below the Box Canyon shale units in the formation of Hades Pass the above the formation of Moosehorn Lake. Redox geochemistry of the Moosehorn Lake formation is not yet known, and obtaining this is of course the next step (along with more detailed, statistically analyzed microfossil work) in testing whether or not the biotic transition in the UMG is related to a eutrophication event. If this transition is related to a eutrophication event, it is potentially a global one restricted to shallow shelf environments (Figure 17); this is suggested by the presence of similar biotic transitions in Neoproterozoic strata of Death Valley, Australia, Tasmania, and the Greenland-East Svaalbard region (Nagy et al., 2009) and implies that this change in biota (at least for these environments) may eventually be used as a global time marker when more robust time constraints are unavailable.

Whether or not this transition in organic-walled microfossil taxa had any impact on the trajectory of eukaryote evolution is yet unknown, and it deserves consideration and further investigation. It seems very counterintuitive that a significant Cryogenian pre-glacial decrease in the diversity and abundance of eukaryotic organisms could somehow spark the rapid radiation of eukaryote groups documented globally in post-glacial (Ediacaran) strata, yet this possibility shouldn't be immediately discounted. It is, however, more likely that this "eutrophication event" is restricted to certain environments and represents a eukaryote evolutionary bottleneck rather than a mass extinction. If this is the case, then we

would expect a smaller-scale shallow shelf ocean geochemical change (Figure 17), even if recorded globally, to affect eukaryotes only temporarily and only result in the extinction of certain phytoplankton taxa; it is important to recall that eukaryotic phytoplankton, including leiosphaerid acritarchs, persist long after the Neoproterozoic ends. On the other hand, a “bloom” of prokaryotic planktonic organisms could have easily resulted in the expansion of organic-rich shallow shelf environments conducive to the proliferation of heterotrophic eukaryotes (e.g. VSMs and other protists) that thrive under such conditions. It has also been suggested that, on a longer timescale than that recorded by the UMG and Chuar Groups, a Neoproterozoic return to ferruginous oceans could have favored eukaryotic over prokaryotic expansion in general, with differential sulfide tolerance between these two groups being a key factor (Johnston et al., 2010). All of these explanations are plausible, and it is likely that what we see in the sedimentary record is a result of their combined effects. Their relative importance - and how they influenced one another - will hopefully be tested by future studies of the links between geochemistry and biota in contemporaneous strata.

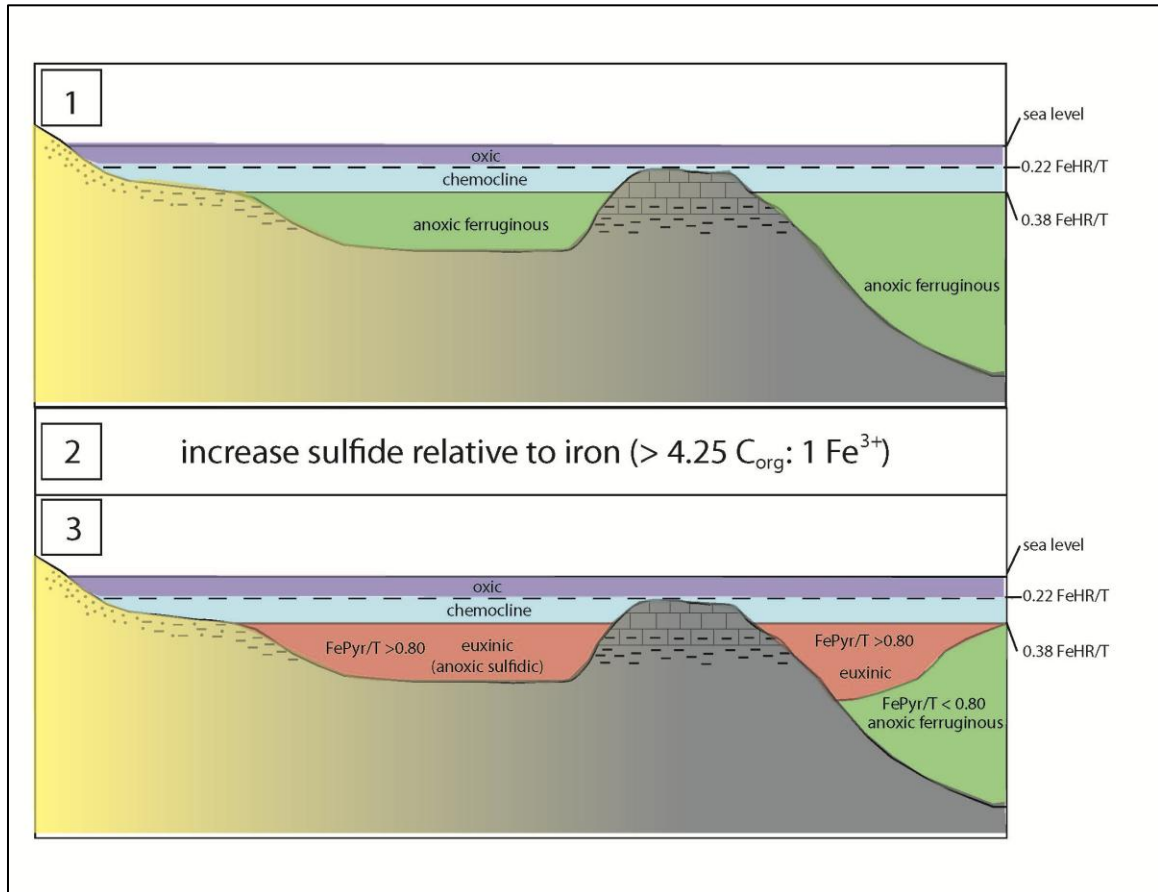


Figure 17. Illustration of chemocline changes in a shallow-shelf eutrophication event. At time 1: ferruginous subsurface ocean redox conditions (majority of UMG strata likely represent this type of shallow shelf environment); time 2: nearshore eutrophication event occurs, causing a “tip” in the organic carbon/Fe ratio that favors sulfidic over ferruginous conditions; time 3: euxinic subsurface conditions in shallow shelf environments (observed in upper Chuar Group & part of upper UMG), ferruginous conditions in deeper open ocean environments.

3.7 - References

Canfield, D.E., Poulton, S.W., Knoll, A.H., Narbonne, G.M., Ross, G., Goldberg, T., and Strauss, H., 2008, Ferruginous conditions dominated later neoproterozoic deep-water chemistry: *Science*, v. 321, p. 949-952.

- Dehler, C.M., Porter, S.M., De Grey, L.D., Sprinkel, D.A., and Brehm, A., 2007, The Neoproterozoic Uinta Mountain Group revisited; a synthesis of recent work on the Red Pine Shale and related undivided clastic strata, northeastern Utah, U. S. A: Proterozoic geology of western North America and Siberia, v. 86, p. 151-166.
- Dehler, C.M., Sprinkel, D.A., and Porter, S.M., 2005, Neoproterozoic Uinta Mountain Group of northeastern Utah; pre-Sturtian geographic, tectonic, and biologic evolution: United States, Geological Society of America : Boulder, CO, United States.
- Dehler, C.M., Fanning, C.M., Link, P.K., Kingsbury, E.M., and Rybczynski, D., 2010, Maximum depositional age and provenance of the Uinta Mountain Group and Big Cottonwood Formation, northern Utah: Paleogeography of rifting western Laurentia: Geological Society of America Bulletin, v. 122, p. 1686-1699.
- , 2004, U-Pb SHRIMP ages of Neoproterozoic (Sturtian) glaciogenic Pocatello Formation, southeastern Idaho: *Geology*, v. 32, p. 881-884.
- Fanning, C.M., and Link, P.K., 2008, Age constraints for the Sturtian Glaciation; data for the Adelaide Geosyncline, South Australia and Pocatello Formation, Idaho: USA Selwyn Symposium 2008 GSA Victoria Division, Abstracts 91, p. 57-61.
- Hansen, W.R., 1964, Geology of the Flaming Gorge area, Utah-Colorado-Wyoming: U.S. Geological Survey Professional Paper 490, p. 196.
- Hayes, D.H., 2010, Stratigraphic, microfossil, and geochemical analysis of the Neoproterozoic Uinta Mountain Group: Evidence for a eutrophication event?: Logan, Utah State University.
- Johnston, D.T., Poulton, S.W., Dehler, C., Porter, S., Husson, J., Canfield, D.E., and Knoll, A.H., 2010, An emerging picture of Neoproterozoic ocean chemistry: Insights from the Chuar Group, Grand Canyon, USA: *Earth and Planetary Science Letters*, v. 290, p. 64-73.
- Karlstrom, K., and Houston, R., 1984, The Cheyenne belt: Analysis of a Proterozoic suture in southern Wyoming: *Precambrian Research*, v. 25, p. 415-446.

- Karlstrom, K.E., Bowring, S.A., Dehler, C.M., Knoll, A.H., Porter, S.M., Des Marais, D.J., Weil, A.B., Sharp, Z.D., Geissman, J.W., Elrick, M.B., Timmons, J.M., Crossey, L.J., and Davidek, K.L., 2000, Chuar Group of the Grand Canyon: Record of breakup of Rodinia, associated change in the global carbon cycle, and ecosystem expansion by 740 Ma: *Geology*, v. 28, p. 619-622.
- Kingsbury-Stewart, E.M., Osterhous, S.L., Link, P.K., and Dehler, C.M., in press, Sequence stratigraphy and formalization of the Middle Uinta Mountain Group (Neoproterozoic), central Uinta Mountains, UT: A closer look at the western Laurentian Seaway at ca. 750 Ma: *Precambrian Research*.
- Knoll, A.H., 1994, Proterozoic and early Cambrian protists: evidence for accelerating evolutionary tempo: *Proceedings of the National Academy of Sciences of the United States of America*, v. 106, p. 1281-1292.
- Knoll, A.H., Blick, N., and Awramik, A.M., 1981, Stratigraphic and ecologic implications of late Precambrian microfossils from Utah: *American Journal of Science*, v. 281, p. 247-263.
- Macdonald, F.A., Schmitz, M.D., Crowley, J.L., Roots, C.F., Jones, D.S., Maloof, A.C., Strauss, J.V., Cohen, P.A., Johnston, D.T., and Schrag, D.P., 2010, Calibrating the Cryogenian: *Science*, v. 327, p. 1241-1243.
- Myer, C.A., 2008, Sedimentology, stratigraphy, and organic geochemistry of the Red Pine Shale, Uinta Mountains, Utah: A prograding deltaic system in a mid-Neoproterozoic interior seaway: Logan, Utah State University.
- Nagy, R.M., 2008, Microfossils from the Neoproterozoic Chuar Group, Grand Canyon, Arizona: taxonomy, paleoecological analysis and implications for life during the onset of Neoproterozoic glaciation: Santa Barbara, University of California Santa Barbara.
- Nagy, R.M., and Porter, S.M., 2005, Paleontology of the Neoproterozoic Uinta Mountain Group: *Uinta Mountain Geology: Utah Geological Association Publication*, v. 33, p. 49-62.
- Nagy, R.M., Porter, S.M., Dehler, C.M., and Shen, Y., 2009, Biotic turnover driven by eutrophication before the Sturtian low-latitude glaciation: *Nature Geoscience*, v. 2, p. 414-417.
- Poulton, S., and Raiswell, R., 2002, The low-temperature geochemical cycle of iron: From continental fluxes to marine sediment deposition: *American Journal of Science*, v. 302, p. 774-805.

- Poulton, S.W., and Canfield, D.E., 2005, Development of a sequential extraction procedure for iron: Implications for iron partitioning in continentally derived particulates: *Chemical Geology*, v. 214, p. 209-221.
- Raiswell, R., and Canfield, D.E., 1998, Sources of iron for pyrite formation in marine sediments: *American Journal of Science*, v. 298, p. 219-245.
- Raiswell, R., Newton, R., and Wignall, P., 2001, An indicator of water-column anoxia: resolution of biofacies variations in the Kimmeridge Clay (Upper Jurassic, UK): *Journal of Sedimentary Research*, v. 71, p. 286-294.
- Rybczynski, D., 2009, Correlation, paleogeography, and provenance of the neoproterozoic eastern Uinta Mountain Group, northeastern UT: Logan, Utah.
- Sanderson, I.D., 1984, The Mount Watson Formation, an interpreted braided-fluvial deposit in the Uinta Mountain Group (Upper Precambrian), Utah: *The Mountain Geologist*, v. 21, p. 157-164.
- Sperling, E. A., Halverson, G.P., Knoll, A.H., MacDonald, F.M., and Johnston, D.T., in review, A basin redox transect at the dawn of animal life: *Earth and Planetary Science Letters*.
- Vidal, G., and Ford, T.D., 1985, Microbiotas from the late Proterozoic Chuar Group and Uinta Mountain Group and their chronostratigraphic implications: *Precambrian Research*, v. 28, p. 349-389.
- Vidal, G., and Moczydlowska, M., 1992, Patterns of phytoplankton radiation across the Precambrian-Cambrian boundary: *Journal of the Geological Society*, v. 149, p. 654-647
- Vidal, G., and Knoll, A.H., 1982, Radiations and extinctions of plankton in the late Proterozoic and early Cambrian: *Nature*, v. 287, p. 57-60.
- Wallace, C.A., 1972, A basin analysis of the upper Precambrian Uinta Mountain Group, Utah: Santa Barbara, California.
- Weil, A.B., Geissman, J.W., and Ashby, J.M., 2006, A new paleomagnetic pole for the Neoproterozoic Uinta Mountain supergroup, Central Rocky Mountain States, USA: *Precambrian Research*, v. 147, p. 234-259.
- Zar, J.H., 2010, *Biostatistical Analysis*: Upper Saddle River, NJ, Pearson Prentice Hall, 944 p.

CHAPTER 4

A NEWLY DESCRIBED NEOPROTEROZOIC POST-GLACIAL CAP CARBONATE SEQUENCE, ANTELOPE ISLAND, GREAT SALT LAKE: DISCOVERY OF THE CRYOGENIAN-EDIACARAN BOUNDARY IN NORTHERN UTAH?³

4.1 - Abstract

The popular yet controversial Snowball Earth hypothesis proposes an Earth almost completely covered in ice at least twice during Neoproterozoic time, predicting the formation of lithologically and isotopically unique “cap carbonate sequences,” precipitated from the oceans nearly instantaneously after these extreme glaciations. About 30 cap carbonate sequences have been described worldwide, with six containing “tube structures,” considered (along with other idiosyncratic features) so distinctive that they may have formed only once in Earth’s history. Thus, despite the lack of direct age constraints, carbonate units of this lithologic style are used to mark the Cryogenian-Ediacaran boundary (635 Ma). We report a newly described Neoproterozoic ($<698 \pm 8$ Ma) cap carbonate sequence with tube structures on Antelope Island, Utah, including four measured stratigraphic sections with $\delta^{13}\text{C}$ and detrital zircon U-Pb age data. Based on lithology alone, this cap carbonate could be interpreted as marking the Cryogenian-Ediacaran boundary. However, detailed C-isotope data do not unequivocally support this correlation, and regional zircon U-Pb age data suggest the carbonate and underlying diamictite were

³ Coauthored by Hayes, D.S., Dehler, C.M., and Yonkee, A.

deposited ca. 685 to 665 Ma. Correlations based only on cap carbonate “style” are thus problematic and need to be tested with additional geochronologic constraints.

4.2 - Introduction

Although preserved globally, most Neoproterozoic Cryogenian successions (~850-635 Ma; Gradstein and Ogg, 2004) are incomplete and direct age constraints rare. In many of these successions, glacial deposits (diamictites) are overlain by lithologically unusual carbonate units, “cap carbonate sequences,” with negative $\delta^{13}\text{C}$ excursions interpreted to record rapid post-glacial flooding and carbonate precipitation (e.g. Hoffman, 2011). In Namibia, Australia, Canada, and China, two stacked sets of diamictite-cap carbonate sequences indicate at least two glacial episodes (Hoffman et al., 1998; Kennedy et al., 1998). The first is dated between 716.5 and 662.4 Ma in NW Canada (Macdonald et al., 2010; Rooney et al., in review) and the second terminated at ~635 Ma in China and Namibia and may have lasted only 10 Myr (Condon et al., 2005; Hoffmann et al., 2004). In Idaho, Utah, China, and Australia, evidence indicates a glacial episode between ~685-665 Ma (Balgord, in review; Dehler et al., 2011; Fanning and Link, 2004; Fanning and Link, 2008; Keeley et al., 2013; Lund et al., 2003; Lund et al., 2010; Zhou et al., 2004).

Based on stratigraphic relationships, lithology, and $\delta^{13}\text{C}$ values, most cap carbonate sequences have been classified as “Sturtian” (older Cryogenian) or “Marinoan” (Cryogenian-Ediacaran boundary; Knoll et al., 2006) without geochronologic constraints. This evolved from an analysis of 12 cap carbonate sequences by Kennedy et al. (1998) describing “Sturtian-style” cap carbonate

sequences as darker-colored, organic-rich, and finely-laminated with negative basal $\delta^{13}\text{C}$ values that increase abruptly to positive values. “Marinoan-style” cap carbonate sequences are lighter-colored, with unusual lithologic features (aragonite fans, tube structures, sheetcrack cements, and giant wave ripples), and negative $\delta^{13}\text{C}$ values that decrease gradually upsection. These criteria are frequently used to designate cap carbonates as “Sturtian” or “Marinoan,” but it is unclear how well they apply to the >15 Neoproterozoic cap carbonate sequences described after 1998. Directly dated cap carbonate sequences, some sharing both “Sturtian” and “Marinoan” features, have disparate age constraints (740 \pm 22, ~663, ~657, ~643, and ~635 Ma; Babinski et al., 2006; Condon et al., 2005; Kendall et al., 2009; Zhou et al. 2004).

The only official geologic period in the Precambrian division of the geologic timescale is the Ediacaran Period, the lower contact of which is formally, yet unconventionally, defined by “Marinoan-style” cap carbonate sequences used as a 635 Ma timeline (Condon et al., 2005; Knoll et al., 2006). Some (Corsetti and Lorentz, 2006; Dehler et al., 2011; Halverson, 2006; Kendall et al., 2009) argue against correlating Neoproterozoic cap carbonates by lithologic “style” because age constraints are lacking and it is based on the Snowball Earth hypothesis (Hoffman et al., 1998), which is controversial (e.g. Allen and Etienne, 2008). The main problem with lithologic correlation is that diagnostic features of these strata are rare and poorly understood. For example, tube structures are reported in the literature from only six successions (Cloud, 1974; Corsetti and Grotzinger, 2005; Hegenberger,

1987; Hoffman and Schrag, 2002; Macdonald et al., 2009a; Macdonald et al., 2010; Marengo and Corsetti, 2002; Nogueira et al., 2003). Only one of these has geochronologic constraints suggesting deposition at ~635 Ma, based on a basin-platform correlation and assumption that the cap-diamictite contact is conformable (Hoffmann et al., 2004). Clearly, more data are needed to test the hypothesis that these features formed only once, along with the global correlations that stem from this idea. We report a new locality of a Neoproterozoic cap carbonate sequence with tube structures from Utah, characterize its sedimentology, physical stratigraphic context, and C-isotope signature, and apply detrital zircon geochronology to provide insight on the timing and style of regional and global cap carbonate deposition.

4.3 - Stratigraphy and sedimentology

A thin succession of Neoproterozoic strata (<80 m), exposed on Antelope Island, Utah, includes a distinctive cap carbonate sequence. This succession is correlated with much thicker (up to 3500 m) Neoproterozoic strata carried from the Willard thrust system to the west (Fig. 18A). On Antelope Island the succession includes a lower diamictite (Mineral Fork Formation) and an upper unit of dolostone and slate to fine-grained quartz arenite (Kelley Canyon Formation; Doelling et al., 1990; Figs. 18B and 19). These strata were deposited during rifting of western Laurentia, culminating in the North American Cordilleran passive margin, and are unconformably overlain by the Cambrian Tintic Quartzite (Yonkee et al., 2000).

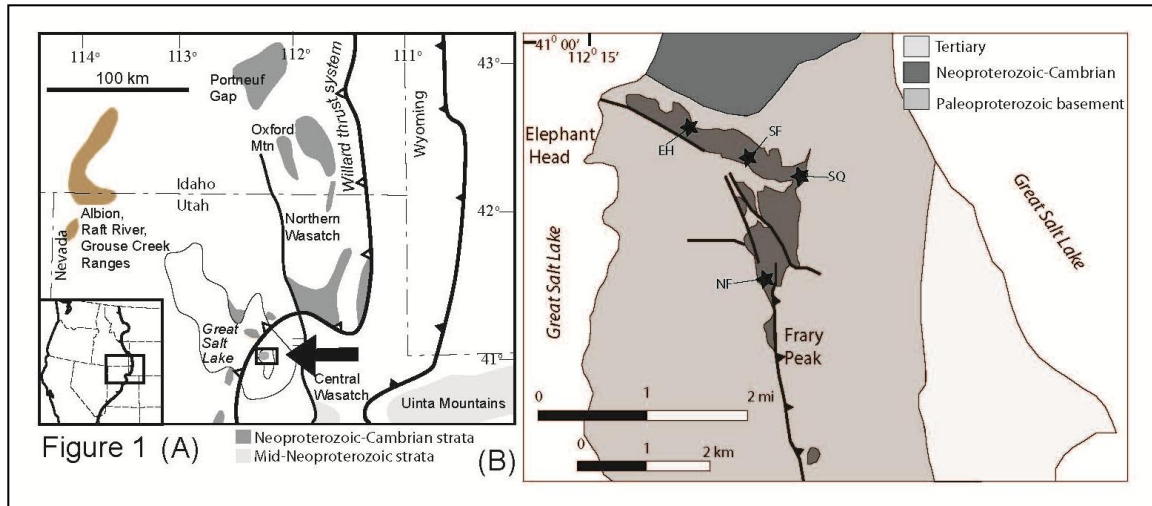


Figure 18. Antelope Island location map. (A) Outcrop distribution of Neoproterozoic to basal Cambrian strata in N Utah & SE Idaho (see key in Fig. 1B). (B) Locations of measured sections in this study (EH = Elephant Head, SF = S. Frary Trail, SQ = Slate Quarry, NF = N. Frary Peak).

The <3- to 30-m-thick diamictite-bearing Mineral Fork Formation nonconformably overlies Paleoproterozoic basement rocks (Farmington Canyon Complex). The diamictite is massive and contains pebble to boulder (up to 4 m) clasts in a sandy matrix (Yonkee et al., 2000, Yonkee et al., 2012). Clasts are sparse to locally concentrated; one layer contains aligned clasts with flattened tops interpreted to represent a boulder pavement (Fig. 20A). Stratified diamictite, wacke, and mudstone with dropstones that deform and pierce laminations are locally present. An overlying interval of siltstone to quartzite contains local angular pebbles, ripple marks and tool marks (Fig. 20B).

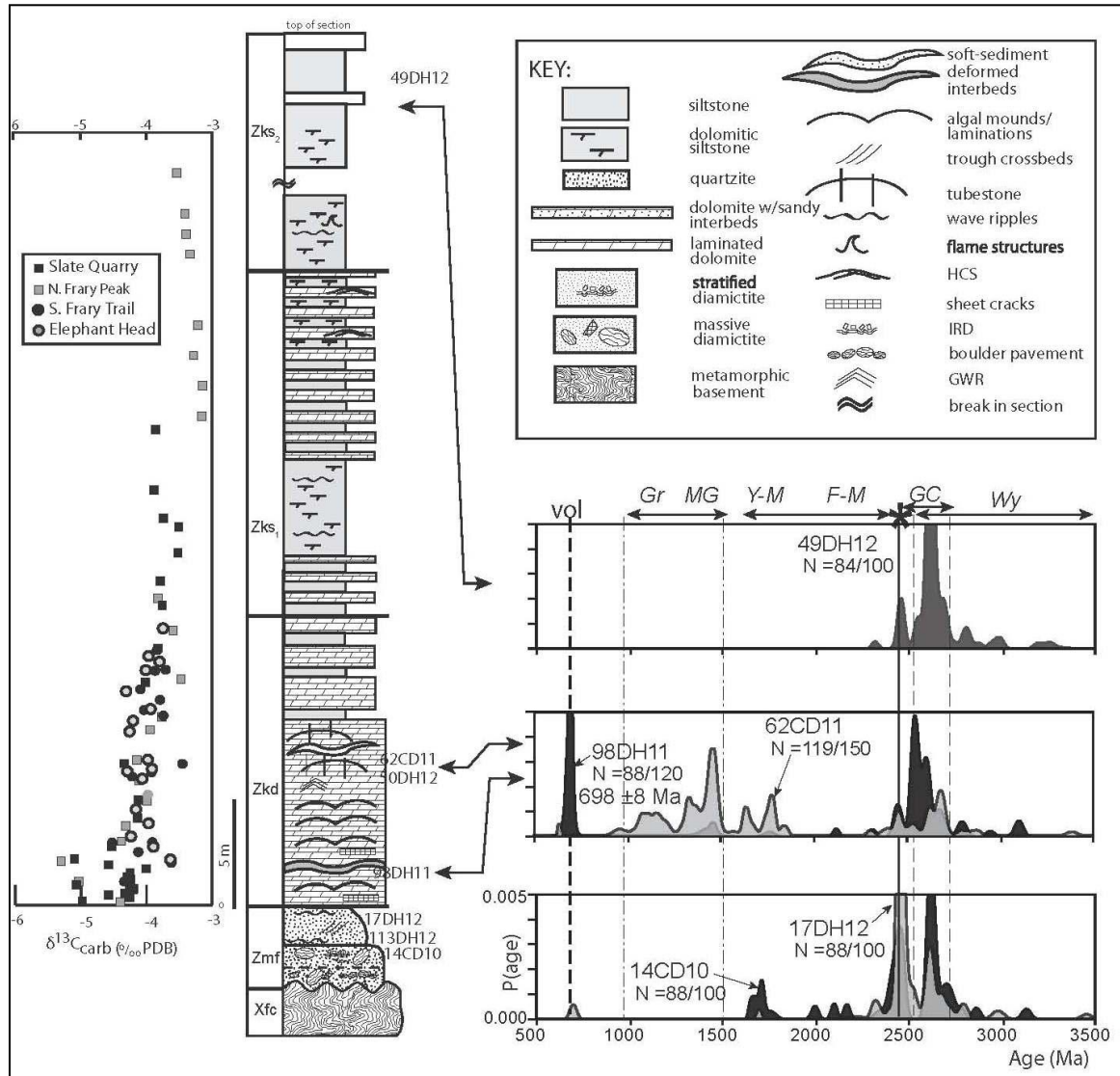


Figure 19. Composite measured section of the Neoproterozoic units on Antelope Island including C-isotope chemostratigraphy and detrital zircon probability density plots. Xfc- Farmington Canyon Complex, Zmf- Mineral Fork Formation.

The 6- to 10-m-thick dolostone member of the Kelley Canyon Formation sharply overlies the diamictite and siltstone-quartzite interval (Fig. 20C). Dolostone is fine-grained and laminated throughout, and displays way to domal structures, brecciated zones with stylolites, sheetcrack cements, giant wave ripples (Fig. 20D),

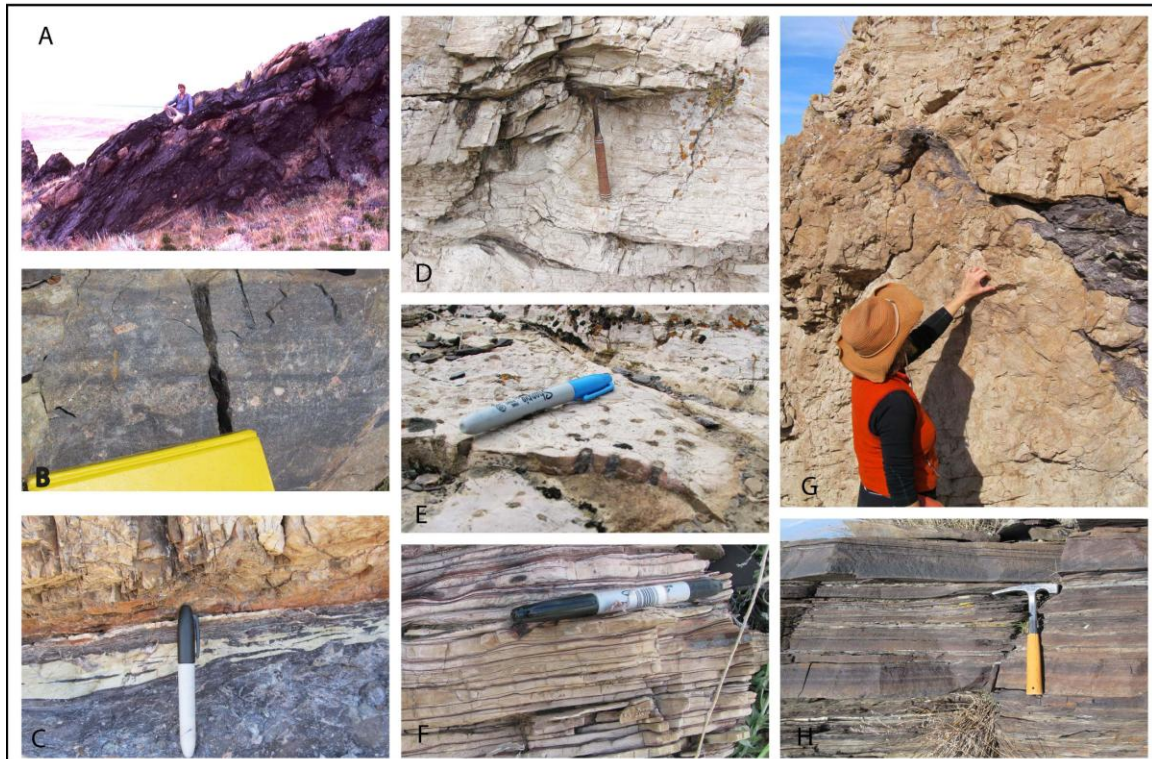


Figure 20. Facies photographs from Antelope Island. (A) Boulder pavement in diamictite, (B) immature quartzite above diamictite, (C) diamictite-cap dolostone contact, (D) giant wave ripple (GWR), (E) tube structures, (F) deformed siliciclastic interbed, (G) lower (dolomitic) slate member, (H) upper slate member.

and distinctive tube structures (Fig. 20E). Locally, dolostone contains disrupted interbeds and sedimentary dikes of purple siltstone and quartzite (Fig. 20F). These thin ($\sim 0.05 - 0.2$ m), discontinuous, contorted interbeds reflect soft sediment deformation and partial injection into the relatively unlithified dolostone. Tectonic veins and fractures related to Cretaceous thrusting locally cross cut sedimentary features. The top of the dolostone member contains silty dolostone to siltstone beds that increase in siliciclastic percentage and bed thickness upwards, grading into the

calcareous lower part of the overlying slate member (Fig. 20G). The upper part of the slate member is mostly thin- to medium-bedded micaceous siltstone and fine-grained quartz arenite (Fig. 20H).

Four stratigraphic sections of the cap carbonate interval were measured and sampled for petrography and stable-isotope analyses (Figs. 18B and 19). The base of the interval comprises buff to pink micropeloidal dolostone that appears massive in weathered outcrops but contains cm-scale laminae visible on fresh surfaces and in thin section. Laminations become more obvious upsection, along with broad domal structures (<0.5 m relief, 0.5-1.0 m wavelength), areas of “frothy” texture where laminae are disrupted, tube structures, and giant wave ripples (Fig. 20D, E, F). Tube structures are concentrated in a ~1-m-thick zone near the top of the dolostone member. They are clustered in m-scale domains separated by areas of laminated strata that lack tubes. Tube structures are generally perpendicular to overall bedding, and in some areas where laminae are gently inclined tube structures appear geoplumb (e.g. Hoffman et al., 2011).

4.4 - Chemostratigraphy

Samples were collected for $\delta^{13}\text{C}$ and $\delta^{18}\text{O}$ analyses at ~1 m intervals within measured stratigraphic sections; higher-resolution samples were collected at ~20 cm intervals in the basal 2 m of the Slate Quarry section (Fig. 19). All samples were processed and analyzed using standard laboratory methods (see supplemental data). $\delta^{13}\text{C}$ values range from -5.10 to -3.51 ‰ VPDB and increase overall upsection in all four sections (Fig. 19). $\delta^{13}\text{C}$ values and $\delta^{18}\text{O}$ values for individual

samples are uncorrelated despite a range in $\delta^{18}\text{O}$ values, supporting the interpretation that $\delta^{13}\text{C}$ values reflect primary or very early diagenetic values (see supplemental data).

4.5 - Detrital zircon geochronology

Six samples were collected from stratigraphic intervals within the Neoproterozoic succession on Antelope Island, including: the Mineral Fork Formation, siliciclastic interbeds in the cap dolostone, and a quartzite in the slate member (Fig. 20). Samples were processed using standard laboratory methods (see supplemental data). Siliciclastic interbeds in the dolostone record input from a wide variety of source areas. A disrupted siltstone interbed (98DH11) contains 2.45 and 2.6–2.8 Ga DZ grains, along with distinctive 2.55 Ga grains interpreted to be sourced from the Grouse Creek block to the west (Strickland et al., 2011) and young (698 ± 8 Ma) grains that give a maximum depositional age and are likely related to synglacial regional felsic volcanism (Balgord et al., in review; Keeley et al., 2013). A sandstone dike (62CD11) in the dolostone has smaller 2.45 and 2.6–2.8 Ga DZ peaks, along with Mesoproterozoic grains.

4.6 - Regional correlations and age constraints

Lithostratigraphic and DZ patterns of Neoproterozoic strata on Antelope Island share similarities with much thicker successions that were deposited to the west, including the Perry Canyon Formation in northern Utah (Balgord et al., in review) and the Pocatello Formation in SE Idaho (Keeley et al., 2013) (see

supplemental data). Both of these formations contain diamictite units overlain by carbonate intervals with negative $\delta^{13}\text{C}$ values comparable to those from Antelope Island (Dehler et al., 2011; Lorentz et al., 2004) and also contain young zircon grains. Zircon grains from a tuffaceous unit in the upper diamictite of the Pocatello Formation record an age of 685.5 ± 0.5 Ma (Keeley et al., 2013) and grains from a reworked tuff above the cap dolostone yield an age of 667 ± 5 Ma (Fanning and Link, 2004). Grains from volcanoclastic sandstone just above the diamictite in the Perry Canyon Formation also have an age of ca. 670 Ma (Balgord et al., in review).

4.7 - Discussion and conclusions

From a sedimentologic perspective, the carbonate interval on Antelope Island more closely resembles a “Marinoan-style” cap than a “Sturtian-style,” and thus could be assumed to have been deposited at ~ 635 Ma and mark the Cryogenian-Ediacaran boundary. However, such lithologic correlations without geochronologic control are problematic, as facies variability in cap carbonate sequences globally could easily lead to erroneous lithologic correlation.

The C-isotope data from the Antelope Island cap carbonate are neither distinctly “Marinoan” nor “Sturtian” style. Unlike the steadily upward-declining $\delta^{13}\text{C}$ values typifying “Marinoan” sequences, the $\delta^{13}\text{C}$ values from Antelope Island vary widely at the base (over $< 1\text{m}$) and then increase. The $\delta^{13}\text{C}$ values do not quickly climb to positive values upsection like those in most “Sturtian” cap carbonate sequences.

With a maximum depositional age of 698 ± 8 Ma, the possibility that the Antelope Island cap carbonate is ~ 635 Ma (“Marinoan”) cannot be ruled out. Correlations with nearby sections in Utah and SE Idaho, however, suggest the diamictite and cap dolostone are older. Dolostone intervals in the Pocatello and Perry Canyon formations with similar C-isotopic signatures as the Antelope Island cap dolostone are overlain by tuffaceous to volcanoclastic beds containing zircon grains with ages of ca. 670 Ma (Balgord et al., in review; Fanning and Link, 2008). Additional support for an older Cryogenian age includes upward younging of zircon U-Pb ages in glacial to post-glacial strata of both the Pocatello and Perry Canyon formations, interpreted to record syndepositional volcanism from ~ 700 -670 Ma (Balgord et al., in review; see supplemental data in Appendix A). Relations in Utah and SE Idaho, combined with the presence of other glacial and cap carbonate sequences of this age (Fanning and Link, 2008; Lund et al., 2010; Zhou et al., 2004), indicate deposition of “Marinoan style” cap carbonates at ~ 665 Ma needs to be considered.

As the GSSP for the base of the Ediacaran period and the top of the evolving Cryogenian period is currently defined globally by the contact between glacial deposits and overlying “Marinoan-style” cap carbonates, the use of lithology and $\delta^{13}\text{C}$ stratigraphy to assign age should be given careful reconsideration. After all, our understanding of what is arguably the most climatologically and biologically dramatic time on Earth – and the geologic timescale itself – depends on it.

4.8 - References

- Allen, P.A., and Etienne, J.L., 2008, Sedimentary challenge to snowball Earth: *Nature Geoscience*, v. 1, p. 817-825.
- Babinski, M., Trindade, R., Alvarenga, C., Boggiani, P., Liu, D., Santos, R., and Brito Neves, B.d., 2006, Chronology of Neoproterozoic ice ages in central Brazil, V: South American Symposium on Isotope Geology, p. 303-306.
- Balgord, E.A., Yonkee, W.A., Link, P.K., and Fanning, C.M., in review, Stratigraphic, geochronologic, and geochemical record of the Cryogenian Perry Canyon Formation, northern Utah: Implications for Rodinian rifting and Snowball Earth glaciation: *Geological Society of America Bulletin*.
- Cloud, P., Wright, L.A., Williams, E.G., Diehl, P., Walter, M.R., 1974, Giant stromatolites and associated vertical tubes from the upper Proterozoic Noonday Dolomite, Death Valley Region, Eastern California: *Geological Society of America Bulletin*, v. 85, p. 1869-1882.
- Condon, D., Zhu, M.Y., Bowring, S., Wang, W., Yang, A.H., and Jin, Y.G., 2005, U-Pb ages from the neoproterozoic Doushantuo Formation, China: *Science*, v. 308, p. 95-98.
- Corsetti, F.A., and Grotzinger, J.P., 2005, Origin and significance of tube structures in Neoproterozoic post-glacial cap carbonates: Example from Noonday Dolomite, Death Valley, United States: *Palaios*, v. 20, p. 348-362.
- Corsetti, F.A., and Lorentz, N.J., 2006, On Neoproterozoic Cap Carbonates as Chronostratigraphic Markers, Neoproterozoic Geobiology and Paleobiology, *in* Xiao, S., and Kaufman, A.J., eds., Volume 27: Topics in Geobiology: Dordrecht, Netherlands, Springer p., 273-294.
- Dehler, C.M., Anderson, K., and Nagy, R., 2011, New descriptions of the cap dolostone and associated strata, Neoproterozoic Pocatello Formation, southeastern Idaho, U.S.A., *in* Evans, J.P., and Lee, J., eds., Geologic Field Trips to the Basin and Range, Rocky Mountains, Snake River Plain, and Terranes of the U.S. Cordillera: *Geological Society of America Field Guide* 21, p. 181-192.
- Doelling, H.H., Willis, G.C., Jensen, M.E., Hecker, S., Case, W.F., and Hand, J.S., 1990, Geologic map of Antelope Island, Davis County, Utah, Utah Geological and Mineral Survey Map 127, 27 p., scale 1:24,000.

- Fanning, C.M., and Link, P.K., 2004, U-Pb SHRIMP ages of Neoproterozoic (Sturtian) glaciogenic Pocatello Formation, southeastern Idaho: *Geology*, v. 32, p. 881-884.
- Fanning, C.M., and Link, P.K., 2008, Age constraints for the Sturtian Glaciation; data for the Adelaide Geosyncline, South Australia and Pocatello Formation, Idaho, USA Selwyn Symposium 2008 GSA Victoria Division, Abstracts 91, p. 57-61.
- Gradstein, F.M., and Ogg, J.G., 2004, Geologic Time Scale 2004 - why, how, and where next!: *Lethaia*, v. 37, p. 175-181.
- Halverson, G.P., 2006, A Neoproterozoic Chronology, *in* Xiao, S.H., and Kaufman, A.J., eds., *Neoproterozoic Geobiology and Paleobiology: Topics in geobiology*: Dordrecht, Netherlands, Springer, p. 300.
- Hegenberger, W., 1987, Gas escape structures in Precambrian peritidal carbonate rocks: *Communications of the Geological Survey of Southwest Africa (Namibia)*, v. 3., p. 62-78.
- Hoffman, P.F., 2011, Strange bedfellows: glacial diamictite and cap carbonate from the Marinoan (635 Ma) glaciation in Namibia: *Sedimentology*, v. 58, p. 57-119.
- Hoffman, P.F., Kaufman, A.J., Halverson, G.P., and Schrag, D.P., 1998, A Neoproterozoic snowball earth: *Science*, v. 281, p. 1342-1346.
- Hoffman, P.F., and Schrag, D.P., 2002, The snowball Earth hypothesis: testing the limits of global change: *Terra Nova*, v. 14, p. 129-155.
- Hoffmann, K.H., Condon, D.J., Bowring, S.A., and Crowley, J.L., 2004, U-Pb zircon date from the Neoproterozoic Ghaub Formation, Namibia: Constraints on Marinoan glaciation: *Geology*, v. 32, p. 817-820.
- Keeley, J.A., Link, P.K., Fanning, C.M., and Schmitz, M.D., 2013, Pre-to synglacial rift-related volcanism in the Neoproterozoic (Cryogenian) Pocatello Formation, SE Idaho: New SHRIMP and CA-ID-TIMS constraints: *Lithosphere*, v. 5, p. 128-150.

- Kendall, B., Creaser, R.A., Calver, C.R., Raub, T.D., and Evans, D.A., 2009, Correlation of Sturtian diamictite successions in southern Australia and northwestern Tasmania by Re–Os black shale geochronology and the ambiguity of “Sturtian”-type diamictite–cap carbonate pairs as chronostratigraphic marker horizons: *Precambrian Research*, v. 172, p. 301-310.
- Kennedy, M.J., Runnegar, B., Prave, A.R., Hoffmann, K.-H., and Arthur, M.A., 1998, Two or four Neoproterozoic glaciations?: *Geology*, v. 26, p. 1059-1063.
- Knoll, A.H., Walter, M.R., Narbonne, G.M., and Christie-Blick, N., 2006, The Ediacaran Period: A new addition to the geologic time scale: *Lethaia*, v. 39, p. 13-30.
- Lorentz, N.J., Corsetti, F.A., and Link, P.K., 2004, Seafloor precipitates and C-isotope stratigraphy from the Neoproterozoic Scout Mountain Member of the Pocatello Formation, southeast Idaho: implications for Neoproterozoic earth system behavior: *Precambrian Research*, v. 130, p. 57-70.
- Lund, K., Aleinikoff, J.N., Evans, K.V., and Fanning, C.M., 2003, SHRIMP U-Pb geochronology of Neoproterozoic Windermere Supergroup, central Idaho: Implications for rifting of western Laurentia and synchronicity of Sturtian glacial deposits: *Geological Society of America Bulletin*, v. 115, p. 349-372
- Lund, K., Aleinikoff, J.N., Evans, K.V., duBray, E.A., Dewitt, E.H., and Unruh, D.M., 2010, SHRIMP U-Pb dating of recurrent Cryogenian and Late Cambrian-Early Ordovician alkalic magmatism in central Idaho: Implications for Rodinian rift tectonics: *Geological Society of America Bulletin*, v. 122, p. 430-453.
- Macdonald, F.A., Schmitz, M.D., Crowley, J.L., Roots, C.F., Jones, D.S., Maloof, A.C., Strauss, J.V., Cohen, P.A., Johnston, D.T., and Schrag, D.P., 2010, Calibrating the Cryogenian: *Science*, v. 327, p. 1241-1243.
- Marenco, P.J., and Corsetti, F.A., 2002, Noonday tubes: observations and reinterpretations based on better preservation from a new locality, *in* Corsetti, F.A., ed., *Proterozoic-Cambrian of the Great Basin and Beyond*, Volume 93: Fullerton, CA, Society for Sedimentary Geology (SEPM) Pacific Section Book, p. 31-42.
- Nogueira, A.C.R., Riccomini, C., Sial, A.N., Moura, C.A.V., and Fairchild, T.R., 2003, Soft-sediment deformation at the base of the Neoproterozoic Puga cap carbonate (southwestern Amazon craton, Brazil): Confirmation of rapid icehouse to greenhouse transition in snowball Earth: *Geology*, v. 31, p. 613-616.

- Rooney, A.D.M., F.M.; Strauss, J.V.; Dudas, F.O.; Hallmann, C.; Selby, D., in review, Weathering the snowball: Geological Society of America Bulletin.
- Strickland, A., Miller, E.L., and Wooden, J.L., 2011, The timing of Tertiary metamorphism and deformation in the Albion–Raft River–Grouse Creek metamorphic core complex, Utah and Idaho: *Journal of Geology*, v. 119, p. 185–206.
- Yonkee, W.A., Willis, G.C., Doelling, H.H., 2000, Proterozoic and Cambrian sedimentary and low-grade metasedimentary rocks on Antelope Island, *in* King, J.K., and Willis, G.C., ed., *The Geology of Antelope Island, Davis County, Utah*: Utah Geological Survey, p. 37-47.
- Yonkee, W.A., Czeck, D.M., Nachbor, A.C., Barszewski, C., Pantone, S., Balgord, E., and Johnson, K.R., 2012, Strain accumulation and fluid-rock interaction in a naturally deformed diamictite, Willard thrust system, Utah (USA): Implications for crustal rheology and strain softening: *Journal of Structural Geology*,
- Zhou, C., Tucker, R., Xiao, S., Peng, Z., Yuan, X., and Chen, Z., 2004, New constraints on the ages of Neoproterozoic glaciations in south China: *Geology*, v. 32, p. 437-440.

CHAPTER 5

GENERAL SUMMARY AND CONCLUSIONS

Redox geochemistry from this study fills an existing knowledge gap in the Proterozoic record of ocean geochemistry (Canfield et al., 2008). The pre-glacial upper part of the Uinta Mountain Group in the area mapped for this study records three relatively short periods of shallow marine anoxia in which ferruginous conditions dominated and euxinia did not occur. This lends support to the Canfield et al. (2008) proposed return of ferruginous subsurface ocean conditions by ~800 Ma, over 100 years before the terminal Proterozoic oxygen enrichment of the oceans. It has been suggested that this change from euxinic to ferruginous subsurface waters, at a large scale (many tens of million years), may have favored eukaryotic expansion (Johnston et al., 2010). There is no evidence, however, that biota (organic-walled microfossil assemblages) in the Leidy/Marsh Peak shale units were influenced by the brief (likely orders of magnitude smaller) anoxic ferruginous events in the paleo-UMG basin. However, when considered at a larger scale the conclusions are different.

Evidence from the composite (vs. just the uppermost) Uinta Mountain Group stratigraphic record suggests a change in biotic assemblages similar to that in the Chuar group. As expected due to the different depositional environments and hypothesized sedimentation rates, the biotic change in the UMG occurs over a much longer section of strata (thousands rather than hundreds of meters). Whether or not this widely spaced biotic change coincides with geochemical indicators of

eutrophication is uncertain, but data from the upper Red Pine Shale suggest a temporary redox shift coincident with a change to very low-diversity biotic assemblages (Hayes, 2010). Additional data from these and the lowermost UMG shale units are needed to test this hypothesis.

This research also lends further support to the correlation of the Uinta Mountain and Chuar Groups - very physically different marine depositional systems that likely shared the same ocean. This provides insight into Neoproterozoic paleogeography and ocean and atmospheric chemistry prior to the most extreme glaciations in the history of our planet – information essential to modeling and understanding how a Snowball Earth could form and persist for millions of years.

In contrast, the study of the post-glacial Antelope Island cap carbonate may enhance our understanding of how Earth responded to the collapse of a Snowball Earth as well as how many Snowball Earth events occurred in the Neoproterozoic Cryogenian Period. The C-isotope, facies, and U-Pb data from this unit raise significant questions about the conventional correlation of post-glacial cap carbonates based solely upon facies and C-isotope curve similarities. Also, the results of this study lend additional support to the possibility of a Snowball Earth glacial-deglacial event ending at ~665 Ma, which would not only change the way these events are correlated, modeled, and understood – it would also change the Precambrian part of the geologic timescale.

REFERENCES

Canfield, D.E., Poulton, S.W., Knoll, A.H., Narbonne, G.M., Ross, G., Goldberg, T., and Strauss, H., 2008, Ferruginous conditions dominated later neoproterozoic deep-water chemistry: *Science*, v. 321, p. 949-952.

Hayes, D.H., 2010, Stratigraphic, microfossil, and geochemical analysis of the Neoproterozoic Uinta Mountain Group: Evidence for a eutrophication event?: Logan, Utah State University

Johnston, D.T., Poulton, S.W., Dehler, C., Porter, S., Husson, J., Canfield, D.E., and Knoll, A.H., 2010, An emerging picture of Neoproterozoic ocean chemistry: Insights from the Chuar Group, Grand Canyon, USA: *Earth and Planetary Science Letters*, v. 290, p. 64-73.

APPENDICES

Appendix A: *Geology* submission data repository items

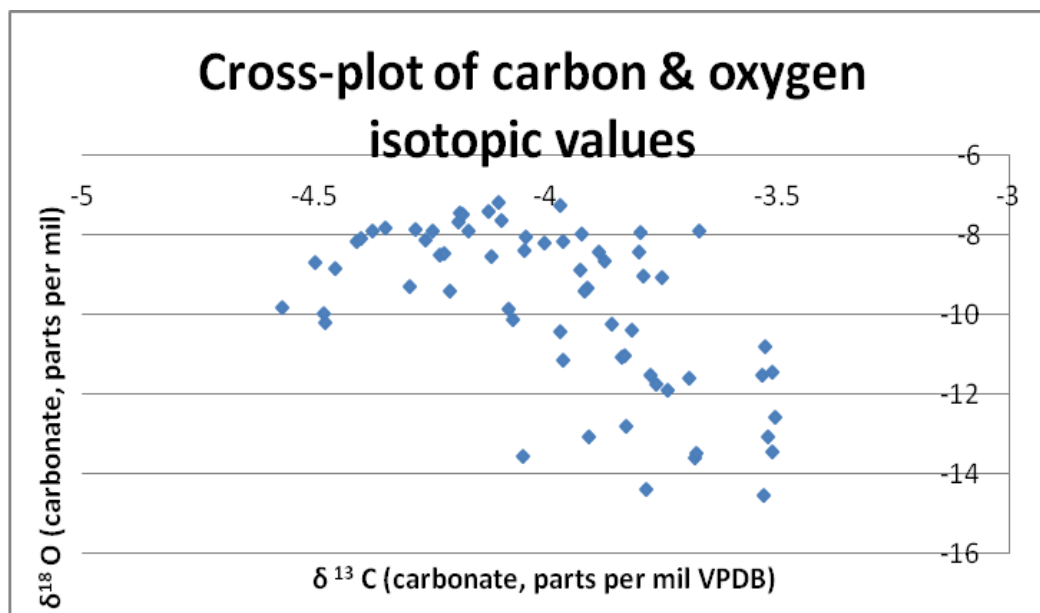
Geology submission data repository items

Procedures for C and O isotope analysis

All samples collected for $\delta^{13}\text{C}$ and $\delta^{18}\text{O}$ analyses were cut perpendicular to lamination to reveal internal textures not visible on weathered surfaces. Approximately 30 – 50 mg of powder were micro-drilled (using a Dremmel Tool) from individual laminations. Veins, stylolites, and lamination boundaries were avoided when drilling. Isotopic analyses were then performed on aliquots of the powders generated by micro-drilling. Carbonate $\delta^{13}\text{C}$ and $\delta^{18}\text{O}$ isotopic data were acquired at the University of New Mexico's Earth and Planetary Sciences Stable Isotope Laboratory using a Delta V Plus Continuous Flow Mass Spectrometer. Approximately 1 mg aliquots of each sample were reacted with phosphoric acid at 50 °C, with an increased reaction time for dolomitic samples, and the evolved CO_2 was then collected and analyzed. Samples were calibrated to VPDB using the Cararra marble standard. A fractionation factor of 1.0106 (after Rosenbaum and Sheppard, 1986) was used for all samples since they were all dolomite rather than calcite. External error (1σ) from standards was better than $\pm 0.1\text{‰}$ for both $\delta^{13}\text{C}$ and $\delta^{18}\text{O}$. Carbon ($\delta^{13}\text{C}$) and oxygen ($\delta^{18}\text{O}$) isotopic results are reported in per mil notation of $^{13}\text{C}/^{12}\text{C}$ and $^{18}\text{O}/^{16}\text{O}$, respectively, relative to the standard VPDB.

Rosenbaum, J., and Sheppard, S.M.F. An isotopic study of siderites, dolomites and ankerites at high temperatures, *Geochimica et Cosmochimica Acta*, Volume 50, Issue 6, June 1986, Pages 1147–1150

Figure DR1



*R-squared value = 0.1073

Results: Table DR1

SAMPLE	d13C	d18O
16aCD10-1	-4.50	-8.69
16aCD10-2	-4.57	-9.82
16eCD10-4	-3.92	-8.88
16fCD10-3	-4.08	-9.86
16gCD10-1	-4.48	-10.18
16gCD10-2	-4.48	-9.96
16gCD10-3	-4.08	-20.73
17CD10	-3.51	-13.43
18aCD10-1	-3.97	-10.40
18aCD10-2	-4.07	-10.10
18cCD10	-3.83	-12.79
18dCD10-1	-3.84	-11.07
18dCD10-2	-3.69	-11.57
18eCD10-2	-3.83	-11.01
18eCD10-3	-3.76	-11.74
18eCD10-4	-3.77	-11.49
18fCD10-1	-3.53	-11.51
18fCD10-2	3.84	2.88
18fCD10-3	-3.52	-10.81
18fCD10-4	-3.51	-11.45
18gCD10-4	-3.74	-11.88
18hCD10-1	-3.81	-10.38
18hCD10-2	-3.96	-11.12
18iCD10-2	-3.86	-10.24
19aCD10-1	-4.19	-7.43
19aCD10-1	-4.10	-7.16
19aCD10-10	-3.80	-7.93
19aCD10-11	-3.67	-7.87
19aCD10-12	-3.92	-7.97
19aCD10-13	-3.50	-12.57
19aCD10-2	-4.12	-7.41
19aCD10-2	-3.97	-7.26
19aCD10-3	-4.41	-8.17
19aCD10-4	-4.37	-7.89
19aCD10-5	-4.17	-7.90
19aCD10-6	-4.24	-7.89
19aCD10-7	-4.40	-8.07
19aCD10-8	-4.34	-7.82
19bCD10-2	-4.05	-8.39
19bCD10-3	-4.28	-7.87
19bCD10-4	-4.26	-8.13
19cCD10-1	-4.19	-7.67
19cCD10-3	-4.18	-7.48
19cCD10-4	-4.10	-7.62
7DH10d	-3.96	-8.15

7DH10e	-3.79	-9.02
7DH10f	-4.00	-8.20
7DH10g	-3.89	-8.40
7DH10h	-4.12	-8.52
7DH10i	-3.78	-14.39
7DH10j	-3.87	-8.65
7DH10k	-3.91	-13.04
7DH10l	-4.04	-8.06
Altube1a	-3.80	-8.41
Altube1b	-3.68	-13.57
Altube1c2	-3.53	-14.54
Altube1c3	-4.23	-8.49
Altube1d1	-4.45	-8.84
Altube1d2	-3.75	-9.06
Altube1e	-4.21	-9.42
Altube2a	-3.52	-13.05
Altube2b1	-3.91	-9.31
Altube2d4	-4.29	-9.27
Altube2d5	-3.92	-9.38
Altube2d6	-3.67	-13.47
Altube2d7	-4.22	-8.46
Altube2d8	-4.05	-13.56
Carrara	2.15	-0.97
Carrara	2.09	-1.45
Carrara	2.06	-1.84
Carrara	2.00	-1.73
Carrara	1.96	-1.87
Carrara	1.93	-2.08
Carrara	1.92	-1.98
Carrara	1.97	-1.93
Carrara	2.03	-1.71
Carrara	1.84	-2.02
Carrara	1.77	-2.12
Carrara	2.17	-1.47
Carrara	2.09	-1.93
03 DH11	-3.41	-9.18
05 DH11	-3.68	-8.84
06 DH11	-4.04	-10.06
07 DH11	-3.73	-9.53
08 DH11	-3.95	-9.09
09 DH11	-3.85	-9.97
10 DH11	-4.07	-10.21
11 DH11	-3.69	-9.54
12 DH11	-3.78	-9.68
14 DH11	-4.02	-9.47
15 DH11	-3.99	-11.00
16 DH11	-3.70	-10.95

17 DH11	-4.09	-10.98
18 DH11	-3.78	-10.31
19 DH11	-3.58	-10.53
20 DH11	-3.74	-10.26
21 DH11	-3.54	-11.42
01DH12	-4.21	-12.16
02DH12	-4.61	-9.62
03DH12	-4.43	-8.74
05DH12	-3.71	-8.51
06DH12	-4.01	-9.68
07DH12	-4.34	-9.34
08DH12	-3.58	-8.49
09DH12	-4.04	-9.92
10DH12	-3.85	-10.13
11DH12	-4.12	-10.26
12DH12	-3.87	-12.16
13DH12	-4.21	-10.56
14DH12	-3.94	-10.55
15DH12	-3.92	-10.81
16DH12	-3.80	-11.27
18DH12	-4.40	-10.67
19DH12	-4.20	-10.29
20DH12	-5.03	-9.13
21DH12	-5.30	-8.57
22DH12	-4.38	-9.95
23DH12	-4.31	-10.52
24DH12	-3.99	-9.66
25DH12	-4.11	-10.31
26DH12	-4.15	-9.02
28DH12	-3.94	-9.03
29DH12	-3.76	-11.15
31DH12	-3.47	-11.43
33DH12	-3.59	-13.34
34DH12	-3.82	-13.25
36DH12	-3.15	-11.57
37DH12	-3.14	-13.08
38DH12	-3.28	-12.56
39DH12	-3.21	-12.02
42DH12	-3.33	-11.22
43DH12	-3.39	-11.75
44DH12	-3.41	-12.01
45DH12	-3.54	-11.46

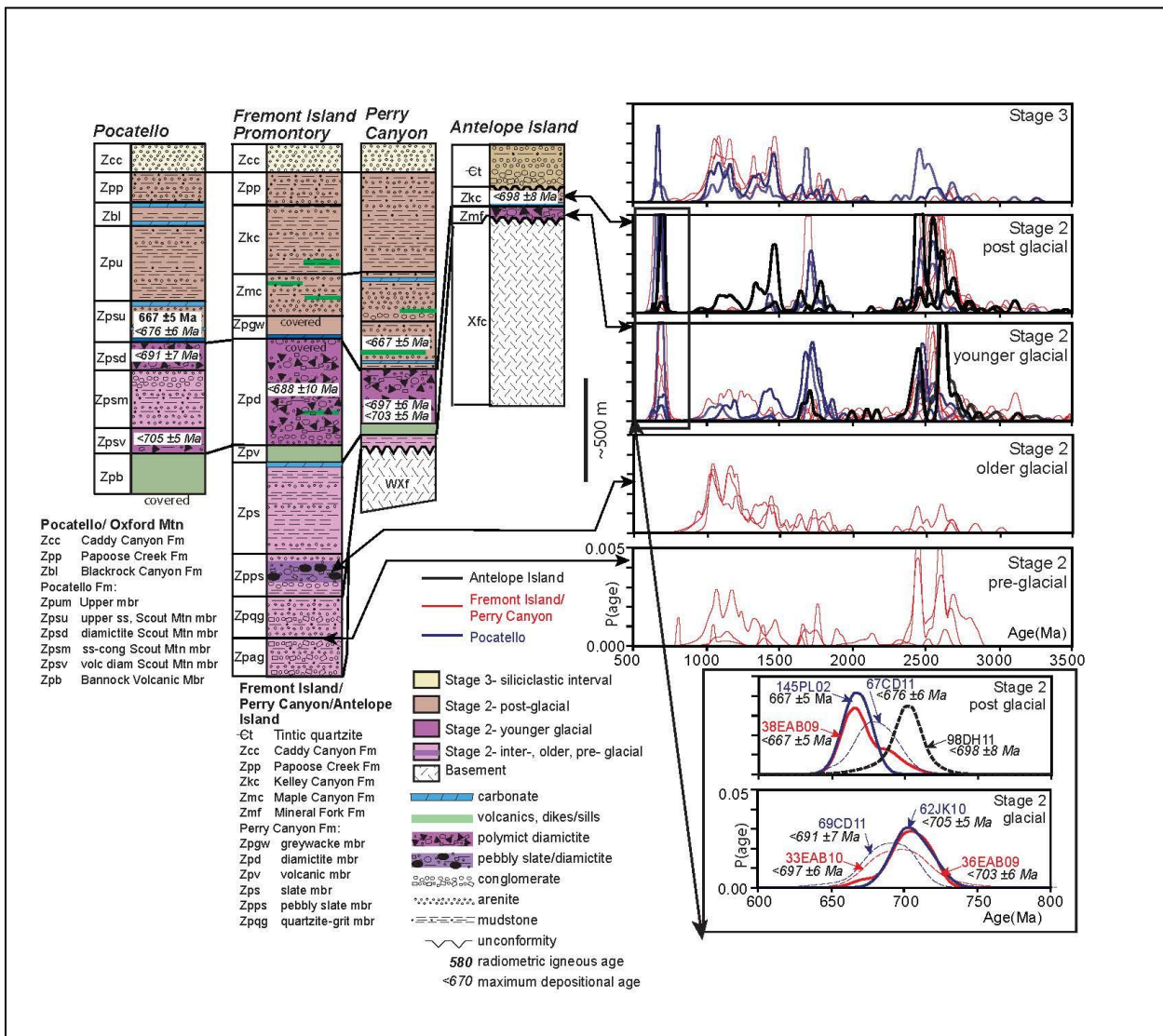
Procedures for detrital zircon U-Pb analysis

Zircon crystals were extracted from samples at Utah State University and Boise State University by traditional methods of crushing and grinding, followed by separation with a Rogers water table, heavy liquids (methylene iodide), and a Frantz magnetic separator. Generally, 500-1000 zircon grains (or as many as can be obtained in rare cases) were incorporated into a 1-inch-radius epoxy mount together with fragments of the Sri Lankan zircon standard. Prior to isotopic analysis, mounts were sanded to ~20 micron depth, polished, imaged, and then cleaned. U-Pb analyses were conducted by laser ablation- multicollector- inductively coupled plasma mass spectrometry (LA-MC-ICPMS) at the Arizona LaserChron Center. Laser ablation of zircon grains was accomplished with a New Wave UP193HE Excimer laser (operating at a wavelength of 193 nm) using a spot diameter of 30 microns, with ablated material then carried (in He gas) into the plasma source of a Nu HR ICPMS, where U, Th, and Pb isotopes were measured simultaneously. Measurements were made in static mode, using Faraday detectors with 3×10^{11} ohm resistors for ^{238}U , ^{232}Th , ^{208}Pb - ^{206}Pb , and discrete dynode ion counters for ^{204}Pb and ^{202}Hg . Each analysis consisted of one 15-second integration on peaks with the laser off (for determination of background levels), 15 one-second integration with the laser firing, and a 30 second delay to purge the previous sample and prepare for the next analysis. ^{204}Hg interference with ^{204}Pb was accounted for by measurement of ^{202}Hg during laser ablation and subtraction of ^{204}Hg according to the natural $^{202}\text{Hg}/^{204}\text{Hg}$ of 4.35, and a Hg correction was applied when necessary. Common Pb correction was accomplished using the Hg-corrected ^{204}Pb and assuming initial Pb compositions from Stacey and Kramers (1975). Uncertainties of ± 1.5 for initial $^{206}\text{Pb}/^{204}\text{Pb}$ and ± 0.3 for $^{207}\text{Pb}/^{204}\text{Pb}$ were applied to assumed compositions based on variation in Pb isotopic compositions in modern crustal rocks. Analysis of fragments of a Sri Lanka zircon standard with known age of 563.5 ± 3.2 Ma (2-sigma error occurred every fifth measurement and were used to correct for Pb/U and Pb isotope fractionation). Analyses >20% discordant (by comparison of $^{206}\text{Pb}/^{238}\text{U}$ and $^{206}\text{Pb}/^{207}\text{Pb}$ ages) or >5% reverse discordant were not included in the results. Data are shown on concordia diagrams and age-probability diagrams using Isoplot (Ludwig, 2008). Age-probability diagrams combine age and uncertainty as a normal distribution for each grain, and then sum distributions from all grains into a single sample distribution. Composite age probability plots will then be made using an Excel program (available from www.geo.arizona.edu/alc).

Stacey, J.S., Kramers, J.D., 1975, Approximation of terrestrial lead isotope evolution by a two stage model: *Earth and Planetary Science Letters*, v. 26, p. 207-221.

Ludwig, K. 2008. Isoplot 3.60, Berkley Geochronology Center Special Publication No. 4, 77p.

Figure DR2



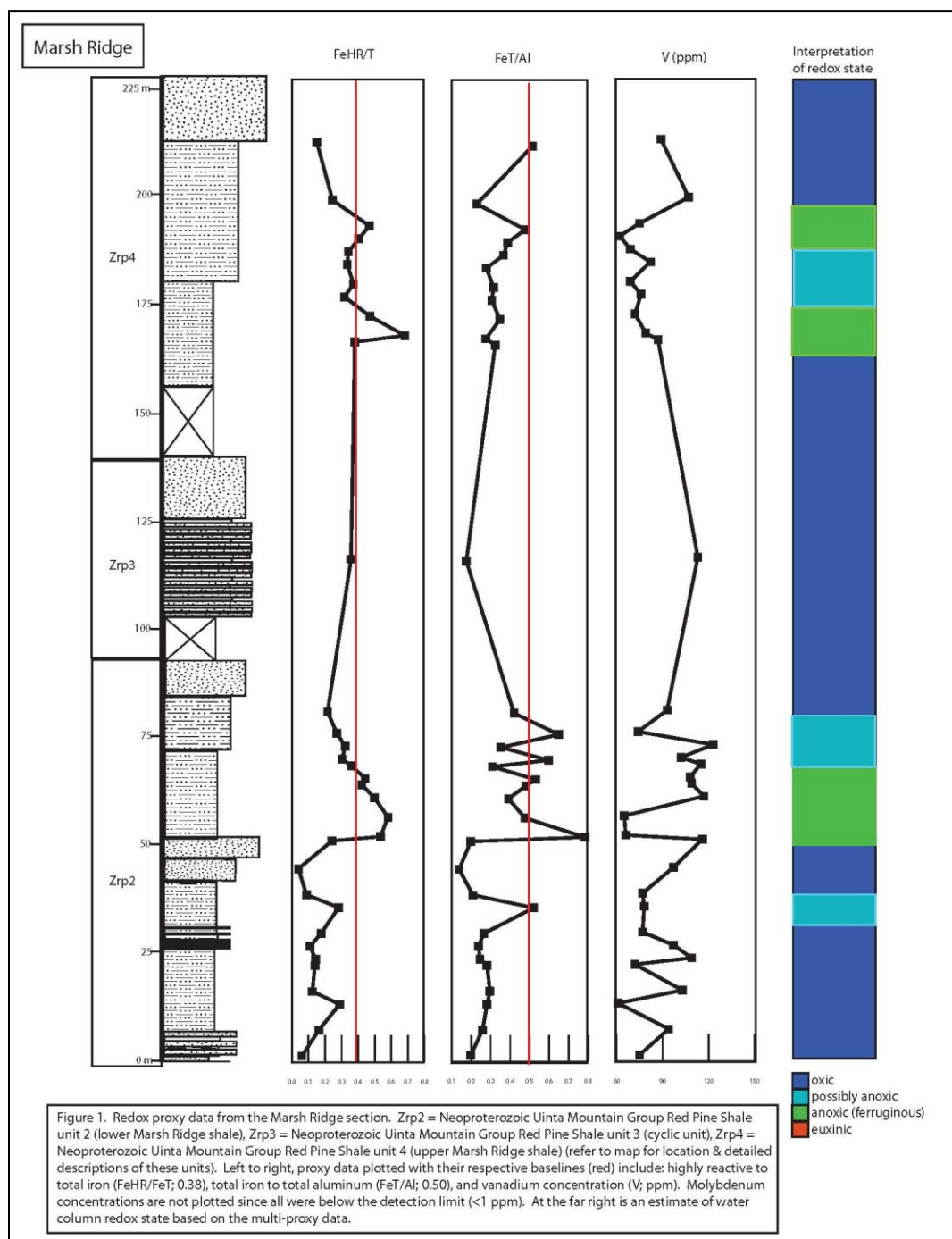
Appendix B: *Precambrian Research* submission data repository items

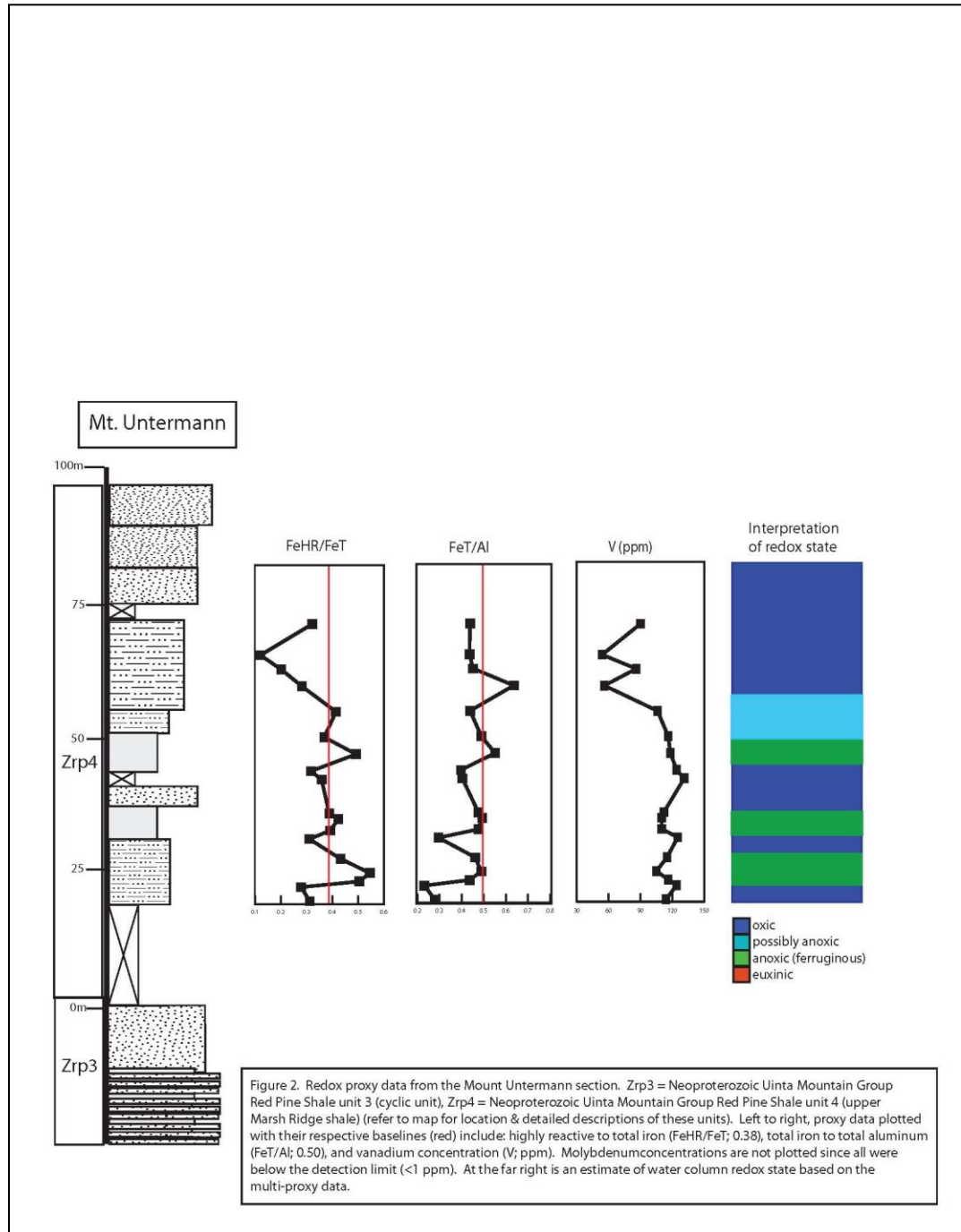
Precambrian Research submission data repository items

Point count data

Sample #	Description	%quartz	%Kspar	%plag	%lithics	%mica	%clay matrix	%other
29DH11	hand sample -coarse arkosic arenite	51	21	18	0	3	5	2
115DH12	hand sample - yellowish arkosic to qtz arenite near top of measured section	75	13	7	0	2	3	0
112DH12	DZ sample -greenish fss w/ x-bedding just below measured sec, above Hades	83	1	0	0	2	14	0
111DH12	DZ sample -sed-struct-rich layer just below measured sec, above red cliffy ss	89	4	1	0	1	6	0
27DH11	hand sample - fine upper to medium lower purple-red quartz arenite w/ some granular layers	99	0	0	0	0	2	0

Redox proxy data





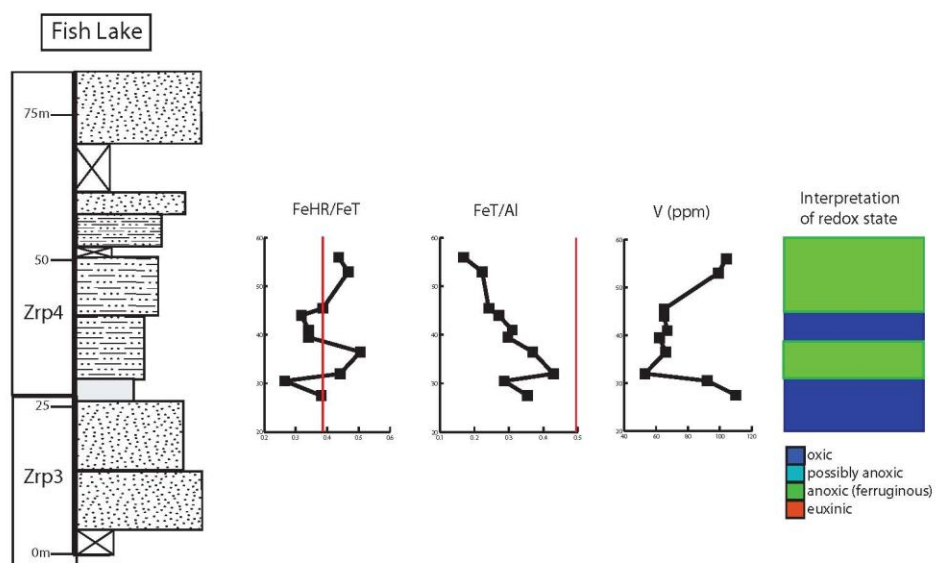


Figure 3. Redox proxy data from the Fish Lake section. Zrp3 = Neoproterozoic Uinta Mountain Group Red Pine Shale unit 3 (cyclic unit), Zrp4 = Neoproterozoic Uinta Mountain Group Red Pine Shale unit 4 (upper Marsh Ridge shale) (refer to map for location & detailed descriptions of these units). Left to right, proxy data plotted with their respective baselines (red) include: highly reactive total iron (FeHR/FeT; 0.38), total iron to total aluminum (FeT/Al; 0.50), and vanadium concentration (V; ppm). Molybdenum concentrations are not plotted since all were below the detection limit (<1 ppm). At the far right is an estimate of water column redox state based on the multi-proxy data.

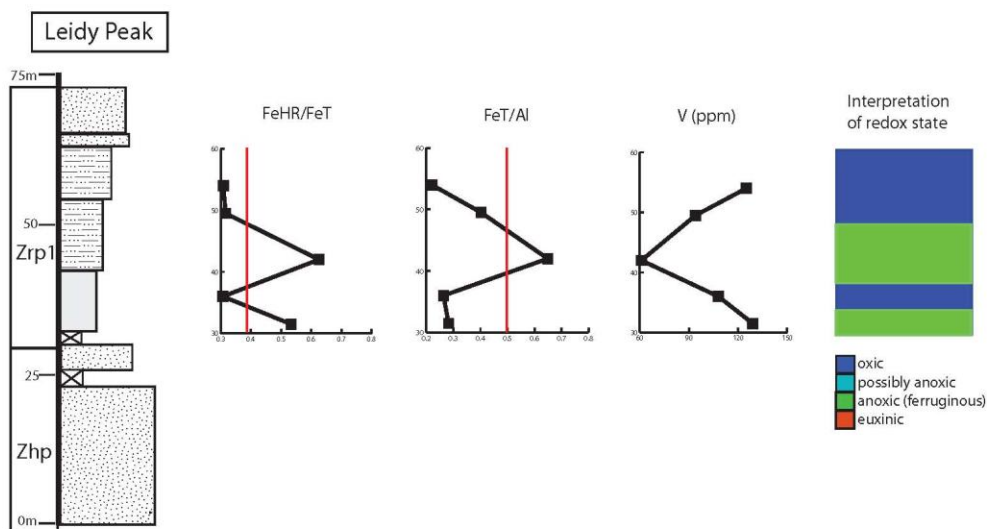


Figure 4. Redox proxy data from the Leidy Peak section. Zhp = Neoproterozoic Uinta Mountain Group formation of Hades Pass, Zrp1 = Neoproterozoic Uinta Mountain Group Red Pine Shale unit 1 (Leidy Peak shale), (refer to map for location & detailed descriptions of these units). Left to right, proxy data plotted with their respective baselines (red) include: highly reactive total iron (FeHR/FeT; 0.38), total iron to total aluminum (FeT/Al; 0.50), and vanadium concentration (V; ppm). Molybdenum concentrations are not plotted since all were below the detection limit (<1 ppm). At the far right is an estimate of water column redox state based on the multi-proxy data.

Iron speciation data

Locality/Section	Sample #	Meters in section	Lab	Fe-acetate %	Fe-dithionite %	Fe-oxalate %	Fe-pyr %	FeT (%)
Box Canyon	DHBCB1	0.5	Johnston	0.19	0.52	0.30	0.00	4.37
Box Canyon	DHBCB1	0.5	Lyons					
Box Canyon	DHBCB2	1.5	Lyons					
Box Canyon	DHBCC3	3	Johnston	0.05	0.53	0.17	0.03	3.15
Box Canyon	DHBCC3	3	Lyons					
Box Canyon	DHBCC4	4.5	Lyons					
Box Canyon	DHBCB4	4.5	Lyons					
Box Canyon	DHBCC6	7.5	Johnston	0.04	1.59	0.23	0.00	3.36
Box Canyon	DHBCC6	7.5	Lyons					
Box Canyon	DHBCC7	9	Lyons					
Box Canyon	DHBCC10	15	Lyons					
Box Canyon	DHBCC14	21	Johnston	0.08	0.56	0.24	0.00	3.34
Box Canyon	DHBCC14	21	Lyons					
Box Canyon	DHBCC16	24	Lyons					
Box Canyon	DHBCC18	28.5	Lyons					
Box Canyon	DHBCC21	34.5	Johnston	0.04	0.58	0.06	0.00	2.61
Box Canyon	DHBCC21	34.5	Lyons					
Box Canyon	DHBCC24	42	Lyons					
Fish Lake	92DH12	27.5	Johnston	0.08	1.20	0.43	0.00	4.49
Fish Lake	94DH12	30.5	Johnston	0.06	0.58	0.23	0.00	3.32
Fish Lake	95DH12	32	Johnston	0.11	1.07	0.17	0.00	3.09
Fish Lake	99DH12	36.5	Johnston	0.07	1.42	0.18	0.00	3.3
Fish Lake	101DH12	39.5	Johnston	0.09	0.61	0.17	0.00	2.55
Fish Lake	102DH12	41	Johnston	0.06	0.62	0.23	0.00	2.66
Fish Lake	104DH12	44	Johnston	0.06	0.54	0.17	0.01	2.42
Fish Lake	105DH12	45.5	Johnston	0.04	0.63	0.13	0.00	2.1
Fish Lake	107DH12	53	Johnston	0.03	0.81	0.22	0.00	2.27
Fish Lake	109DH12	56	Johnston	0.13	0.73	0.02	0.00	2.02
Leidy	DHLPA1	31.5	Johnston	0.02	1.66	0.10	0.00	3.36
Leidy	DHLPA4	36	Johnston	0.03	0.72	0.14	0.00	2.9
Leidy	DHLPA8	42	Johnston	0.05	2.30	0.52	0.00	4.58
Leidy	DHLPA13	49.5	Johnston	0.05	0.81	0.39	0.00	3.95

Leidy	DHLPA16	54	Johnston	0.03	0.70	0.11	0.00	2.71
Leidy Peak	DHLPA1	31.5	Lyons					
Leidy Peak	DHLPA3	34.5	Lyons					
Leidy Peak	DHLPA4	36	Lyons					
Leidy Peak	DHLPA6	39	Lyons					
Leidy Peak	DHLPA8	42	Lyons					
Leidy Peak	DHLPA11	46.5	Lyons					
Leidy Peak	DHLPA13	49.5	Lyons					
Leidy Peak	DHLPA14	51	Lyons					
Leidy Peak	DHLPA16	54	Lyons					
Leidy Peak	DHLPA17	55.5	Lyons					
Marsh Ridge 1	29DH11	1.5	Johnston	0.02	0.04	0.07	0.00	2.13
Marsh Ridge 1	31DH11	7.5	Johnston	0.02	0.23	0.09	0.01	2.15
Marsh Ridge 1	35DH11a	13.5	Johnston	0.02	0.42	0.06	0.00	1.75
Marsh Ridge 1	38DH11	16.5	Johnston	0.02	0.20	0.08	0.00	2.38
Marsh Ridge 1	41DH11	22.5	Johnston	0.03	0.15	0.08	0.00	1.82
Marsh Ridge 1	42DH11	24	Johnston	0.02	0.25	0.06	0.00	2.34
Marsh Ridge 1	44DH11	27	Johnston	0.02	0.15	0.06	0.00	2.12
Marsh Ridge 1	46DH11	30	Johnston	0.02	0.27	0.05	0.00	1.97
Marsh Ridge 1	47DH11	36	Johnston	0.05	0.82	0.26	0.00	4.04
Marsh Ridge 1	48DH11	39	Johnston	0.02	0.08	0.03	0.00	1.49
Marsh Ridge 1	50DH11	45	Johnston	0.01	0.03	0.00	0.00	1.25
Marsh Ridge 1	51DH11	51.5	Johnston	0.00	0.38	0.11	0.00	2.02
Marsh Ridge 1	52DH11	52.5	Johnston	0.01	1.61	0.77	0.00	4.47
Marsh Ridge 1	55DH11	57	Johnston	0.02	1.27	0.41	0.00	2.93
Marsh Ridge 1	58DH11	61.5	Johnston	0.03	1.19	0.81	0.00	4.07
Marsh Ridge 1	60DH11	64.5	Johnston	0.02	1.16	0.73	0.00	4.53
Marsh Ridge 1	61DH11	66	Johnston	0.02	1.42	0.81	0.00	5.1
Marsh Ridge 1	63DH11	69	Johnston	0.03	0.72	0.36	0.00	3.08
Marsh Ridge 1	64DH11	70.5	Johnston	0.06	1.24	0.45	0.00	5.77
Marsh Ridge 1	70DH11	73.5	Johnston	0.04	0.79	0.57	0.00	4.35
Marsh Ridge 1	72DH11	76.5	Johnston	0.10	0.87	0.36	0.00	4.92
Marsh Ridge 1	74DH11	81.5	Johnston	0.06	0.66	0.33	0.00	4.87
Marsh Ridge 1	76DH11	117	Johnston	0.02	0.57	0.10	0.00	1.95
Marsh Ridge 2	78DH11	167.5	Johnston	0.02	0.93	0.31	0.00	3.33
Marsh Ridge 2	79DH11	169	Johnston	0.04	1.61	0.13	0.00	2.62
Marsh Ridge 2	81DH11	173.5	Johnston	0.03	1.00	0.40	0.00	3.03
Marsh Ridge 2	82DH11	178	Johnston	0.05	0.59	0.24	0.00	2.77
Marsh Ridge 2	83DH11	181	Johnston	0.06	0.64	0.22	0.00	2.5
Marsh Ridge 2	85DH11	185.5	Johnston	0.03	0.64	0.21	0.00	2.64
Marsh Ridge 2	86DH11	188.5	Johnston	0.03	0.62	0.37	0.00	3

Marsh Ridge 2	87DH11	191.5	Johnston	0.03	0.77	0.44	0.00	3.1
Marsh Ridge 2	88DH11	194.5	Johnston	0.09	1.36	0.54	0.00	4.26
Marsh Ridge 2	90DH11	200.5	Johnston	0.03	0.45	0.10	0.00	2.34
Marsh Ridge 2	92DH11	214	Johnston	0.06	0.37	0.26	0.00	4.58
Nameless Creek	65DH11	0	Johnston	0.15	0.40	0.21	0.01	3.4
Nameless Creek	66DH11	1.5	Johnston	0.06	0.48	0.33	0.00	3.21
Nameless Creek	67DH11	3	Johnston	0.05	0.73	0.28	0.00	3.1
Untermann	52DH12	20.5	Johnston	0.08	0.65	0.17	0.00	2.88
Untermann	55DH12	23	Johnston	0.04	0.56	0.11	0.00	2.54
Untermann	56DH12	24	Johnston	0.07	1.54	0.62	0.00	4.44
Untermann	57DH12	25.5	Johnston	0.04	2.06	0.65	0.00	5.03
Untermann	59DH12	28	Johnston	0.03	1.37	0.61	0.00	4.66
Untermann	61DH12a	31.5	Johnston	0.08	0.76	0.16	0.00	3.22
Untermann	63DH12	33	Johnston	0.03	1.11	0.66	0.00	4.61
Untermann	64DH12	35	Johnston	0.05	1.39	0.65	0.00	4.92
Untermann	65DH12	36	Johnston	0.03	1.25	0.47	0.00	4.53
Untermann	66DH12	42	Johnston	0.03	1.03	0.61	0.00	4.68
Untermann	67DH12	43.5	Johnston	0.02	0.79	0.60	0.00	4.48
Untermann	69DH12	46.5	Johnston	0.03	2.32	0.58	0.00	5.95
Untermann	71DH12	49.5	Johnston	0.07	1.23	0.65	0.00	5.28
Untermann	74DH12	54	Johnston	0.04	1.26	0.66	0.00	4.73
Untermann	77DH12	58.5	Johnston	0.06	1.07	0.25	0.00	4.92
Untermann	79DH12	61.5	Johnston	0.10	0.61	0.19	0.00	4.46
Untermann	80DH12	64	Johnston	0.04	0.21	0.15	0.00	3.32
Untermann	81DH12	69.5	Johnston	0.08	1.15	0.20	0.00	4.47

Sample #	Meters in section	Al (%)	Fe/Al	FeHR %	FeP/FeHR	FeHR/T	Al	Fe	Mo	V
DHBCB1	0.5	9.87	0.443	1.012	0.494	0.232	9.87	4.37	<1	78
DHBCB1	0.5		0.399			0.127				
DHBCB2	1.5		0.377			0.121				
DHBCC3	3	12.5	0.252	0.775	3.87	0.246	12.5	3.15	<1	117
DHBCC3	3		0.19			0.156				
DHBCC4	4.5		0.475			0.184				
DHBCB4	4.5		0.39			0.15				
DHBCC6	7.5	11.2	0.3	1.864	4.024	0.555	11.2	3.36	4	124
DHBCC6	7.5		0.297			0.165				
DHBCC7	9		0.137			0.16				
DHBCC10	15		0.55			0.15				
DHBCC14	21	10.1	0.331	0.884	23.76	0.265	10.1	3.34	<1	104
DHBCC14	21		0.322			0.142				
DHBCC16	24		0.437			0.199				
DHBCC18	28.5		0.563			0.149				
DHBCC21	34.5	11.7	0.223	0.691	49.9	0.265	11.7	2.61	1	107
DHBCC21	34.5		0.166			0.137				
DHBCC24	42		0.267			0.16				
92DH12	27.5	12.7	0.354	1.71	16.08	0.381	12.7	4.49	<1	110
94DH12	30.5	11.6	0.286	0.878	34.73	0.265	11.6	3.32	<1	92
95DH12	32	7.19	0.43	1.363	23.48	0.441	7.19	3.09	<1	53
99DH12	36.5	8.94	0.369	1.668	21.88	0.505	8.94	3.3	<1	66
101DH12	39.5	8.59	0.297	0.87	45.43	0.341	8.59	2.55	<1	62
102DH12	41	8.59	0.31	0.908	45.16	0.341	8.59	2.66	<1	67
104DH12	44	8.94	0.271	0.77	57.15	0.318	8.94	2.42	<1	65
105DH12	45.5	8.69	0.242	0.811	56.08	0.386	8.69	2.1	<1	65
107DH12	53	10.2	0.223	1.061	49.96	0.467	10.2	2.27	<1	99
109DH12	56	12	0.168	0.881	63.56	0.436	12	2.02	<1	104
DHLPA1	31.5	11.9	0.282	1.792	17.58	0.533	11.9	3.36	<1	129
DHLPA4	36	11	0.264	0.891	40.4	0.307	11	2.9	<1	108
DHLPA8	42	7.06	0.649	2.866	14.65	0.626	7.06	4.58	<1	61
DHLPA13	49.5	9.81	0.403	1.25	39.61	0.316	9.81	3.95	<1	94
DHLPA16	54	12.3	0.22	0.836	64.56	0.309	12.3	2.71	<1	125
DHLPA1	31.5		0.247			0.197				
DHLPA3	34.5		0.32			0.147				

DHLPA4	36		0.224			0.131				
DHLPA6	39		0.377			0.165				
DHLPA8	42		0.384			0.181				
DHLPA11	46.5		0.381			0.183				
DHLPA13	49.5		0.348			0.143				
DHLPA14	51		0.334			0.151				
DHLPA16	54		0.191			0.17				
DHLPA17	55.5		0.266			0.138				
29DH11	1.5	10.8	0.197	0.129	11.61	0.061	10.8	2.13	0	75
31DH11	7.5	8.31	0.259	0.349	21.46	0.163	8.31	2.15	0	94
35DH11a	13.5	6.21	0.282	0.504	26.79	0.288	6.21	1.75	0	61
38DH11	16.5	8.04	0.296	0.294	56.12	0.124	8.04	2.38	0	103
41DH11	22.5	6.46	0.282	0.253	88.8	0.139	6.46	1.82	0	72
42DH11	24	9.54	0.245	0.332	72.24	0.142	9.54	2.34	0	109
44DH11	27	8.9	0.238	0.233	115.7	0.11	8.9	2.12	0	97
46DH11	30	7.44	0.265	0.348	86.33	0.176	7.44	1.97	0	77
47DH11	36	7.76	0.521	1.137	31.66	0.281	7.76	4.04	0	78
48DH11	39	7.12	0.209	0.131	297	0.088	7.12	1.49	0	77
50DH11	45	9.01	0.139	0.049	913.6	0.039	9.01	1.25	0	97
51DH11	51.5	10.2	0.198	0.488	105.6	0.241	10.2	2.02	0	116
52DH11	52.5	5.71	0.783	2.389	21.98	0.534	5.71	4.47	0	66
55DH11	57	6.15	0.476	1.7	33.52	0.58	6.15	2.93	0	65
58DH11	61.5	10.4	0.391	2.029	30.31	0.498	10.4	4.07	0	117
60DH11	64.5	9.42	0.481	1.91	33.77	0.422	9.42	4.53	0	109
61DH11	66	9.62	0.53	2.257	29.24	0.443	9.62	5.1	0	108
63DH11	69	9.98	0.309	1.103	62.54	0.358	9.98	3.08	0	115
64DH11	70.5	9.67	0.597	1.752	40.25	0.304	9.67	5.77	0	102
70DH11	73.5	12.3	0.354	1.398	52.58	0.321	12.3	4.35	0	123
72DH11	76.5	7.58	0.649	1.337	57.22	0.272	7.58	4.92	0	74
74DH11	81.5	11.6	0.42	1.049	77.71	0.215	11.6	4.87	0	93
76DH11	117	11.1	0.176	0.696	168.1	0.357	11.1	1.95	0	113
78DH11	167.5	10.3	0.323	1.263	132.6	0.379	10.3	3.33	0	87
79DH11	169	9.5	0.276	1.785	94.66	0.681	9.5	2.62	0	79
81DH11	173.5	8.72	0.347	1.429	121.4	0.472	8.72	3.03	0	72
82DH11	178	9.06	0.306	0.878	202.7	0.317	9.06	2.77	1	76
83DH11	181	7.94	0.315	0.929	194.7	0.372	7.94	2.5	0	69
85DH11	185.5	9.49	0.278	0.882	210.2	0.334	9.49	2.64	0	82
86DH11	188.5	8.2	0.366	1.024	184.1	0.341	8.2	3	0	69
87DH11	191.5	8.01	0.387	1.253	152.8	0.404	8.01	3.1	0	62
88DH11	194.5	8.92	0.478	1.993	97.59	0.468	8.92	4.26	0	75
90DH11	200.5	10.2	0.229	0.574	349.2	0.245	10.2	2.34	0	107

92DH11	214	8.9	0.515	0.69	310.2	0.151	8.9	4.58	0	89
65DH11	0	8.27	0.411	0.766	0	0.225	8.27	3.4	<1	70
66DH11	1.5	9.43	0.34	0.866	1.731	0.27	9.43	3.21	<1	89
67DH11	3	8.6	0.36	1.066	2.814	0.344	8.6	3.1	<1	90
52DH12	20.5	10.3	0.28	0.899	22.79	0.312	10.3	2.88	<1	114
55DH12	23	11	0.231	0.708	32.47	0.279	11	2.54	<1	124
56DH12	24	10.2	0.435	2.242	10.7	0.505	10.2	4.44	<1	116
57DH12	25.5	10.3	0.488	2.746	9.285	0.546	10.3	5.03	<1	105
59DH12	28	10.1	0.461	2.014	13.9	0.432	10.1	4.66	<1	115
61DH12a	31.5	10.9	0.295	1.002	31.45	0.311	10.9	3.22	<1	125
63DH12	33	9.69	0.476	1.806	18.27	0.392	9.69	4.61	<1	110
64DH12	35	9.98	0.493	2.084	16.8	0.423	9.98	4.92	<1	110
65DH12	36	9.53	0.475	1.759	20.47	0.388	9.53	4.53	<1	112
66DH12	42	11.6	0.403	1.678	25.03	0.359	11.6	4.68	<1	131
67DH12	43.5	11.3	0.396	1.421	30.62	0.317	11.3	4.48	<1	124
69DH12	46.5	10.8	0.551	2.931	15.87	0.493	10.8	5.95	<1	118
71DH12	49.5	10.8	0.489	1.948	25.41	0.369	10.8	5.28	<1	116
74DH12	54	10.8	0.438	1.959	27.57	0.414	10.8	4.73	<1	106
77DH12	58.5	7.74	0.636	1.387	42.17	0.282	7.74	4.92	<1	56
79DH12	61.5	9.87	0.452	0.898	68.52	0.201	9.87	4.46	<1	86
80DH12	64	7.63	0.435	0.4	160.1	0.12	7.63	3.32	<1	54
81DH12	69.5	10.2	0.438	1.438	48.32	0.322	10.2	4.47	<1	90

Microfossil data

Section	Meters	Sample	Leiosphaerids	Operculosphaerids	Filaments	Colonial forms	<i>E. moorei</i>	<i>S. variabilis</i>	acritarchs	Assemblage
Box Canyon	0.5	DHBCB1	16	1	6	3	0	4	0	Leiosphaerids
Box Canyon	1.5	DHBCB2	15	0	5	2	0	4	0	Leiosphaerids
Box Canyon	3	DHBCC3	20	0	8	0	0	0	0	filaments/leiosphaerids
Box Canyon	4.5	DHBCB4	20	2	9	5	0	3	0	filaments/leiosphaerids
Box Canyon	4.5	DHBCC4	95	0	4	0	0	1	0	Leiosphaerids
Box Canyon	7.5	DHBCC6	33	1	6	1	0	0	5	?ornamented?
Box Canyon	9	DHBCC7	56	0	4	0	0	0	6	Leiosphaerids
Box Canyon	15	DHBCC1	0	0	0	0	0	0	0	barren
Box Canyon	21	DHBCC1	39	0	3	0	0	4	0	filaments/leiosphaerids
Box Canyon	24	DHBCC1	30	0	8	0	0	5	0	Leiosphaerids
Box Canyon	28.	DHBCC1	0	0	0	0	0	0	0	barren
Box Canyon	34.	DHBCC2	0	0	0	0	0	1	0	barren
Box Canyon	5	DHBCC2	73	5	2	1	0	9	0	Leiosphaerids
Box Canyon	42	DHBCC2	50	0	5	0	0	5	0	Leiosphaerids
Fish Lake	5	92DH12	2	0	0	1	0	0	0	barren
Fish Lake	32	95DH12	86	4	4	1	0	1	0	Leiosphaerids
Fish Lake	36.	99DH12	64	0	3	0	0	0	0	Leiosphaerids
Fish Lake	41	102DH1	49	0	7	0	0	0	0	Leiosphaerids
Fish Lake	44	104DH1	10	6	1	0	0	4	1	Leiosphaerids

		2	9	2						
		107DH1		1						
Fish Lake	53	2	83	3	0	4	0	0	0	Leiosphaerids
	31.					1				
Leidy	5	DHLPA1	78	3	2	7	7	0	0	Leiosphaerids
	34.									
Leidy	5	DHLPA3	10	0	0	0	0	0	0	Leiosphaerids
Leidy	36	DHLPA4	61	0	3	5	0	0	0	Leiosphaerids
						1				
Leidy	39	DHLPA6	83	0	7	0	0	0	0	Leiosphaerids
						2				
Leidy	42	DHLPA8	68	0	8	0	0	4	0	Leiosphaerids
	46.	DHLPA1				1		3		
Leidy	5	1	59	0	1	0	0	0	0	Leiosphaerids
	49.	DHLPA1						2		
Leidy	5	3	63	4	5	4	0	5	0	Leiosphaerids
		DHLPA1	24	1	3					
Leidy	51	4	6	3	2	7	0	5	0	Leiosphaerids
		DHLPA1				1		1		
Leidy	54	6	68	0	2	0	0	3	0	Leiosphaerids
	55.	DHLPA1	27		1	2				
Leidy	5	7	5	0	4	5	0	2	0	Leiosphaerids
Marsh	13.	35DH11								
Ridge	5	a	0	0	0	0	0	0	0	barren
Marsh	16.									
Ridge	5	38DH11	25	0	0	0	0	0	0	Leiosphaerids
Marsh										
Ridge	39	48DH11	0	0	0	0	0	0	0	barren
Marsh	52.					1				
Ridge	5	52DH11	83	2	3	2	0	0	0	Leiosphaerids
Marsh	61.					1				
Ridge	5	58DH11	80	5	7	5	0	0	4	Leiosphaerids
Marsh						1				
Ridge	66	61DH11	75	0	8	2	0	3	0	Leiosphaerids
Marsh	70.									
Ridge	5	64DH11	2	1	2	1	0	0	0	barren
Marsh	16					1				
Ridge	9	79DH11	81	0	4	4	0	1	0	Leiosphaerids
Marsh	18					1				
Ridge	1	83DH11	70	8	8	4	0	2	0	Leiosphaerids
Marsh	19									
Ridge	2	87DH11	81	9	8	2	0	0	0	Leiosphaerids
Marsh	20	90DH11	66	6	2	5	0	0	0	Leiosphaerids

Ridge	1				3					
Unterman	24	56DH12	31	0	4	2	0	0	0	Leiosphaerids
Unterman	28	59DH12	90	6	0	4	0	0	0	Leiosphaerids
Unterman	32	62DH12	86	5	2	7	0	0	0	Leiosphaerids
Unterman	42	66DH12	87	1	0	3	0	0	0	Leiosphaerids
Unterman	46.	5	69DH12	18	2	0	0	0	0	Leiosphaerids
Unterman	49.	5	71DH12	82	1	6	2	0	0	Leiosphaerids
Unterman	54	74DH12	77	1	0	7	1	0	0	Leiosphaerids
Unterman	61.	5	79DH12	20	0	0	1	0	0	Leiosphaerids

Diversity index & evenness data

Analysing 7 variables x 48 cases

Shannon's method

Log base e

Sample	Diversity Index		Evenness	Number of taxa
DHBCB1	1.269	0.789	5.000	
DHBCB2	1.120	0.808	4.000	
DHBCC3	0.692	0.998	2.000	
DHBCB4	1.268	0.788	5.000	
DHBCC4	0.224	0.203	3.000	
DHBCC6	0.955	0.593	5.000	
DHBCC7	0.985	0.711	4.000	
DHBCC10	****	****	0.000	
DHBCC14	0.848	0.772	3.000	
DHBCC16	0.814	0.741	3.000	
DHBCC18	****	****	0.000	
DHBCC21	0.819	0.509	5.000	
DHBCC24	0.566	0.515	3.000	
92DH12	0.637		0.918	2.000
95DH12	0.458		0.285	5.000
99DH12	0.183		0.264	2.000
102DH12	0.377	0.544	2.000	
104DH12	0.660	0.410	5.000	
107DH12	0.619	0.446	4.000	
DHLPA1	0.876	0.544	5.000	
DHLPA3	0.000	0.000	1.000	
DHLPA4	0.435	0.396	3.000	
DHLPA6	0.456	0.658	2.000	
DHLPA8	0.747	0.680	3.000	
DHLPA11	0.915	0.833	3.000	
DHLPA13	1.045	0.649	5.000	
DHLPA14	0.696	0.433	5.000	
DHLPA16	0.768	0.699	3.000	
DHLPA17	0.492	0.355	4.000	

35DH11a	****	****	0.000	
38DH11		0.000	0.000	1.000
48DH11	****		****	0.000
52DH11		0.593	0.427	4.000
58DH11		0.940	0.584	5.000
61DH11		0.773	0.558	4.000
64DH11		1.330	0.959	4.000
79DH11		0.705	0.438	5.000
83DH11		0.968	0.602	5.000
87DH11		0.668	0.482	4.000
90DH11		0.931	0.671	4.000
56DH12		0.546	0.497	3.000
59DH12		0.392	0.357	3.000
62DH12		0.544	0.392	4.000
66DH12		0.457	0.416	3.000
69DH12		0.325	0.469	2.000
71DH12		0.534	0.486	3.000
74DH12		0.647	0.467	4.000
79DH12		0.191	0.276	2.000

**** = barren sample

Special t-test for comparing two diversity indices (Zar, 2010):

$$t = \frac{H'_1 - H'_2}{S_{H'_1 - H'_2}}, \text{ where } S_{H'_1 - H'_2} = \sqrt{S^2_{H'_1} + S^2_{H'_2}}$$

$$\text{and } v = \frac{(S^2_{H'_1} + S^2_{H'_2})^2}{\left(\frac{S^2_{H'_1}}{n_1} + \frac{S^2_{H'_2}}{n_2}\right)}$$

H'_1 = Box Canyon diversity index = 0.40412, H'_2 = Leidy/Marsh diversity index = 0.332293

$S^2_{H'_1}$ = Box Canyon variance = 0.000267, $S^2_{H'_2}$ = Leidy/Marsh variance = 7.76E-05

$$t = 3.871168$$

$$v = 317.6804$$

$$t_{0.05(2), 317} = 1.968$$

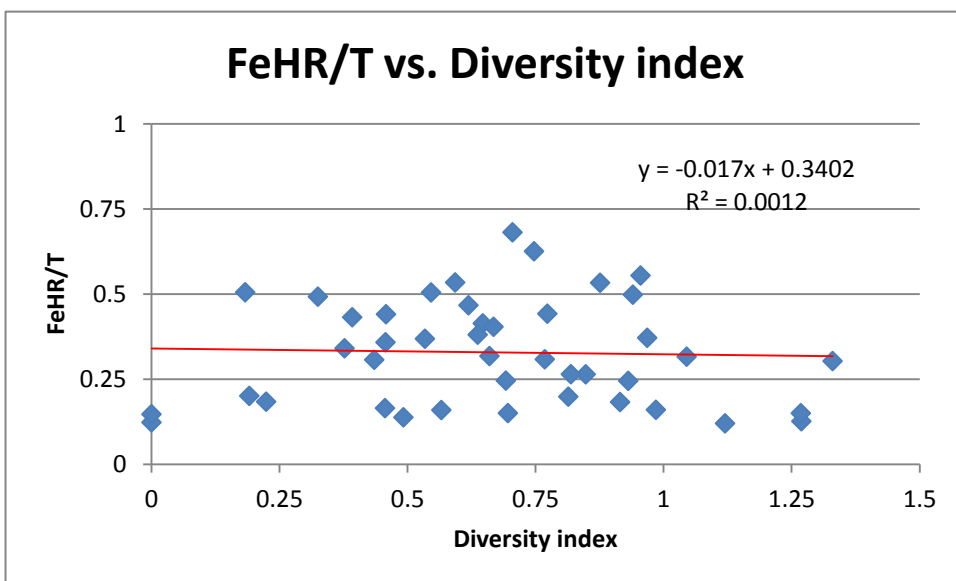
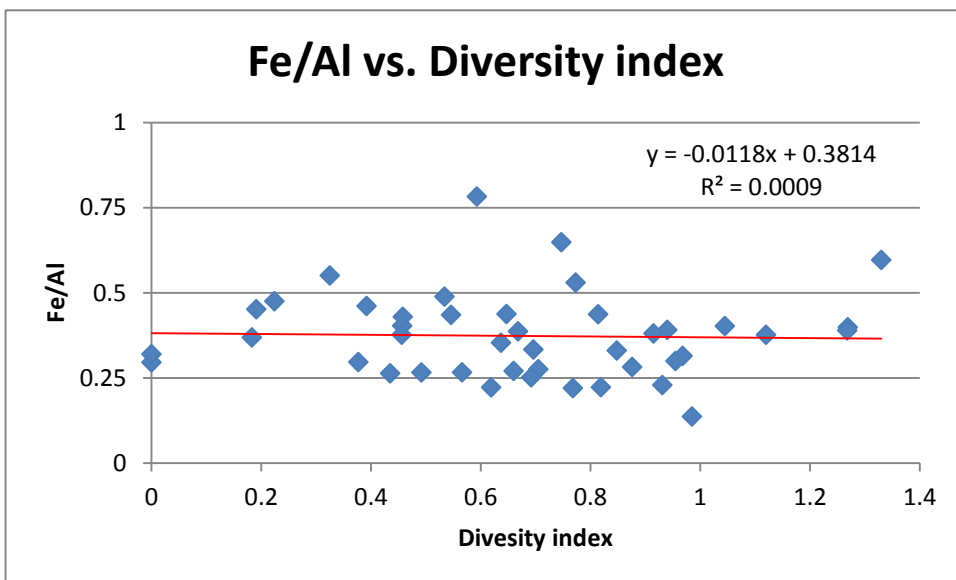
Therefore, the null hypothesis (equal diversity) should be rejected. The conclusion is that the diversity of microfossil taxa in the Box Canyon sections is significantly different from the diversity of microfossil taxa in the Leidy/Marsh Peak sections.

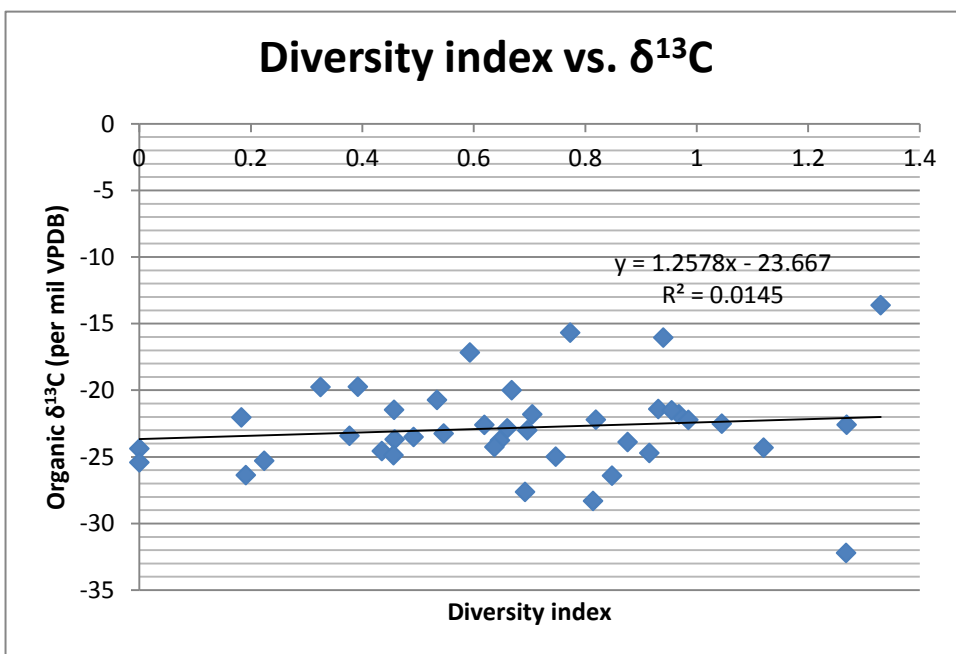
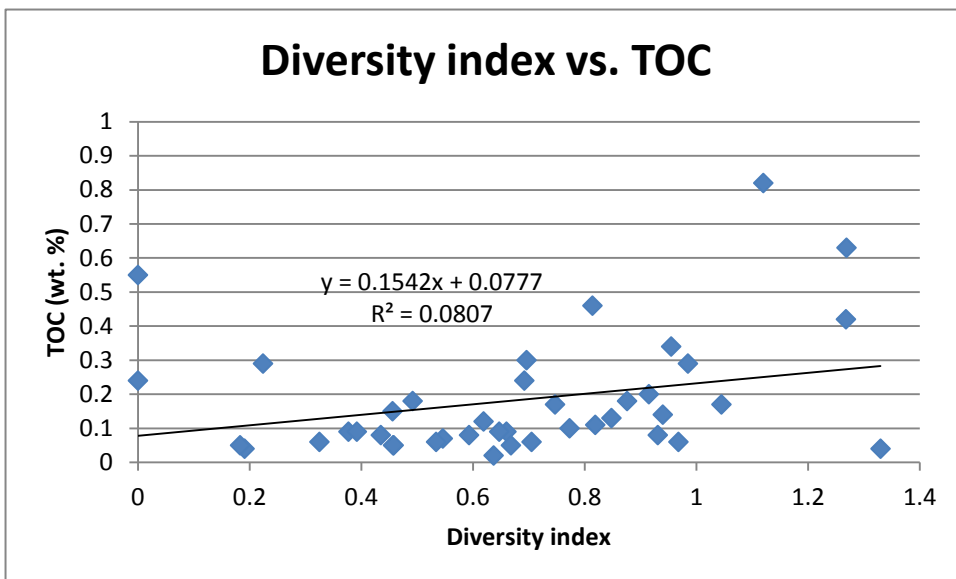
Organic carbon data

Sample #	Locality/Section	Meters	TOC (%)	d13C
DHBCB1	Box Canyon	0.5	0.63	-22.58
DHBCC3	Box Canyon	3	0.25	-26.75
DHBCC6	Box Canyon	7.5	0.31	-20.80
DHBCC14	Box Canyon	21	0.07	-24.41
DHBCC21	Box Canyon	34.5	0.13	-20.53
92DH12	Fish Lake	27.5	0.02	-24.25
94DH12	Fish Lake	30.5	0.04	-23.74
95DH12	Fish Lake	32	0.05	-23.68
99DH12	Fish Lake	36.5	0.05	-22.03
101DH12	Fish Lake	39.5	0.05	-22.84
102DH12	Fish Lake	41	0.09	-23.41
104DH12	Fish Lake	44	0.09	-22.85
105DH12	Fish Lake	45.5	0.08	-22.75
107DH12	Fish Lake	53	0.12	-22.59
109DH12	Fish Lake	56	0.17	-18.70
DHLPA1	Leidy Peak	31.5	0.18	-23.88
DHLPA4	Leidy Peak	36	0.12	-23.77
DHLPA8	Leidy Peak	42	0.08	-22.43
DHLPA13	Leidy Peak	49.5	0.12	-22.18
DHLPA16	Leidy Peak	54	0.24	-21.08
29DH11	Marsh Ridge 1	1.5	0.06	-25.15
31DH11	Marsh Ridge 1	7.5	0.15	-19.38
35DH11a	Marsh Ridge 1	13.5	0.05	-23.94
38DH11	Marsh Ridge 1	16.5	0.55	-24.37
41DH11	Marsh Ridge 1	22.5	0.22	-24.32
42DH11	Marsh Ridge 1	24	0.11	-23.38
44DH11	Marsh Ridge 1	27	0.08	-23.98
46DH11	Marsh Ridge 1	30	0.08	-23.90
47DH11	Marsh Ridge 1	36	0.05	-25.70
48DH11	Marsh Ridge 1	39	0.06	-25.74
50DH11	Marsh Ridge 1	45	0.06	-25.58
51DH11	Marsh Ridge 1	51.5	0.11	-23.41
52DH11	Marsh Ridge 1	52.5	0.08	-17.16
55DH11	Marsh Ridge 1	57	0.09	-19.40
58DH11	Marsh Ridge 1	61.5	0.14	-16.04

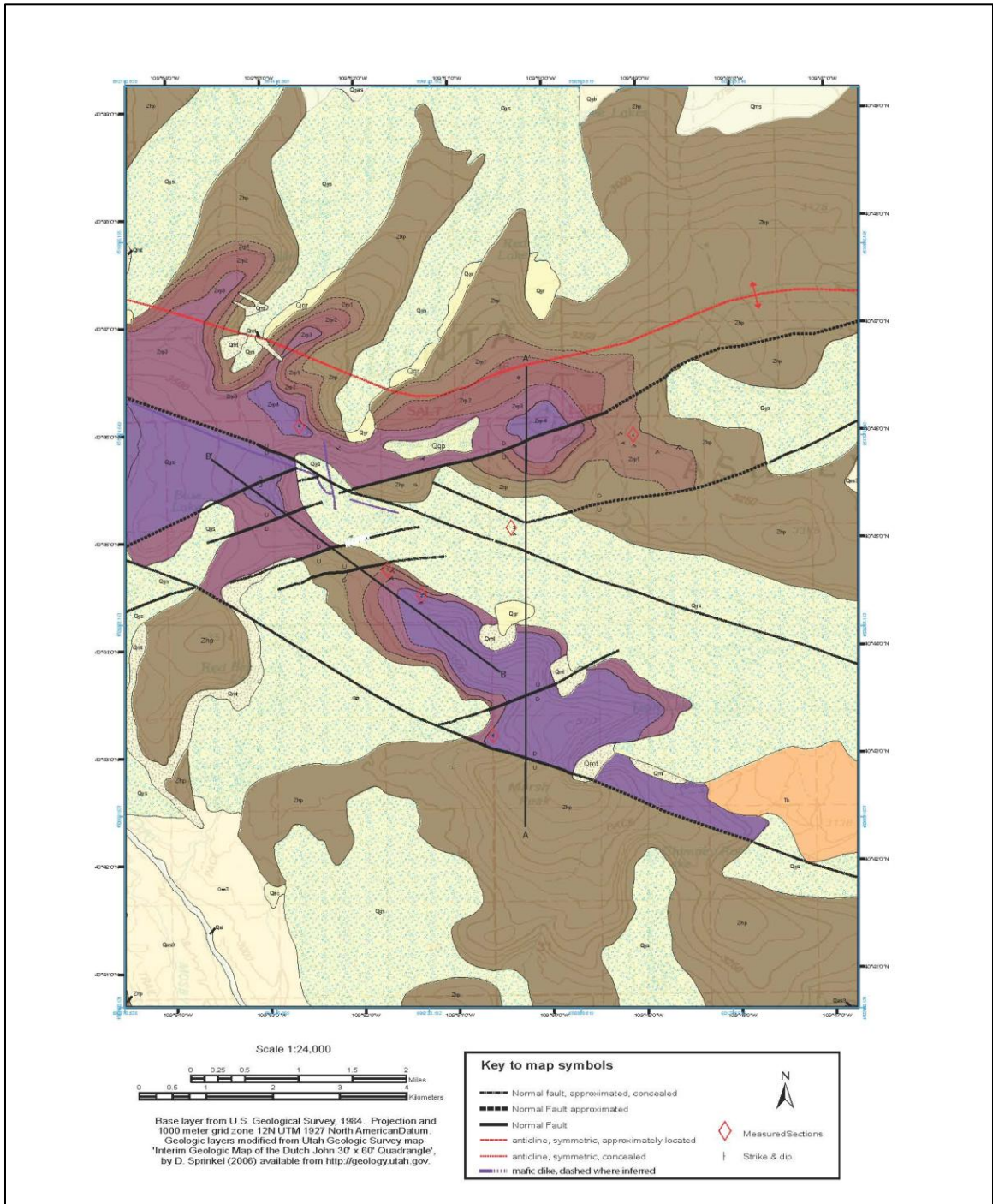
60DH11	Marsh Ridge 1	64.5	0.10	-16.56
61DH11	Marsh Ridge 1	66	0.10	-15.67
63DH11	Marsh Ridge 1	69	0.07	-17.30
64DH11	Marsh Ridge 1	70.5	0.04	-13.61
70DH11	Marsh Ridge 1	73.5	0.13	-18.60
72DH11	Marsh Ridge 1	76.5	0.76	-24.51
74DH11	Marsh Ridge 1	81.5	0.02	-22.09
76DH11	Marsh Ridge 1	117	0.07	-17.40
78DH11	Marsh Ridge 2	167.5	0.05	-21.46
79DH11	Marsh Ridge 2	169	0.06	-21.80
81DH11	Marsh Ridge 2	173.5	0.06	-21.33
82DH11	Marsh Ridge 2	178	0.04	-21.41
83DH11	Marsh Ridge 2	181	0.06	-21.80
85DH11	Marsh Ridge 2	185.5	0.07	-21.22
86DH11	Marsh Ridge 2	188.5	0.07	-21.14
87DH11	Marsh Ridge 2	191.5	0.05	-19.99
88DH11	Marsh Ridge 2	194.5	0.05	-18.40
90DH11	Marsh Ridge 2	200.5	0.08	-21.40
92DH11	Marsh Ridge 2	214	0.03	-25.52
65DH11	Nameless Creek	0	0.06	-23.10
66DH11	Nameless Creek	1.5	0.05	-22.75
67DH11	Nameless Creek	3	0.05	-23.03
55DH12	Untermann	23	0.07	-23.24
56DH12	Untermann	24	0.16	-22.00
57DH12	Untermann	25.5	0.17	-21.28
59DH12	Untermann	28	0.09	-19.73
61DH12a	Untermann	31.5	0.07	-22.84
63DH12	Untermann	33	0.06	-19.72
64DH12	Untermann	35	0.06	-21.66
65DH12	Untermann	36	0.05	-21.32
66DH12	Untermann	42	0.05	-21.46
67DH12	Untermann	43.5	0.06	-21.58
69DH12	Untermann	46.5	0.06	-19.75
71DH12	Untermann	49.5	0.06	-20.72
74DH12	Untermann	54	0.09	-23.75
77DH12	Untermann	58.5	0.03	-23.96
79DH12	Untermann	61.5	0.04	-26.36
81DH12	Untermann	69.5	0.10	-27.48

Correlations

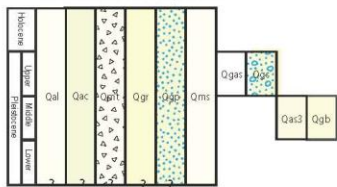




Appendix C: Geologic Map



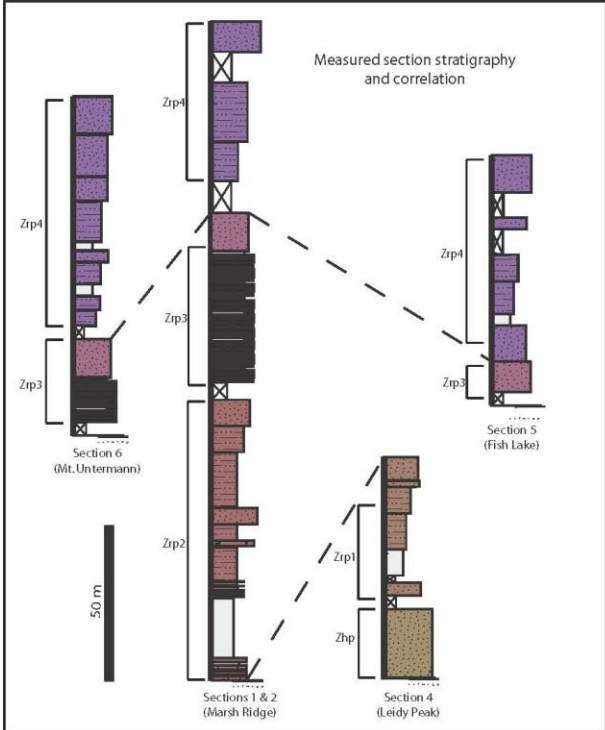
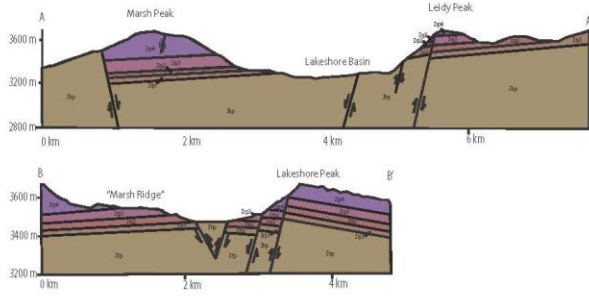
Correlation of Map Units



Description of Map Units

- Qal** Flood-plain alluvium (Holocene) - Unconsolidated silt, sand, and gravel
- Qac** Mixed colluvium and alluvium (Pliocene and Pleistocene) - Unconsolidated, poorly to moderately sorted mud, silt, sand and gravel
- Qm1** Talus deposits (Holocene and Pleistocene) - Unconsolidated, poorly to moderately sorted sand, gravel, cobbles, and boulders
- Qgr** Back-glacier deposits (Holocene and Pleistocene) - Unconsolidated cliques that have "humped-crest" topographic photographs
- Qms** Slides, slumps, and flows (Holocene and Pleistocene) - Earthflows, slumps, and slides some Qms units share a common boundary with adjoining mass movement
- Qgp** Patterned ground (Holocene and Pleistocene (?)) - Soil structures developed on bedrock unit Zhp, composed generally of fine-grained materials surrounded by unconsolidated boulders that are roughly arranged into polygon shapes less than 10 m in diameter; boulders are angular sandstone fragments of the Uinta Mountain Group, mapped on the saddle west of Leidy Peak
- Qgs** Smiths Fork fill (Upper Pleistocene) - Unconsolidated, poorly sorted, angular to rounded boulders, cobbles, and pebbles mostly of red sandstone and quartzite (Uinta Mountain Group); generally forms low ridges, knobs, and terraces with a smooth to subrounded hummocky surface with well-developed soils; correlated to Bull Lake glaciation by Munroe (2001), less than 5 m thick
- Qas3** Smiths Fork outwash (Upper Pleistocene) - Unconsolidated, well-rounded boulders, cobbles, and pebbles, and sand of mostly red sandstone and quartzite (Uinta Mountain Group); deposited by meltwaters of Smiths Fork-age glaciers (Munroe, 2001), less than 5 m thick
- Qgb** Backs Fork fill (Middle Pleistocene) - Unconsolidated, poorly sorted, angular to rounded boulders, cobbles, and pebbles mostly of red sandstone and quartzite (Uinta Mountain Group); generally forms steep ridges, knobs, and terraces with a smooth to hummocky surface with thin soils; correlated to Friesdale glaciation by (Munroe and Laabs, 2009), 1 - 50 m thick
- Qas3** Older south flank piedmont alluvium (Middle Pleistocene) - Unconsolidated to poorly consolidated, poorly sorted silt, sand, gravel, and cobble to boulder deposits; subangular to subrounded clasts dominated by quartz sandstone and quartzite of Uinta Mountain Group; mostly matrix-supported with clay-supported channel deposits; well-developed soil profile with irregular carbonate cementation; some clasts coated with iron-manganese; boulders are scattered on surface as lag deposit
- Tb** Bishop Conglomerate (Oligocene) - Light gray to pinkish-gray, friable sandstone and poorly sorted, loosely cemented boulder conglomerate mapped on the north and south flank of the Uinta Mountains; contains light gray to white air-fall tuff interbeds; siltstone and horribles from tuff bed X dated at about 29 Ma (Benson, 1986); X bed part from sample near top of Bishop 40473A dated at 30.5 Ma and from lower in the section 40473W dated at 34.03 Ma (Kowallis et al., 2008) 10 - 150 m thick
- Zhp4** Uinta Mountain Group (Eoprotozoic) Red Pine Shale (?) Unit 4—Upper Marsh Ridge shale Overall coarsening upward section (minimum thickness of 80 m); lower part is medium brownish-gray clay shale coarsening upward to grey-green siltstone. Upward, the siltstone is interbedded with thin beds of fine-grained quartz arenite and beds thicken upward to medium beds. Includes a system of cracks, parting laminations, tool marks, ripples, and intra-beds. The upper part of the unit is red laggy medium-grained sandstone fining upward into fine-grained cross-bedded quartz arenite. Prominent on Marsh Ridge, above Fish Lake, and on Mount Unteremann. Section Unit 4 has an eroded top.
- Zhp3** Uinta Mountain Group (Eoprotozoic) Red Pine Shale (?) Unit 3—Cyclic unit Stacked to six cycles in ~75 m thick section of alternating coarse silty sandstone and siltstone; capped by purple, red, cross-bedded medium-grained sandstone lower part and fine to fine-grained quartz arenite. Prominent on Marsh Ridge and in the saddle between Mt. Unteremann and Leidy Peak. Section Unit 3 and overlain by Unit 4.
- Zhp2** Uinta Mountain Group (Eoprotozoic) Red Pine Shale (?) Unit 2—Lower Marsh Ridge shale Coarsening upward package (40-60 m thick) of alternating medium-bedded fine to medium-grained purple red quartz arenite and grey silty shale. Upward increasing shale, w coarse arkosic arenite channels and fine-grained thin to medium bedded lower quartz arenite. The greenish-grey siltstone and fine-grained quartz arenite and subarkosic interbeds, coarsen upward to a fine to medium grained quartz arenite, medium to thick bedded. Sits sharply on Unit 1 and overlain by Unit 3.
- Zhp1** Uinta Mountain Group (Eoprotozoic) Red Pine Shale (?) Unit 1—Leidy Peak shale Generally coarsening upward package ~70 m thick, upper part of unit comprises variable composition arenite including coarse-grained weathered arkosic sandstone and overlying red laggy fine-medium bedded, medium-grained sandstone interval. The top of this is a thick bedded fine-grained cross-bedded quartz arenite. Sits gradually on classic Hades Pine quartzite and overlain by Unit 2.
- Zhp** Uinta Mountain Group (Eoprotozoic) formation of Hades Pine—Bed plane is coarse grained quartzite with thin beds and lenses of pebbly sandstone; pebbles comprise quartzite and yellow chert. Tough cross-bedded and arcuate surfaces. Overlain by medium-bedded fine-grained greenish sandstone and thin shale interbeds (?) with trough crossbeds, symmetric and asymmetric ripples, toolmarks, mudcrack beds, pressure cracks, esposito casts, soil sediment deformation, intra-beds. Overlain sharply by Unit 1 Leidy Peak shale of Red Pine Shale. Minimum thickness of 415 m in map area.

*Tertiary and Quaternary descriptions modified from Sprinkel, 2006 and Munroe and Laabs 2009



Sources of geologic information:

Dehler, C.M., Fanning, C.M., Link, P.K., Kingsbury, E.M., and Pylczynski, D., 2010. Maximum depositional age and provenience of the Uinta Mountain Group and Big Cottonwood Formation, northern Utah: Paleogeography of drifting western Laurentia. Geological Society of America Bulletin, v. 122, p. 1686-1699.

Hansen, W. R., 1986. Neogene tectonics and geomorphology of the eastern Uinta Mountains in Utah, Colorado, and Wyoming. U.S. Geological Survey Professional Paper 1356, 78 p.

Kowallis, B.J., Christiansen, E.H., Balls, Elizabeth, Hezler, M.T., and Sprinkel, D.A., 2005. The Bishop Conglomerate ash beds, south flank of the Uinta Mountains, Utah—are they pyroclastic fall beds from the Oligocene ignimbrites of western Utah and eastern Nevada. in DeHler, C.M., Pederson, J.L., Sprinkel, D.A., and Kowallis, B.J., editors. Uinta Mountain geology. Utah Geological Association Publication 33, p. 131-145.

Munroe, J.S. and Laabs, B.J.C., 2009. Glacial Geologic Map of the Uinta Mountains Area, Utah and Wyoming. Utah Geological Survey, Miscellaneous Publication 09-40M.

Sprinkel, D.A., 2006. Interim geologic map of the Dutch John 30' x 60' quadrangle, Daguerre and Uintah Counties, Utah, Moffat County, Colorado, and Sweetwater County, Wyoming. Utah Geological Survey, <http://geology.utah.gov/map/geomaps/30b30p/df04-431.pdf>

Wallace, C.A., and Criffenden, M.D., 1969. The stratigraphy, depositional environment and correlation of the Precambrian Uinta Mountain Group, western Uinta Mountains, Utah. in Lindsey, J.D., ed., Geologic Guidebook of the Uinta Mountains, Intermountain Association of Geologists 16th Annual Field Conference, p. 127-142.

VITA

Dawn Schmidli Hayes

711 E 200 N • Logan, UT 84321
 321.368.9497 • dawn.schmidli.hayes@aggiemail.usu.edu

CAREER OBJECTIVE 1) Contribute to the advancement of petroleum systems science by applying sedimentologic, stratigraphic, and geochemical techniques to solve complex hydrocarbon-related geologic problems and 2) do so in a motivating and supportive environment where collaboration, accountability, and excellence are the norm.

ACADEMIC QUALIFICATIONS Department of Geology, Utah State University, Logan, Utah
Doctor of Philosophy in Geology, May 2013 GPA: 4.0
 Dissertation: *Two scenes from Utah's stratigraphic record: Neoproterozoic Snowball Earth, Before and After*

Department of Geology, Utah State University, Logan, Utah
Master of Science in Geology, May 2011
 Thesis: *Stratigraphic, microfossil, and geochemical analysis of the Neoproterozoic Uinta Mountain Group, Utah: evidence of a eutrophication event?* GPA: 4.0

Idaho State University, Pocatello, Idaho
Bachelor of Science in Secondary Education, May 2002
 GPA: 4.0 High Honors Major: Biology Minor: Geology/Earth Science

DePauw University, Greencastle, Indiana
Bachelor of Arts in Biological Sciences, May 1999
 GPA: 3.2 Minor: Geology

PROFESSIONAL EXPERIENCE **Geoscience Intern**, summer 2012
Anadarko Petroleum Corporation, The Woodlands, Texas
 Project: *Maximizing Marcellus production: development and integration of a lithofacies model*

Geology Instructor for USU Summer Science Academy, June – July 2011 *Utah State University, Logan, Utah*
 Courses taught: Physical Geology (GEO 1110), & Lab (GEO 1115)
 •Planned and taught an integrated college-level laboratory & lecture course for advanced high school students

Graduate Teaching Assistant, May 2009 – present

Utah State University, Logan, Utah

- Natural Disasters course, summer 2009
- Mineralogy & Crystallography, fall 2009 & spring 2011
- Earth Through Time, spring 2010, 2012, 2013
- Sedimentology & Stratigraphy, fall 2010

GK-12 Graduate Fellow, August 2008-June 2009

Idaho State University & Irving Middle School, Pocatello, Idaho

- Partnered with 8th grade teacher to engage Earth Science students in inquiry-based lessons
- Planned two science lessons & spent 15 hr/week in the classroom
- Coordinated student research projects that utilized university resources & technology
- Involved students in locally relevant university research

Chemistry Instructor, August 2005 – July 2007

Florida Air Academy, Melbourne, Florida

Courses taught: Chemistry 1, Honors Chemistry

- Selected chemistry curriculum and planned all classroom and laboratory activities
- Responsible for laboratory inventory, MSDS/chemical hygiene plan, ordering and preparation of laboratory materials, and laboratory safety training
- Participated in the school-wide tutoring program and the summer-school program, sponsored the Academic Team, and mentored local undergraduate students
- Selected as a high-performing teacher by the Florida Council of Independent Schools

Master Teacher, June 2005

University of South Carolina – Aiken, Aiken, South Carolina

Course taught: Advanced Placement Biology Institute

- Collaborated with USCA professors Drs. William Jackson and Andrew Dyer to plan lectures, activities, laboratory exercises, and assessments for the course
- Ordered laboratory supplies, prepared lab materials, and provided instruction for the laboratory section of the course

Science Teacher, August 2002 – May 2005

Midland Valley High School, Graniteville, South Carolina

Courses taught: Physical Science, Biology 1, Applied Biology 2, Chemistry 1 Honors Chemistry 1, Advanced Placement Biology

- Successfully completed ADEPT evaluation program in May 2004
- Taught alternative school and summer school in 2003-2004
- Coached cheerleading 2003-05 & assisted with Student Council 2002-03

College of Education Research Assistant, August 2001 – January 2002 *Idaho Classrooms of Accomplished Teachers (ICAT) Project*, Pocatello, Idaho

- Collected data & designed surveys to evaluate ICAT program effectiveness
- Conducted literature searches & wrote literature reviews used to gain project funding
- Assisted Dr. Traci Bliss, ICAT Project Director, in designing & coordinating ICAT seminars

Teaching & Research Assistant, June 1999 – May 2000
Idaho State University Department of Biological Sciences, Pocatello, Idaho

Courses taught: “Biology & Human Concerns” and “General Ecology”

- Conducted field analysis of streams, collecting benthic macroinvertebrate, chlorophyll, and water samples
- Tested stream water samples in the laboratory (pH, BOD, alkalinity, hardness, and ion analysis) and performed chlorophyll analysis and benthic macroinvertebrate identification
- Responsible for activity planning, materials preparation, instruction, and assessment for the laboratory course sections

PROFESSIONAL ACTIVITIES

Memberships: Sigma Xi Scientific Society, Geological Society of America, American Association of Petroleum Geologists, American Geophysical Union, National Science Teachers’ Association, Alpha Phi Fraternity, Idaho State University Geology Club, Utah State University Geology Club, Logan Geological Society

Conferences/meetings attended: Geological Society of America Rocky Mountain Cordilleran Section 2008, Geological Society of America Rocky Mountain Section 2009, Society of Mining Engineers/Idaho Association of Petroleum Geologists (2008-09 monthly meetings), University of Montana Thompson-Winston Symposium 2009, International Conference & Field Meeting on Precambrian Life, Time and Environments: Evolving Concepts and Modern Analogues 2010, Geological Society of America National Conference Denver 2010, Geological Society of America Rocky Mountain Cordilleran Section 2011, Geological Society of America National Conference Minneapolis 2011, American Geophysical Union Annual Meeting San Francisco 2011

Meeting Presentations:

Detrital zircons from the newly discovered quartzite of Island Lake, Neoproterozoic Uinta Mountain Group, High Uintas Wilderness, GSA Rocky Mountain Section Meeting 2009, Orem, Utah, USA

Stratigraphic, microfossil, and geochemical analysis of the Neoproterozoic Uinta Mountain Group, Utah: Evidence of biotic change driven by eutrophication?, International Conference & Field Meeting on Precambrian Life, Time and Environments: Evolving Concepts and Modern Analogues 2010, Lucknow, India

A new locality of Neoproterozoic tube structures in northern Utah: Insight into genesis and age of a cap carbonate, GSA Rocky Mountain Cordilleran Section Meeting 2011, Logan, Utah, USA

Description and stable isotope record of newly discovered Neoproterozoic (Cryogenian?) tube structures, northern Utah, AGU Annual Meeting 2011, San Francisco, CA, USA

FUNDING RECEIVED

EDMAP project, 2011, semester research assistantship
 Geological Society of America, 2011, \$3500 research grant
 Sigma Xi Grant-In-Aid of Research, 2010, \$800 research grant
 The Society for Organic Petrology Spackman Award, 2009-2010, \$1000 research grant
 Utah State University Teaching Assistantship, 2009-present, \$12,000/year stipend, tuition
 National Science Foundation GK-12 Fellowship, 2008-2009, \$30,000 stipend & full tuition
 Geological Society of America Student Travel Grant, 2009, \$400

AWARDS & HONORS

Outstanding Graduate Researcher, 2013
 Beryl O. and Tura H. Springer Memorial Scholarship, 2011
 J. Stewart Williams Graduate Fellowship, 2010
 Outstanding Graduate Teaching Assistant, 2010 & 2011
 USU College of Science Zobell Scholarship Finalist, 2010
 SEPM-RMS Edwin McKee Award honorable mention, 2010
 National Science Foundation GK-12 Fellow, 2008-2009
 Florida Council of Ind. Schools High-Performing Teacher, 2007
 Dean's List & High Honors Diploma, Idaho State Univ., 2000-2002
 President's List, College of Charleston, 1997